12-15-2014

# Surface Functionalization of Inorganic Substrates with Polymeric Ligands Using Raft Polymerization

Anand Viswanath
*University of South Carolina - Columbia*

# SURFACE FUNCTIONALIZATION OF INORGANIC SUBSTRATES WITH POLYMERIC LIGANDS USING RAFT POLYMERIZATION

by

Anand Viswanath

Bachelor of Science
Furman University, 2009

---

Submitted in Partial Fulfillment of the Requirements

For the Degree of Doctor of Philosophy in

Chemistry

College of Arts and Sciences

University of South Carolina

2014

Accepted by:

Brian C. Benicewicz, Major Professor

Chuanbing Tang, Committee Member

Thomas Vogt, Committee Member

MVS Chandrasekhar, Committee Member

Lacy Ford, Vice Provost and Dean of Graduate Studies

# ACKNOWLEDGEMENTS

I would like to thank Dr. Brian Benicewicz for his guidance and mentorship though my Ph.D. work, especially in developing my technical skillset in polymeric materials and his encouragement in leadership activities. His support and belief throughout the rigors of my Ph.D. career was invaluable in the success of my research. I would also like to thank my doctoral committee members – Prof. Chaunbing Tang, Prof. Tom Vogt and Prof. MVS Chandrasekhar for their encouragement and assistance during graduate school.

This work would not be possible without the feedback and new ideas brainstormed with various collaborators. I would like to thank my collaborator Prof. Linda Schadler (Rensselaer Polytechnic Institute) and her graduate students, Peng Tao and Ying Li for their valuable contributions in this work. Furthermore, I would also like to acknowledge my collaborator Prof. Andrew Greytak for his guidance, and his graduate students Yi Shen and Pravin Paudel. I would also like to acknowledge Dr. Gordon Calundann and Warren Steckle for their contributions in this work.

I am very thankful for the support and great work environment provided by membersss of the Benicewicz group, past and present. In particular, Brandon Cash and Atri Rungta were very helpful mentors. Alexandra Green also provided vital contributions to this work, and I am grateful for her insight and assistance.

Finally, I would also like to thank my family and friends– my parents, my brother Arun and Reena for their continuous inspiration through my Ph.D. work.

## ABSTRACT

This work focused on using polymers to modify the surface of various inorganic substrates, ranging from $TiO_2$, ITO, CDSe and CdS nanostructures to micron sized silica particles. The synthesis of the polymers using the RAFT technique and the characterization of the functionalized substrates were analyzed in detail to provide insights into their use for various applications.

In the first part of this work, novel phosphate based RAFT agents and phosphate containing polymers, including poly(methyl methacrylate) (PMMA), poly(glycidyl methacrylate) (PGMA) and poly(dimethyl siloxane) (PDMS) were synthesized. Alkyne functionalized PGMA was used to click to ITO surfaces in a grafting-to method, and a phosphate based RAFT agent was utilized to demonstrate the first example of PMMA grafted from ITO nanoparticles. Using commercially available hydroxyl-modified PDMS, the PDMS-phosphate was synthesized and anchored to $TiO_2$ nanoparticles using both monomodal and bimodal approaches.

The second part of this thesis focused on the development of imidazole functionalized polymers for attachment to quantum dot materials. Activated esters were directly copolymerized with poly(ethylene glycol) methacrylate (PEGMA) followed by postmodification with histamine to obtain water soluble multidentate imidazole copolymers. The applicability of these polymers in functionalizing and stabilizing CdSe

quantum dots was investigated, resulting in good quantum yields of the functionalized dots as well as excellent dispersions in water. Detailed polymerization studies were conducted to determine the reactivity ratios for this important monomer pair.

In the third section, the earlier fundamental studies on the polymerization of activated esters were expanded by adding a boc-protected methacrylamide to the methacrylate based activated ester and PEGMA. Due to the intrinsic differences in the electronegativity of the groups next to the vinyl bond, the vinyl groups displayed unique NMR signals, and allowed for the measurement of the individual monomer conversions in the terpolymer system. The terpolymer was postmodified with imidazole units, followed by the boc-deprotection of the amine terminal groups. The resulting poly(imid-PEGMA-MAMimine) provided water solubility, dye loading capability and well as the ability to coordinate with CdS surfaces using the imidazole units. Upon the attachment of a rhodamine dye, studies to analyze the potential of such polymers to modify CdS nanowires were performed using florescence spectroscopy. The results also showed that the carefully designed terpolymers were more effective as a labeling species than the free dyes.

Finally, the fourth part of the thesis investigated additional monomer classes and particle types for functionalized polymer applications. In this section, the synthetic toolbox was expanded by studying the growth of poly(acrylic acid) and poly(acrylamide) (PAM) on larger porous silica particles (5.5 μm) using RAFT. Additionally, a novel activated azo initiator was also shown to polymerize methyl methacrylate and styrene from the silica surface as a cost-effective alternative to RAFT. In a demonstration of this technology for environmentally friendly fracturing fluids, migration studies were

designed by passing the silica-polymer samples through columns of filter material to show that the polymer-anchored samples were retained in the filter media more than unfunctionalized silica particles.

# TABLE OF CONTENTS

# LIST OF TABLES

# LIST OF FIGURES

# LIST OF SCHEMES

# CHAPTER 1

## INTRODUCTION

### 1.1. Reversible Addition-fragmentation Chain Transfer Polymerization

Reversible addition-fragmentation chain transfer (RAFT) polymerization[1] has become one of the leading controlled radical polymerization (CRP) methods, along with nitroxide mediated polymerization (NMP) and atom transfer radical polymerization (ATRP). These CRP methods enable the highly precise control over several molecular variables in the polymerization system. These include, but are not limited to the molecular weight, molecular weight distribution and the integrity of functional end groups in the polymer. In particular, RAFT polymerization has been extensively utilized to prepare a variety of polymeric architectures, mainly due to its ability to tolerate various functional groups and its usage under mild reaction conditions.[1,2]

In the RAFT process, the chain transfer agent (CTA) is essential for control in the polymerization. The CTA, which ranges from dithioesters, trithiocarbonates or xanthates achieves control via a two-step addition-fragmentation mechanism. The living characteristics of the polymerization depends on the equilibrium between the active propagating radicals ($P_n$ and $P_m$) and the dormant polymeric CTA (Scheme 1.1).[3] Reinitation and propagation steps usually occur quickly in the RAFT process, with the termination step being suppressed. The choice of an appropriate R and Z group is crucial for control in a given monomer system, and can be varied according to the needs of the polymer product. The Z group controls the stability of the S=C bond and the radical

intermediate in the chain transfer step, while the R group is designed to be a good leaving group and to allow the expelled radical to reinitiate efficiently. The choice of the appropriate Z and R groups for a particular monomer system is shown in Figure 1.1 and 1.2.

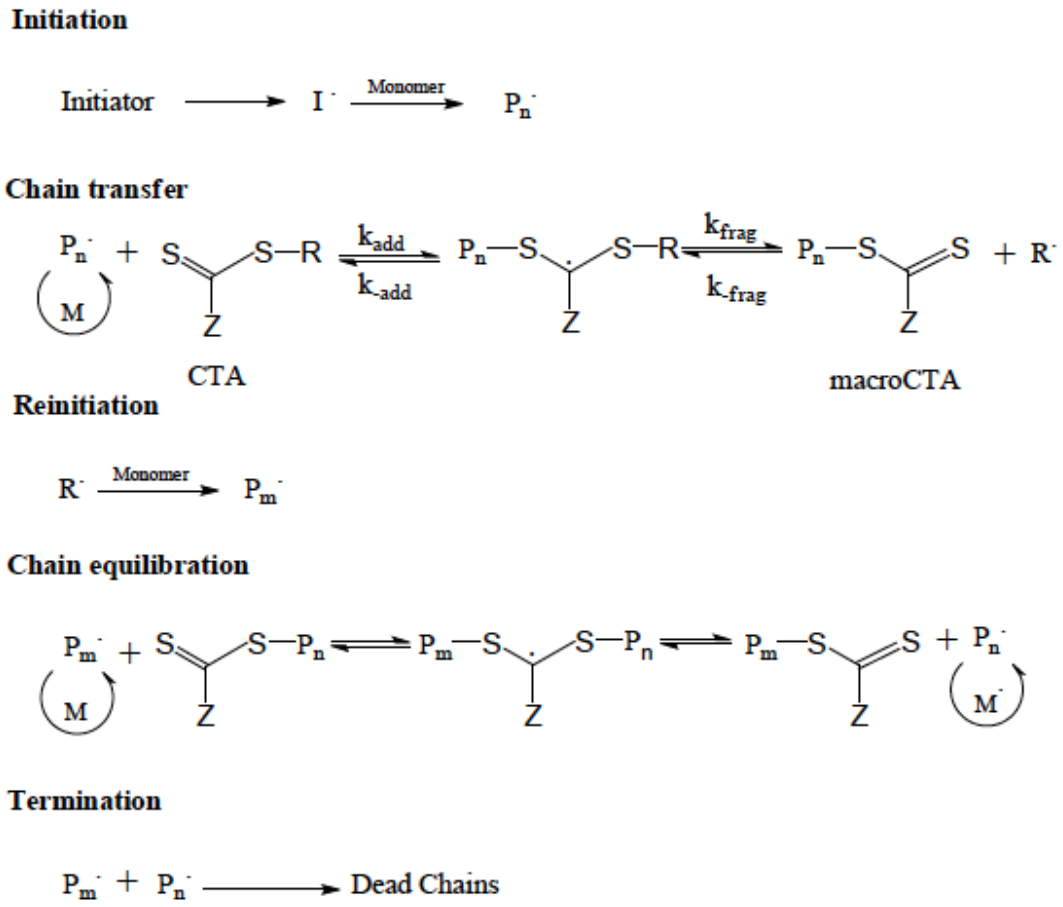


Scheme 1.1: Mechanism of RAFT polymerization.

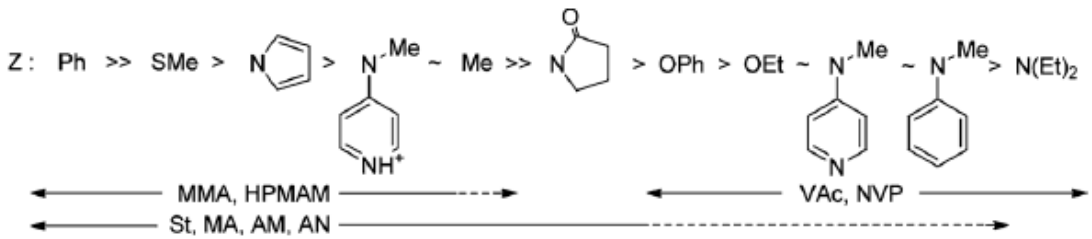

Figure 1.1: Ideal choices of Z groups of the RAFT agent for various monomer systems.[3]

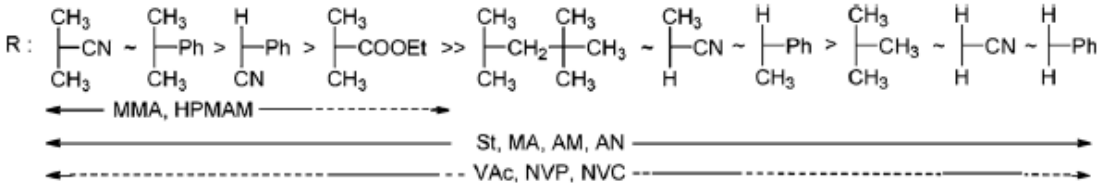


Figure 1.2: Ideal choices of R groups of RAFT agents for various monomer systems.[3]

## 1.2 Ligands for substrate functionalization

Inorganic substrates are often functionalized with polymers and organic compounds in order to alter their properties or behavior for various applications.[4,5] For effective functionalization, surface anchoring groups need to be present on the organic molecule to facilitate the attachment. Such materials are commonly referred to as ligands, where the head group contains a polar functionality that can coordinate to the inorganic surface via electrostatic attraction, hydrogen bonding or covalent binding (Figure 1.3). The backbone of the ligand varies widely, and is commonly present as alkyl chains of different lengths. In cases where the post modification reactions are needed, a functional group is added to the backbone of the ligand. It must be noted that these functional groups are designed/protected to withstand the reaction conditions for the substrate functionalization step.

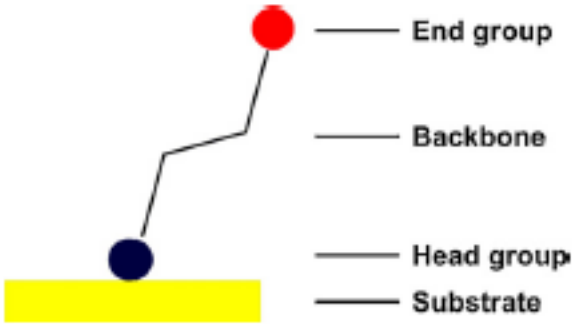


Figure 1.3: Ligand structure details for substrate functionalization.[6]

In all substrate modifications, the choice of the ligand for the particular substrate is important. Additionally, the outlook in terms of the application for the functionalized substrate product also plays a significant role in dictating the appropriate ligand choice. For example, in applications where silica needs to be strongly bound (such as stationary phase materials in chromatography), robust covalent attachment is required, which can be obtained via silane ligands.[7] If a weaker attachment is preferred for silica, non-covalently binding ligands such as carboxylic acids or phosphonic acids can be considered. For metal oxides, the trend is the opposite where the phosphonic acid/phosphates provide a stronger binding than the carboxylic acid or silane based ligands.[8] Phosphorus containing ligands tend to favor the formation of M-O-P (where M is metal), which are more stable than M-O-Si or M-O-C bonds. As seen in Figure 1.4, the P-O bond can also be manifested in a variety of binding modes for added stability, including monodentate, bidentate and tridentate modes.

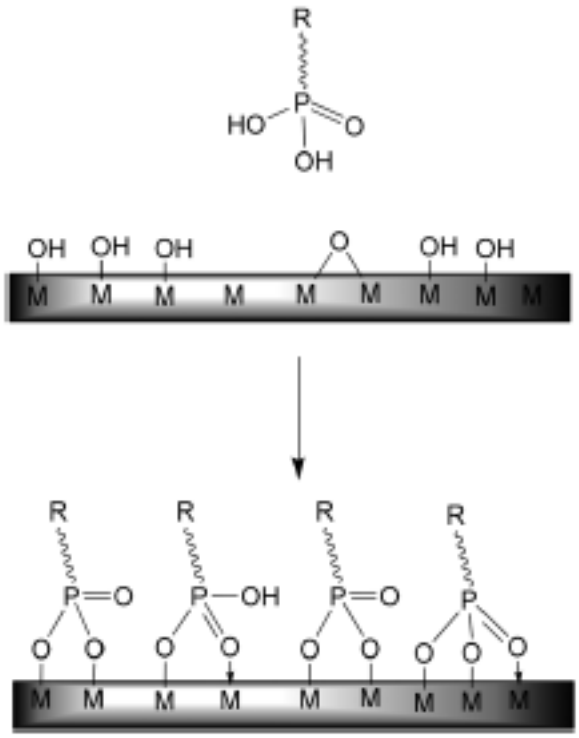


Figure 1.4: Binding of phosphorus-based ligands on metal oxide surfaces, and the presence of different binding modes.

In the chapters that follow, a variety of ligands will be explored with a focus towards specific applications. Phosphate based ligands are explored with metal oxide nanoparticles for robust attachment for well-dispersed nanocomposites. Imidazole ligands are investigated as contenders for strong adsorbers (non-covalent) for semiconductor quantum dots and nanowires in optical applications. Finally, silane functional ligands are utilized for the purpose of robust attachment of polymers to silica in order to prevent any cleavage of the polymer for environmentally friendly fracturing fluids.

### 1.3 Grafting Methods Overview

In terms of attachment methods to substrate materials, there are several methods for functionalization using polymeric materials. These methods are highly effective for aiding in preventing aggregation of the nanomaterials, and the steric hindrance between the inorganics due to the large polymeric chains plays a role in maintaining good dispersions of the nanomaterial.[9,10] There are three main methods, and include physisorption, grafting-to and grafting-from techniques (Figure 1.5). In physisorption, ligands range from weak to strong adsorbents, and typically bind via an electrostatic or hydrogen bonding approach.[11] With extended washing of the functionalized substrate, the ligand can be completely removed, with the rate of dissociation dependent upon the ligand binding strength. In the grafting-to approach, the substrate is modified with a ligand bearing different end functionality, such that the functionality is available for post-modification. In recent decades, click chemistry has proven to be a popular strategy, where polymers are functionalized with azide/alkyne moieties.[12,13] One disadvantage with this approach is that the post-modification yields are dependent upon the molecular weight of the polymer, with higher yields favoring smaller molecular weight polymers. In the grafting from approach, ligands containing CTAs are commonly utilized followed by the growth of polymer chains from the surface. Highly dense brushes can be achieved by this method, as polymer growth is dependent upon the diffusion of monomers to the growing chain end.

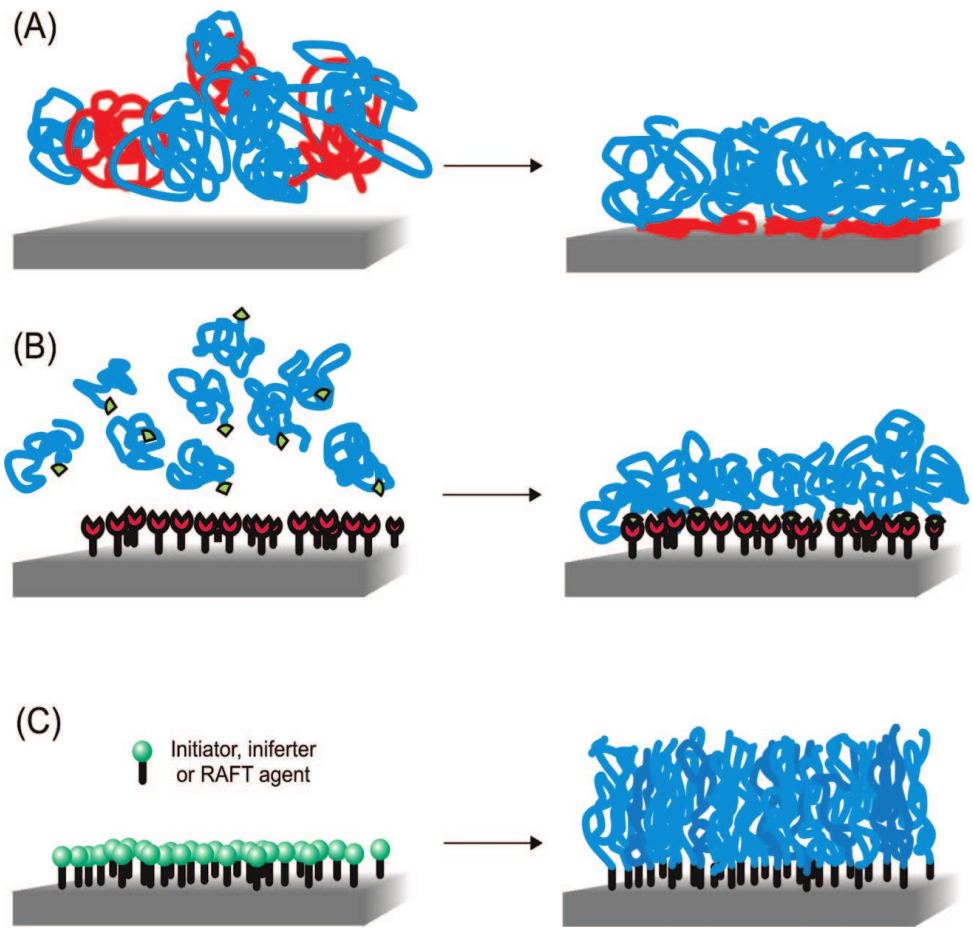


Figure 1.5: Overview of grafting polymers to substrates, including (a) physisorption, (b) grafting-to and (c) grafting-from methods.

In this Ph.D. work, physisorption is investigated using imidazoles on quantum dots and nanowires, both grafting-to and from methods for the attachment to $TiO_2$ and Indium Tin Oxide (ITO) nanoparticles, and the grafting from method explored as a viable solution for the growth of polymer chains on silica substrates.

### 1.4 Phosphate functionalized polymers for metal oxide nanoparticle modification

After several reports provided definitive proof of the ability of phosphorus containing ligands to bind strongly with metal oxides, interest on the use of these ligands on ITO and $TiO_2$ followed quickly.[8,14,15] Tin-doped indium oxide (ITO) has been reported to be a favorable energy efficient material due to its combination of high transparency in the visible range, high infrared reflectivity, UV-light absorption and high thermal stability.[16,17] $TiO_2$ nanoparticles have a high refractive index (2.45 and 2.7 for anatase and rutile phase respectively) and a very low absorption coefficient in the visible range, and are useful as components in high refractive index nanocomposites.[18–20] With ITO, Hansen and coworkers have investigated the use of a phosphonic acid based oligothiophene to alter the electronic properties of ITO flat substrates.[21] The preparation of ITO nanocomposites was investigated by Capozzi et al., where ITO was blended with poly(methyl methacrylate) to reveal 3D nanowire-like formations of the ITO within the composite.[22] In the area of ligand modified ITO and its use in nanocomposites, there is a lack of detailed studies in the literature. However, $TiO_2$ has seen a surge of research in nanocomposite work using carboxylic acid as ligands, including both grafting-to and grafting-from methods.[23–26] Phosphonic acid/phosphate ligands for $TiO_2$ nanocomposites is less well represented, and work by Tchoul and coworkers[27] through a click chemistry grafting-to method for high refractive index nanocomposites and Aslan et al.[28] regarding $TiO_2$-poly(vinylphosphonic acid) composites for membranes are a few examples using phosphorus based ligands. One of the goals of this dissertation is to develop a more fundamental understanding of the synthesis and characterization of phosphorus based

ligands on $TiO_2$ and ITO nanoparticles using different grafting methods for usage as nanocomposite applications.

### 1.5 Activated esters for postmodification

The homopolymerization of monomers with succinimide based activated ester groups via CRP has been documented in the literature extensively, with good control under mild reaction conditions. Copolymers with other monomers have also been explored, where the choice of monomer is dependent upon its reactivity ratio with N-methacryloxy succinimide (NMS) and the solvent conditions. Tew and coworkers have investigated the copolymerization of NMS with styrene, methyl methacrylate (MMA) and PEGMA using ATRP.[29] Alternatively, NHS based carbonates have also been introduced on the end of longer alkyl chain methacrylates and copolymerized with MMA and PEGMA.[30] N-acryloxy succinimide (NAS) and acrylamides with alkyl linkers bearing succinimide groups have been copolymerized with MMA to develop polyurethanes with soft segments.[31] For polymers incorporating organic/nonpolar side groups, PEG functional groups have been widely used to improve the water solubility for applications in biomedicine. Fukukawa et al. have utilized a PEG based NMP initiator to polymerize NAS and DMA for core shell star copolymers for biodistribution studies.[32] NMS has also been incorporated through RAFT to make terpolymers for similar biodistribution and imaging studies.[32] In all these cases, the succinimide group has been used for postmodification reactions to attach new functionalities to the polymer. Using a similar approach, this work demonstrates a facile synthetic strategy for the preparation of water soluble polymers and their modification with multidentate histamine ligands that can efficiently coordinate semiconductor materials.

## 1.6 Grafting polymers from silica particles through RAFT polymerization

In the area of grafting polymers from silica using RAFT, Benicewicz and coworkers have designed a robust and versatile platform for the synthetic process.[33,34] This involves the use of aminopropyl silane to initially functionalize the silica surface, followed by the use of an activated RAFT agent (CPDB) to anchor on the silica particles.[34] By controlling the ratio of aminosilane to silica particles, the grafting density of the resulting RAFT functionalized silica can be controlled. Furthermore, the synthetic toolbox developed through these methods enables the substitution of other activated RAFT agents. This becomes important as CPDB, being a dithioester with a phenyl Z group, is good at polymerizing methacrylate and styrene derivatives. In applications requiring polymers from less reactive monomers, such as acrylamide, CPDB tends to suffer from retardation in the polymerization process.[3] Furthermore, dithioesters have limited stability in basic environments, and any degradation of the acrylamide monomer into ammonia can limit the polymerization process. In chapter 5, trithiocarbonate based RAFT agents will be explored which do not suffer from these limitations. In particular, the attachment of trithiocarbonate based RAFT agents on the silica surface will be investigated and adds to the synthetic foundation on grafting work by the Benicewicz group.

## 1.7. Dissertation Motives and Outline

This thesis will focus on expanding the synthetic toolbox for the functionalization of various inorganic materials. This is performed by designing unique synthetic ligands for functionalization, and analyzing the use of various polymer attachment methods

including physisorption, grafting-to and grafting from. Furthermore, this work expands the choice of inorganic substrates for polymer modification, such as TiO2, ITO, CdSe, CdS and silica. Chapter 2 focuses on the use of new phosphate based polymers for the modification of $TiO_2$ and ITO. A novel RAFT-phosphate ligand is synthesized which allows the grafting-from polymerization of PMMA from ITO nanoparticles to be demonstrated for the first time. Chapter 3 lays the foundation of a simple post-modification of activated ester copolymers with imidazole units, along with an understanding of the kinetics of the acrylate based activated ester and methacrylate derivative copolymerization as well as its quantitative reactivity ratio analysis. The use of such imidazole copolymers in binding with quantum dots is also illustrated. Chapter 4 utilizes the synthetic foundation set in the earlier chapter, and builds on it by adding a methacrylamide in a terpolymer system. The individual monomer conversions are monitored by NMR due to the unique arrangement of the monomer peaks in the NMR. The applicability of these terpolymers to be postmodified with imidazole units, and their binding to semiconductor CdS nanowires is also demonstrated. Finally, in chapter 5, larger silica particles (5.5 μm) were functionalized with activated dithioesters and trithiocarbonates for the polymerization of acrylic acid and acrylamide. These robustly anchored polymer-silica composites were tested to display high retention efficiency of these samples in various soil materials, and points to its applicability in environmentally friendly fracturing fluids with improved oil and gas yields.

## 1.8 References


(1) Chiefari, J.; Chong, Y. K. (Bill); Ercole, F.; Krstina, J.; Jeffery, J.; Le, T. P. T.; Mayadunne, R. T. A.; Meijs, G. F.; Moad, C. L.; Moad, G.; Rizzardo, E.; Thang, S. H. *Macromolecules* **1998**, *31*, 5559.

(2) Moad, G.; Rizzardo, E.; Thang, S. H. *Aust. J. Chem.* **2009**, *62*, 1402.

(3) Barner-Kowollik, C. *Handbook of RAFT Polymerization*; John Wiley & Sons, 2008; p. pg. 245.

(4) Kango, S.; Kalia, S.; Celli, A.; Njuguna, J.; Habibi, Y.; Kumar, R. *Prog. Polym. Sci.* **2013**, *38*, 1232.

(5) Kumar, S. K.; Jouault, N.; Benicewicz, B.; Neely, T. *Macromolecules* **2013**, *46*, 3199.

(6) Olivier, A.; Meyer, F.; Raquez, J.-M.; Damman, P.; Dubois, P. *Prog. Polym. Sci.* **2012**, *37*, 157.

(7) Minakuchi, H.; Nakanishi, K.; Soga, N.; Ishizuka, N.; Tanaka, N. *Anal. Chem.* **1996**, *68*, 3498.

(8) Mutin, P. H.; Guerrero, G.; Vioux, A. *J. Mater. Chem.* **2005**, *15*, 3761.

(9) Rungta, A.; Natarajan, B.; Neely, T.; Dukes, D.; Schadler, L. S.; Benicewicz, B. C. *Macromolecules* **2012**, *45*, 9303.

(10) Li, Y.; Tao, P.; Viswanath, A.; Benicewicz, B. C.; Schadler, L. S. *Langmuir* **2013**, *29*, 1211.

(11) Norsten, T. B.; Jeoung, E.; Thibault, R. J.; Rotello, V. M. *Langmuir* **2003**, *19*, 7089.

(12) Helms, B.; Mynar, J. L.; Hawker, C. J.; Fréchet, J. M. J. *J. Am. Chem. Soc.* **2004**, *126*, 15020.

(13) Binder, W. H.; Sachsenhofer, R. *Macromol. Rapid Commun.* **2008**, *29*, 952.

(14) Guerrero, G.; Mutin, P. H.; Vioux, A. *Chem. Mater.* **2001**, *13*, 4367.

(15) Guerrero, G.; Alauzun, J. G.; Granier, M.; Laurencin, D.; Mutin, P. H. *Dalton Trans.* **2013**, *42*, 12569.

(16) Granqvist, C. G.; Hultåker, A. *Thin Solid Films* **2002**, *411*, 1.

(17) Tao, P.; Viswanath, A.; Schadler, L. S.; Benicewicz, B. C.; Siegel, R. W. *ACS Appl. Mater. Interfaces* **2011**, *3*, 3638.

(18) Liu, J.; Nakamura, Y.; Ogura, T.; Shibasaki, Y.; Ando, S.; Ueda, M. *Chem. Mater.* **2008**, *20*, 273.

(19) Su, H.-W.; Chen, W.-C. *J. Mater. Chem.* **2008**, *18*, 1139.

(20) Tao, P.; Li, Y.; Rungta, A.; Viswanath, A.; Gao, J.; Benicewicz, B. C.; Siegel, R. W.; Schadler, L. S. *J. Mater. Chem.* **2011**, *21*, 18623.

(21) Hanson, E. L.; Guo, J.; Koch, N.; Schwartz, J.; Bernasek, S. L. *JACS* **2005**, 10058.

(22) Capozzi, C. J.; Li, Z.; Samuels, R. J.; Gerhardt, R. a. *J. Appl. Phys.* **2008**, *104*, 114902.

(23) Khaled, S. M.; Sui, R.; Charpentier, P. A.; Rizkalla, A. S. *Langmuir* **2007**, *23*, 3988.

(24) Matsuno, R.; Otsuka, H.; Takahara, A. *Soft Matter* **2006**, *2*, 415.

(25) Hojjati, B.; Charpentier, P. A. *J. Polym. Sci. Part A: Polymer Chem.* **2008**, *46*, 3926.

(26) Hojjati, B.; Sui, R.; Charpentier, P. A. *Polymer (Guildf).* **2007**, *48*, 5850.

(27) Tchoul, M. N.; Fillery, S. P.; Koerner, H.; Drummy, L. F.; Oyerokun, F. T.; Mirau, P. A.; Durstock, M. F.; Vaia, R. A. *Chem. Mater.* **2010**, *22*, 1749.

(28) Aslan, A.; Bozkurt, A. *J. Mater. Res.* **2012**, *27*, 3090.

(29) Aamer, K. A.; Tew, G. N. *J. Polym. Sci. Part A: Polym. Chem.* **2007**, *45*, 5618.

(30) Cengiz, N.; Kabadayioglu, H.; Sanyal, R. *J. Polym. Sci. Part A: Polym. Chem.* **2010**, *48*, 4737.

(31) Eschweiler, N.; Keul, H.; Millaruelo, M.; Weberskirch, R.; Moeller, M. *Polym. Int.* **2014**, *63*, 114.

(32) Fukukawa, K.; Rossin, R.; Hagooly, A.; Pressly, E. D.; Hunt, J. N.; Messmore, B. W.; Wooley, K. L.; Welch, M. J.; Hawker, C. J. *Biomacromolecules* **2008**, *9*, 1329.

(33) Li, C.; Han, J.; Ryu, C. Y.; Benicewicz, B. C. *Macromolecules* **2006**, *39*, 3175.

(34) Li, Y.; Benicewicz, B. C. *Macromolecules* **2008**, *41*, 7986.

# CHAPTER 2

## PHOSPHATE DERIVATIZED RAFT AGENTS AND POLYMERS: AVENUES FOR METAL OXIDE NANOPARTICLE FUNCTIONALIZATION

### 2.1 Introduction

The preparation of polymer nanocomposites through the incorporation of inorganic nanomaterials into a polymer matrix has been extensively explored to provide new and improved properties (as compared to the matrix polymer) for a variety of applications.[1–5] Polymer nanocomposites have shown significant improvements in optical[2,6] and electrical[7] properties, as well as an ability to tune processing variables including viscosity[8] and the glass transition temperature[9] of the nanocomposite. However, the precise applicability of the nanocomposite depends heavily on preventing any aggregation of the inorganic nanoparticles (NPs) within the matrix due to their high Van der Waals core-core attraction forces.[10] Aggregation or clumping behavior of the inorganic materials results in nanocomposites which have poor mechanical stability and low optical transparency (as the inorganics are no longer in the nano size regime), thus hindering its use in the envisaged application.

There are two main methods for ensuring aggregation free nanocomposites: (a) electrostatic forces in aqueous media to provide good dispersions and (b) functionalized polymers that can adsorb to the NP and prevent interparticle attraction.[11,12] Polymeric materials that can anchor to the surface of the NP possess a distinct advantage in that organic media can be used for nanocomposite processing. Furthermore, functionalized

polymers have shown ability to tune the dispersion of the inorganic NPs in the composite depending on the molecular variables of the polymer system.[13,14]

Since inorganic metal oxide nanomaterials have a higher surface energy than organic materials,[15] surface modification of the metal oxide is commonly used to obtain good dispersion in polymer matrices. Small molecule ligands are typically used for surface modification, and include silanes, carboxylic acids and phophonates. Such ligands are able to complex with the metal oxide via coordinative, electrostatic or hydrogen bonding.[16,17] In this work, where the metal oxides investigated include titanium dioxide ($TiO_2$) and Indium Tin Oxide (ITO), phosphorous containing ligands have been reported to be more promising that the other ligands.[16,17] This is mainly due to the lack of homocondensation between phosphonic acid/phosphate ligands, as compared to silanes, which tend to homocondense in the presence of metal oxides. Phosphonic acid/phosphate ligands have also shown to have a higher binding strength to the metal oxide NPs than carboxylic acids, and hence provide improved dispersions of the NPs.[18]

This chapter focuses on the development of phosphate functionalized RAFT agents and the polymers obtained from such RAFT agents. This relies on using the phosphorous moiety on the end of the RAFT agent to anchor to the NPs, while the RAFT agent can be used for grafting polymers "from" the NP surface. In an alternative scenario, polymers obtained in solution from the phosphate functionalized RAFT agent retain the phosphate end group, and can be used to graft such polymers "to" the NP surface. Additionally, grafting-to reactions can be done via phosphate modifications to commercially available polymers. The development of synthetic methods for the phosphate RAFT agents and

polymers provides a vantage point for the development of well-dispersed metal oxide nanocomposites and their usage in a variety of industrially relevant applications.

## 2.2 Experimental

### 2.2.1 Materials

All reagents were used as received from Fisher Scientific unless stated otherwise below. Prop-2-ynyl 4-cyano-4-(phenyl carbonothioylthio) pentanoate (AL-CPDB),[19] bis(dithiobenzoyl) disulfide[20] and 11-azidoundecyl dihydrogen phosphate[21] were synthesized according to established procedures. Azobisisobutyronitrile (AIBN) was purchased from Sigma Aldrich and recrystallized from ethanol thrice prior to use. Glycidyl methacrylate (in THF) was passed through a neutral alumina column to remove the inhibitor, followed by removal of the solvent by rotary evaporation. $POCl_3$ (99.99%) and $NaN_3$ were obtained from Sigma Aldrich. N,N,N',N",N"-Pentamethyldiethylenetriamine (PMDETA), hydroxyl ethyl bromoisobutyryl bromide and 11-bromo-1-undecanol were purchased from Acros. Cu(I)Br (99.999%, Aldrich) was purified with glacial acetic acid and washed with diethyl ether and ethanol prior to use. $TiO_2$ (5 nm) and ITO (6.6 nm) NPs were obtained through the Schadler research lab.

### 2.2.2 Characterization

NMR spectra were recorded on a Varian Mercury 300 spectrometer using $CDCl_3$ or $D_2O$ as the solvent. The molecular weights and molecular weight distributions were determined using a Waters gel-permeation chromatograph equipped with a 515 HPLC pump, a 2410 refractive index detector, three Styragel columns (HR1, HR3, HR4 in the effective molecular weight range of 100−5000, 500−30000, and 5000−500000,

respectively). Tetrahydrofuran (THF) was used as the eluent at 30°C and a flow rate of 1.0 mL/min. The GPC system was calibrated with polystyrene standards obtained from Polymer Laboratories. Thermal gravimetric analysis (TGA) was performed on a Perkin Elmer Series 7 instrument. The sample was heated from 30 to 1000˚C under a 60mL/min nitrogen flow at a heating rate of 10˚C/min.

### 2.2.3 Preparation of alkynyl poly(glycidyl methacrylate) (AL-PGMA)

In a Schlenk tube, glycidyl methacrylate (10.7g, 75.27 mmol) was dissolved in THF (20 ml). AL-CPDB (0.03g, 0.0946 mmol) was added to the mixture, followed by a 5mM solution of AIBN in THF (1.89 ml, 0.00946 mmol). The Schlenk tube was capped and subjected to three cycles of freeze-pump-thaw. The tube was then heated at 65°C for 25h. The polymerization was quenched in ice water and the mixture precipitated in hexane. The mixture was centrifuged at 3000 rpm for 5 min and redispersed in 20 mL of THF. This precipitation-redispersion process was repeated twice to obtain alkynyl poly(glycidyl methacrylate) with Mn: 60k, PDI: 1.20.

### 2.2.4 Click attachment of AL-PGMA to azide functional ITO

A mixture of as-synthesized ITO particles and 11-azidoundecyl dihydrogen phosphate with a weight ratio of 1:1 dispersed in chloroform was stirred and refluxed at 75˚C overnight. The phosphate treated particles were washed 3 times with ethanol and finally dispersed into THF. In a typical “click” reaction, 0.5 g of phosphate treated ITO NPs, 0.4 g of AL-PGMA, and 20 μL of PMDETA ligand were added into 60 mL of

anhydrous THF. Ten milligrams of CuBr was added into the flask, and the solution was bubbled with argon gas for 5 min. The flask was transferred into an oil bath at 55˚C for 48 h. The ITO-PGMA was precipitated into methanol, followed by centrifugation at 20000 rpm for 10 min and redispersion into chloroform.

### 2.2.5 Synthesis of 2-methyl-propionic acid 2-hydroxy-ethyl ester dithiobenzoate

Bis(dithiobenzoyl) disulfide (92.75 mg, 0.3 mmol), CuBr (23.4 mg, 0.163 mmol) and Cu(0) (51.9 mg, 0.81 mmol) were added to a round bottom Schlenk tube equipped with a magnetic stirrer. The flask was purged with $N_2$ for 20 min. In a separate Schlenk tube, Hydroxyl ethyl bromoisobutyrate (HeBib) (127.5 mg, 0.61 mmol), N,N,N',N',N''-pentamethyldiethylenetriamine (PMDETA) (56.6 mg, 0.33 mmol) and anhydrous toluene (4 mL) were subjected to four cycles of freeze-pump-thaw. Using a syringe backfilled with $N_2$, the liquid contents were transferred to the first tube. The mixture was then heated at 82˚C for 6h. The mixture was passed through a neutral alumina column to obtain the product in a 98% yield. $^1$H NMR (300 MHz, CDCl3), δ(ppm form TMS): 1.55 (s, 9H), 3.53 (t, 2H), 4.25 (t, 2H), 7.3-7.6 (m, 5H). LRMS (ES-TOF) m/z: [M-H] calcd for $C_{13}H_{16}O_3S_2$: 284.05 Found: 284.

### 2.2.6 Synthesis of 2-methyl-propionic acid 2-phosphonic acid-ethyl ester dithiobenzoate (RAFT-phosphate)

2-Methyl-propionic acid 2-hydroxy-ethyl ester dithiobenzoate (0.466g, 1.64 mmol) was dissolved in anhydrous THF (10 mL) in a 2-neck round bottom flask and purged with $N_2$ for 10 min. Anhydrous triethylamine (0.183g, 1.81 mmol) was added, and the mixture was cooled to 0˚C. $POCl_3$ (0.278g, 1.81 mmol) was added dropwise to the solution. The reaction was allowed to warm to room temperature and stirred for 3h. The reaction was quenched with $H_2O$ (10 ml) and the pH was observed to be less than 2. It was extracted with $CHCl_3$ (3 x 10ml), the combined organic extracts were filtered over $MgSO_4$ and the solvent removed via rotary evaporation. The liquid was then dried under vacuum to give the product (0.354g, 58%) as a dark red oil. $^1$H NMR (300 MHz, CDCl3), δ(ppm form TMS): 1.55 (s, 9H), 3.94 (t, 2H), 4.25 (t, 2H), 7.3-7.6 (m, 5H). $^{31}$P NMR (400 MHz, CDCl3): 1.19. LRMS (ES-TOF) m/z: [M-H] calcd for $C_{13}H_{17}O_6PS_2$: 364.02 Found: 363.

### 2.2.7 Functionalization of ITO nanoparticles with the RAFT-phosphate

ITO nanoparticles (0.05g) and RAFT-phosphate (0.01g, 0.027 mmol) were dispersed in anhydrous THF (5 ml) with the aid of ultrasonication for 20 min. The mixture was precipitated into hexanes, followed by centrifugation and redispersion in THF.

### 2.2.8 Preparation of poly(methyl methacrylate) grafted from ITO NPs

RAFT modified ITO (0.072g, 0.002mmol RAFT), methyl methacrylate (MMA) (4.7g, 47 mmol), THF (4 mL) and AIBN (0.03 mg, 0.0002 mmol) were added to a Schlenk tube equipped with a stir bar. The tube was subjected to three cycles of freeze-pump-thaw and was stirred for 6h at 60˚C. The polymerization was stopped by quenching the flask in ice water. The mixture was precipitated into hexanes to remove any traces of excess monomer. The particles were centrifuged at 20000 rpm for 5 min and redispersed with THF. This centrifugation-redispersion process was repeated twice more to obtain ITO-poly(methyl methacrylate) (ITO-PMMA).

### 2.2.9 Cleavage of polymers from ITO NPs

0.2 g of the ITO-PMMA was dissolved in THF (5ml) in a 25 ml round bottom flask, followed by the addition of 0.2 ml of 12M HCl. The mixture was refluxed overnight, and then dried in a Teflon petri dish. The dried mixture was suspended in THF, and centrifuged at 5000 rpm for 10 min. The supernatant was collected and dried to obtain the cleaved polymer. The polymer sample was then subjected to analysis by GPC.

### 2.2.10 Synthesis of phosphate functionalized Poly(dimethyl siloxane)

PDMS chains were prepared via a single step modification of commercially available hydroxyl terminated PDMS. In a typical reaction, a tetrahydrofuran (THF) solution of hydroxyl terminated PDMS (5000 g/mol) was cooled to 0˚C using an ice-

water bath under stirring, and $Et_3N$ (0.2g, 2 mmol) was added to the mixture. $POCl_3$ (0.306g, 2 mmol) was added dropwise to the stirred solution. The solution was then allowed to warm to ambient temperature as the ice melted. After 2 days, the reaction was terminated by adding deionized water and the pH value was adjusted below 2. The modified PDMS chains were extracted with $CH_2Cl_2$ and filtered over $Na_2SO_4$. The $CH_2Cl_2$ solvent was removed via rotary evaporation. Similar reactions were performed with other PDMS-OH (Mn ranging from 1k - 36K) where a ratio of 1:10:10 of PDMS-OH:$Et_3N$:$POCl_3$ was used to obtain phosphate functionalized PDMS.

### 2.2.11 Grafting PDMS to $TiO_2$ NP Surfaces

The phosphate modified PDMS was added to the transparent $TiO_2$ NP chloroform solution and refluxed under stirring for 24 h. The grafted NPs in the solution were precipitated using ethanol and then centrifuged under 10,000 rpm for 10 min. The precipitates were then dispersed in chloroform. The precipitation-redispersion process was repeated twice to remove residual free polymer chains to obtain monmodal $TiO_2$-PDMS samples. Bimodal distributions of PDMS were obtained with one further modification, where a 36k PDMS-phosphate was added to the $TiO_2$ NP first and the mixture was refluxed under stirring for 24 h. The grafted NPs in the solution were precipitated using ethanol and then centrifuged under 10,000 rpm for 10 min. The precipitates were then dispersed in chloroform. The precipitation-redispersion process was repeated twice to remove residual free polymer chains, followed by repeating the

same procedure using lower molecular weight PDMS-phosphate to obtain bimodal $TiO_2$-PDMS samples.

## 2.3 Results and Discussion

### 2.3.1 Grafting polymers to ITO using Al-PGMA and azide functional ITO NPs

In order to investigate the grafting-to approach, click chemistry was used to react AL-PGMA with azide functionalized ITO NPs (Scheme 2.1). The azide modified phosphate ligand was synthesized according to procedures outlined by Tao et al.[21] Given that the azide-alkyne click reaction provides high yields and mild reaction conditions, this synthetic strategy allowed grafting to the ITO surface in a versatile manner. The alkynyl group was added onto CPDB using a simple DCC procedure as established in earlier work by our group.[19] This click reaction is generally followed by means of FTIR, where the disappearance of the azide peak at 2100 $cm^{-1}$ confirms the product. As seen in Figure 2.1, there is a decrease in the azide peak and appearance of the carbonyl peak of the attached polymer after the reaction with AL-PGMA. Another method of characterization that confirmed the attachment of the polymer is TGA, and Figure 2.2 illustrates the increase in mass loss upon the attachment of the azide-phosphate ligand as well as a larger mass loss upon polymer attachment. Furthermore, the integrity of the nanocomposite was maintained to obtain aggregation-free thin films when the PGMA-ITO composite was cured in an epoxy resin (Section 2.3.7).

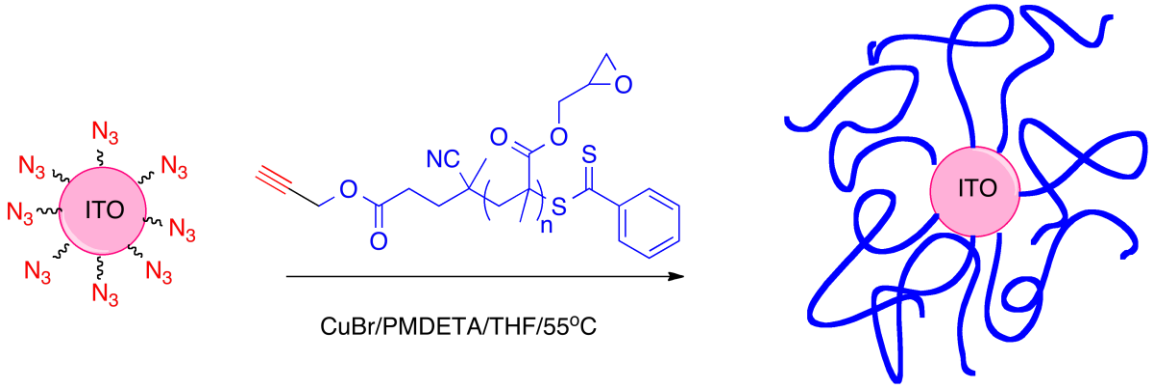


Scheme 2.1: Grafting to reaction of AL-PGMA onto azide functionalized ITO NPs.

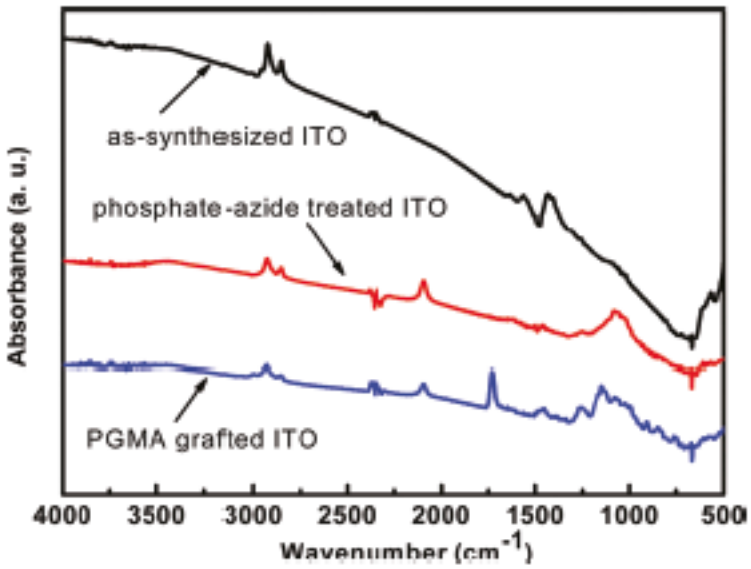


Figure 2.1: FTIR spectra of as-synthesized ITO, phosphate-azide treated ITO, and PGMA grafted ITO nanoparticles.

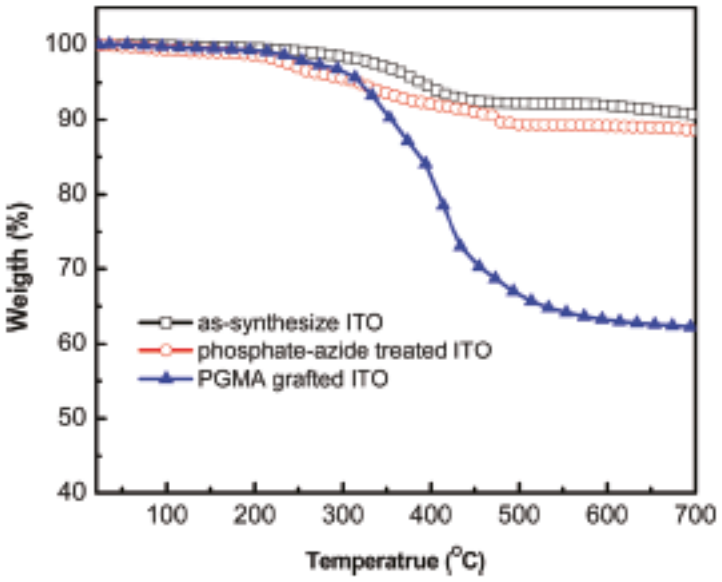


Figure 2.2: TGA curves of as-synthesized ITO nanoparticles, phosphate-azide treated ITO nanoparticles, and PGMA grafted ITO particles.

### 2.3.2 Synthesis of phosphate functionalized RAFT agents

Although the grafting-to method demonstrated the ability of phosphate based ligands to coordinate to the ITO surface, the grafting-from method can provide several advantages, including the absence of the role of steric repulsion for the attachment of high molecular weight polymers and the ability to grow dense polymer brushes. Hence, the grafting-from strategy for metal oxides requires the synthesis of a phosphate functional RAFT agent.

Several synthetic routes can be envisaged for the attachment of phosphates to commercially available carboxylic acid functionalized RAFT agents, but there are some key requirements, including (i) synthetic steps that do not degrade the dithioester group in the RAFT agent (ii) simple reactions that do not involve protection/deprotection steps as

these can affect the integrity of the RAFT agent and (iii) high yields. Given these requirements, common reactions such as DCC coupling or azide-alkyne reactions cannot be used as the P-OH bond in the phosphate tends to be involved in these reactions to give multiple unwanted side products. Phosphates are typically synthesized by reacting $POCl_3$ with R-OH, where R represents alkyl/aryl groups. In the process of this reaction phosphorochloridate intermediates are formed, but hydrolyze to the phosphate and HCl upon the addition of water.[22] In order to prevent the degradation of other reactive groups in the product, triethylamine is added to complex with the HCl. Since a hydroxyl group is needed for conversion to the phosphate, a hydroxyl functional RAFT agent is required.

One convenient method for the synthesis of hydroxyl functionalized RAFT agents is the use of a common ATRP initiator – hydroxy ethyl bromoisobutyrate. In the presence of heat and a cleaved disulfide, radical coupling complexes the tertiary bromide to form an unconventional dithioester RAFT agent (Scheme 2.2). The reaction is known as ATRAF (atom transfer radical addition-fragmentation), and results in high yields and minimal purification (alumina column to remove copper based catalysts).[23] In this case, a 98% yield was obtained. The corresponding phosphate modification of the hydroxyl group on the dithioester occurs through the reaction with $POCl_3$, and a 58% yield is obtained. The phosphate modification was also confirmed by $^{31}$P-NMR, where a singlet at 1.19 ppm was observed, as compared to a lack of signals in the hydroxyl functional dithioester starting material.

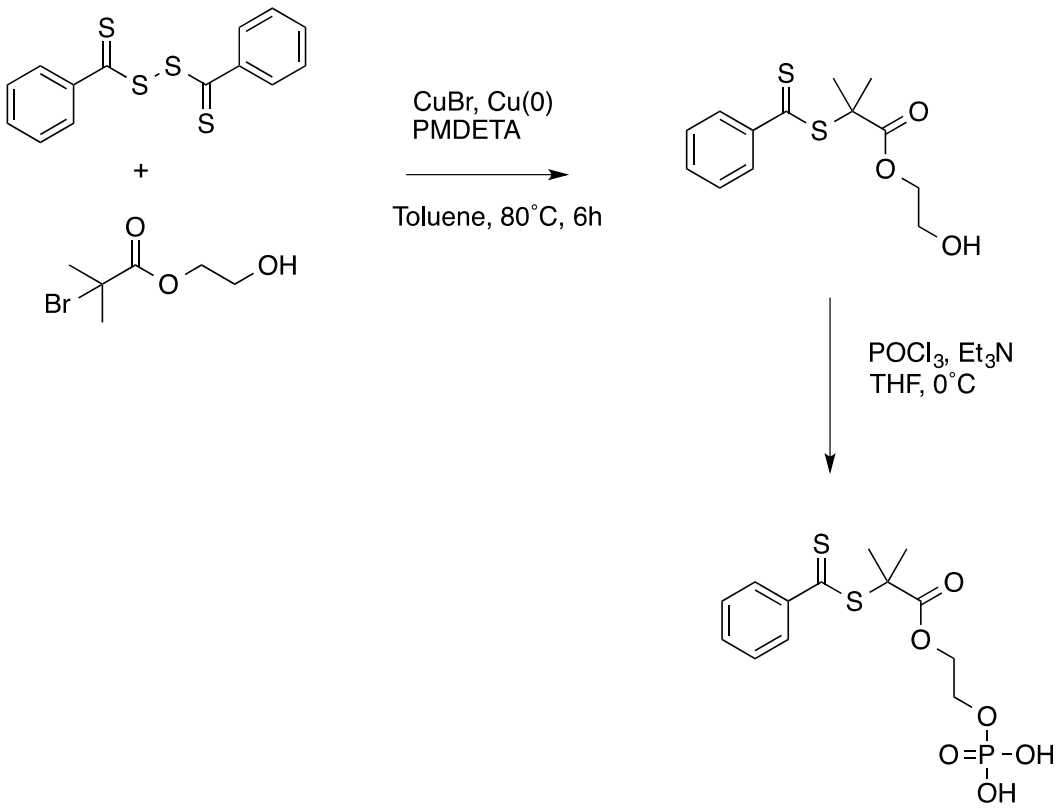


Scheme 2.2: Synthesis of the hydroxyl functional RAFT agent and its corresponding phosphate modification.

### 2.3.3 ITO functionalization with the RAFT-phosphate

ITO nanoparticles were functionalized with the RAFT-phosphate using a variety of solvents, including toluene, THF and chlorobenzene. THF served as the most effective solvent as no aggregation or degradation of the RAFT agent was observed. After functionalization, ITO particles precipitated instantly with ethanol, and were centrifuged at 20000 rpm for 5 min to remove any free RAFT agent. Repetition of this process thrice successfully removed any free RAFT agent, as was observed by the lack of the red color (characteristic of the RAFT agent) in the supernatant.

### 2.3.4 Polymerization of methyl methacrylate from ITO-RAFT

For the polymerization of methyl methacrylate (MMA) (Scheme 2.3), ITO nanoparticles with a graft density of 0.5 chains/nm$^2$ (from TGA, see Section 2.3.5) were used to obtain various molecular weights ranging from 87k to 203k (Figure 2.3). Due to the nature of the tertiary R group (two $CH_3$ units and an ester linkage), the polymerization does not have a high degree of control for methacrylates. Chong and coworkers have also employed a RAFT agent with a similar R group for the polymerization of MMA and reported polydispersities ranging from 1.89-1.5 with the corresponding lack of correlation of theoretical and actual molecular weights at low conversions.[24] Chong postulated that the R group used herein has a low transfer constant ($C_{tr}$ ~2) at 60˚C for MMA polymerization. In the current work, a linear increase of Mn with respect to monomer conversion was observed at 65˚C. Also, the polydispersity was initially very high at low conversions but gradually decreased to the range of 1.34-1.4 at higher conversions. It should be noted that conversions above 40% were unfeasible in this study due to the increasing viscosity of the mixture and gelation at high conversions. Conversions were measured gravimetrically and GPC samples were prepared by cleaving the PMMA from the nanoparticles with concentrated HCl.

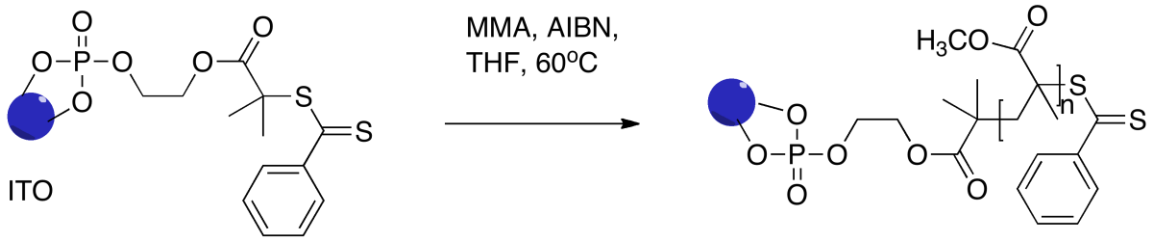


Scheme 2.3: Polymerization of MMA from ITO NPs.

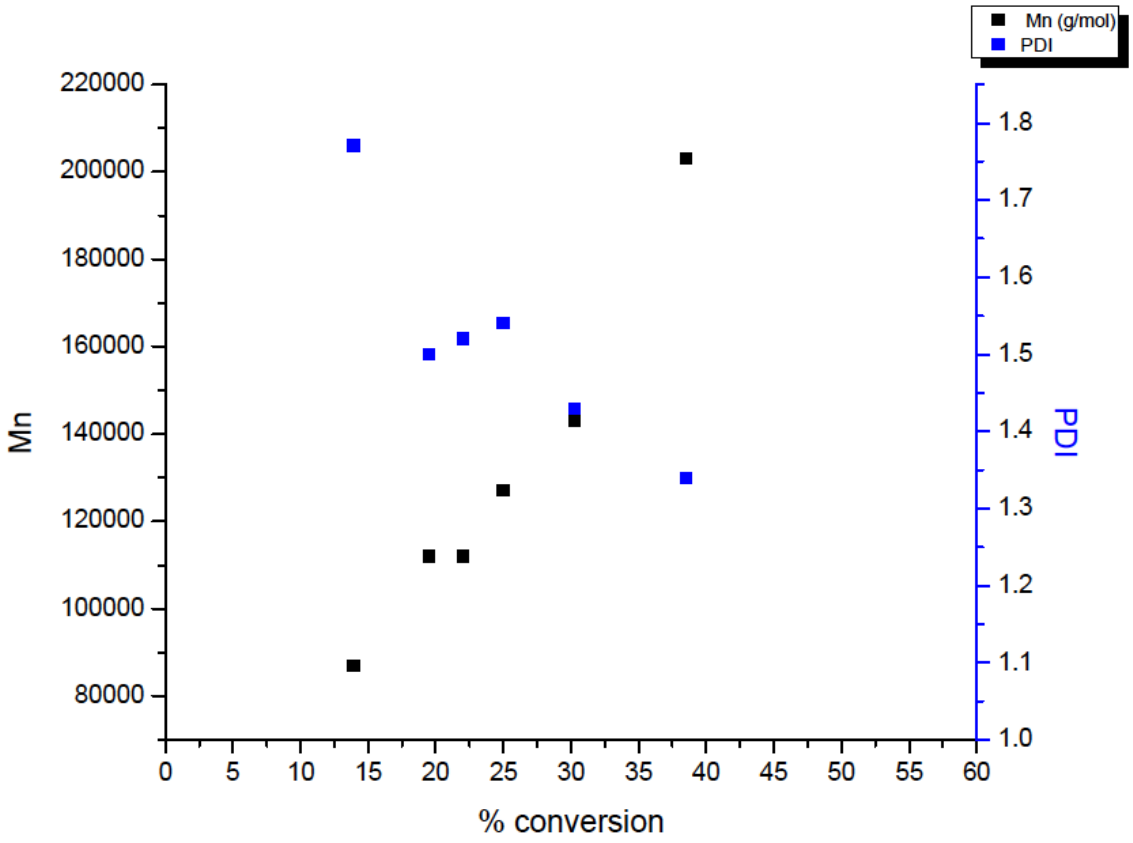


Figure 2.3: Kinetics of MMA polymerization from ITO-RAFT (0.0104g, 0.0011 mmol of RAFT content, 0.5 ch/nm$^2$), MMA (0.55g, 5.5 mmol), AIBN (0.00011 mmol) in THF (0.586 ml) at 65˚C.

### 2.3.5 FTIR and TGA Analysis

IR spectroscopy was used (Figure 2.4) to elucidate the exact nature of the bonding, i.e. whether a bi or tri-dentate form of coupling was employed in the complexation. FTIR spectra showed a peak at 1040 cm$^{-1}$ which corresponded to the P-O stretching vibrations of the bound phosphate and the P=O stretch at 1300 cm$^{-1}$. As the P=O presence on the bound ITO indicates the lack of involvement of the P=O in binding, it is more likely a mixture of the bi and tri-dentate coupling.

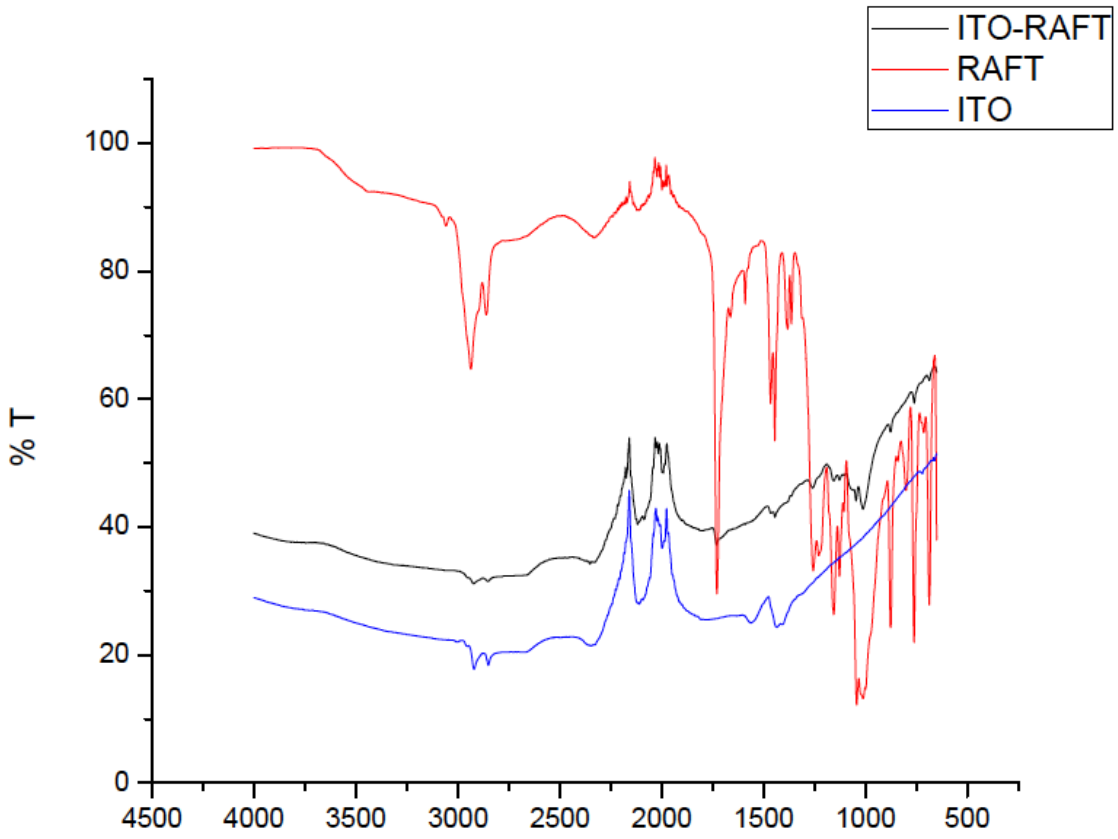


Figure 2.4: FTIR of the bare ITO (blue, bottom), free RAFT-phosphate (red, top) and RAFT functionalized ITO NPs (black, middle).

The grafting density (ch/nm$^2$) was calculated by thermal gravimetric analysis (Figure 2.5), where the amount of phosphate was calculated by subtracting the weight loss of the bare ITO from the phosphate functionalized ITO. Graft densities using this procedure gave values ranging from 0.3-0.5 ch/nm$^2$. Traditionally, graft densities of RAFT agents on other nanoparticles are usually measured by UV-vis spectroscopy, where the dithioester absorption at 298 nm can provide the concentration of the RAFT agent in a given sample of nanoparticles by means of a calibration curve. However, as the ITO absorbs heavily in the 300 nm region it was difficult to calculate the graft density

in this manner. Although the TGA is not as accurate as the UV-vis method for calculating grafting densities, an approximate reading of the graft density can be obtained by comparing the weight loss at 700˚C.

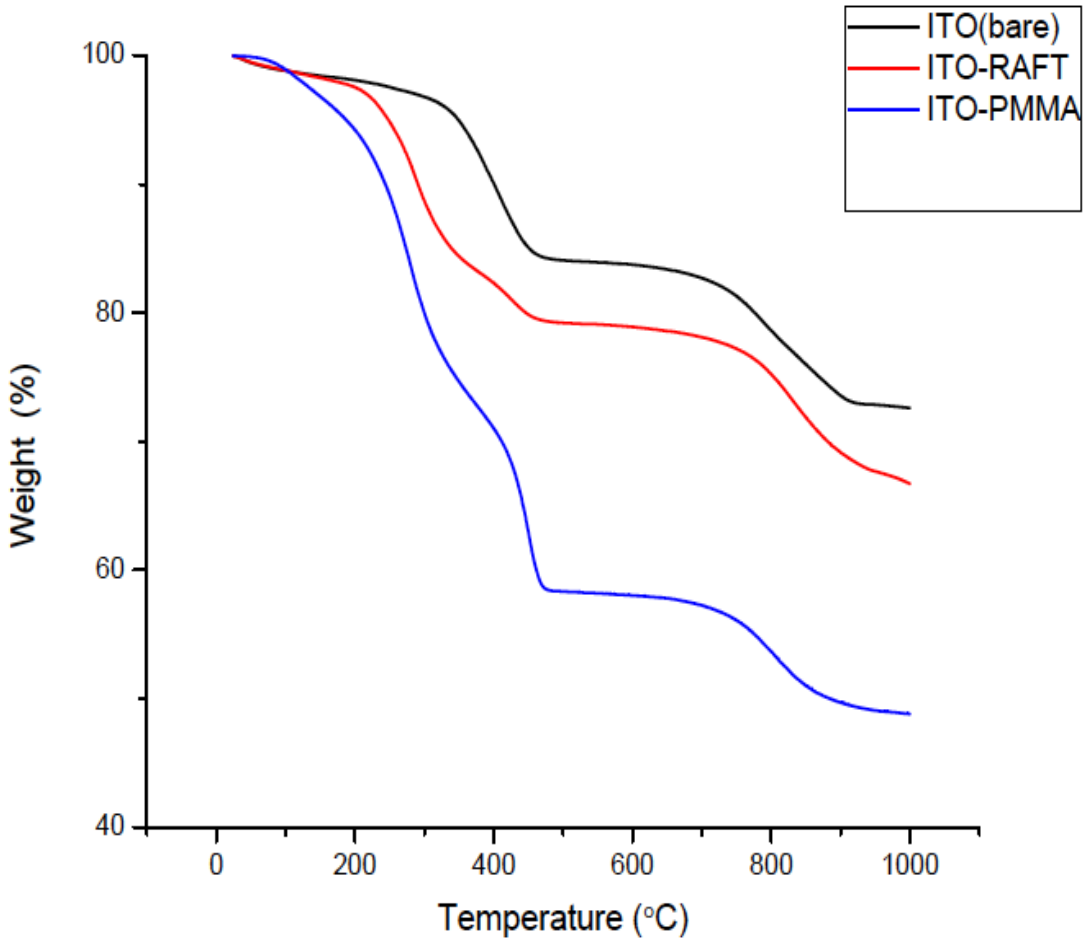


Figure 2.5: TGA curves illustrating the weight loss attributed to the attachment of the RAFT agent and the PMMA functionalized ITO.

### 2.3.6 Phosphate functionalized PDMS

To compatibilize the as-synthesized $TiO_2$ NPs in the silicone matrix, organophosphate terminated PDMS chains were grafted onto NP surfaces via a ligand exchange process (Scheme 2.4).[25] The phosphate terminated PDMS polymers were

prepared through a single step modification of commercial hydroxyl-terminated PDMS with $POCl_3$. A ten-fold excess of the $POCl_3$ was used to convert the hydroxyl groups, and the mixture was stirred for two days. The phosphate group has stronger binding capability with the metal oxide and can partially replace the original synthetic oleic acid ligands on the $TiO_2$. The successful conversion of phosphate-terminated PDMS was detected from the $^{31}P$ NMR spectrum. As shown in Figure 2.6, the large singlet at 1.57 ppm indicates that the main product was monophosphate PDMS, while smaller peaks at −8 to −12 ppm are diphosphate esters. For the smaller molecular weight PDMS (1k-10k), the conversion of the hydroxyl to the phosphate was monitored by $^{31}P$ NMR. With the larger molecular weight PDMS (>10k), this becomes difficult as the concentration of the terminal phosphate in the NMR sample decreases significantly.

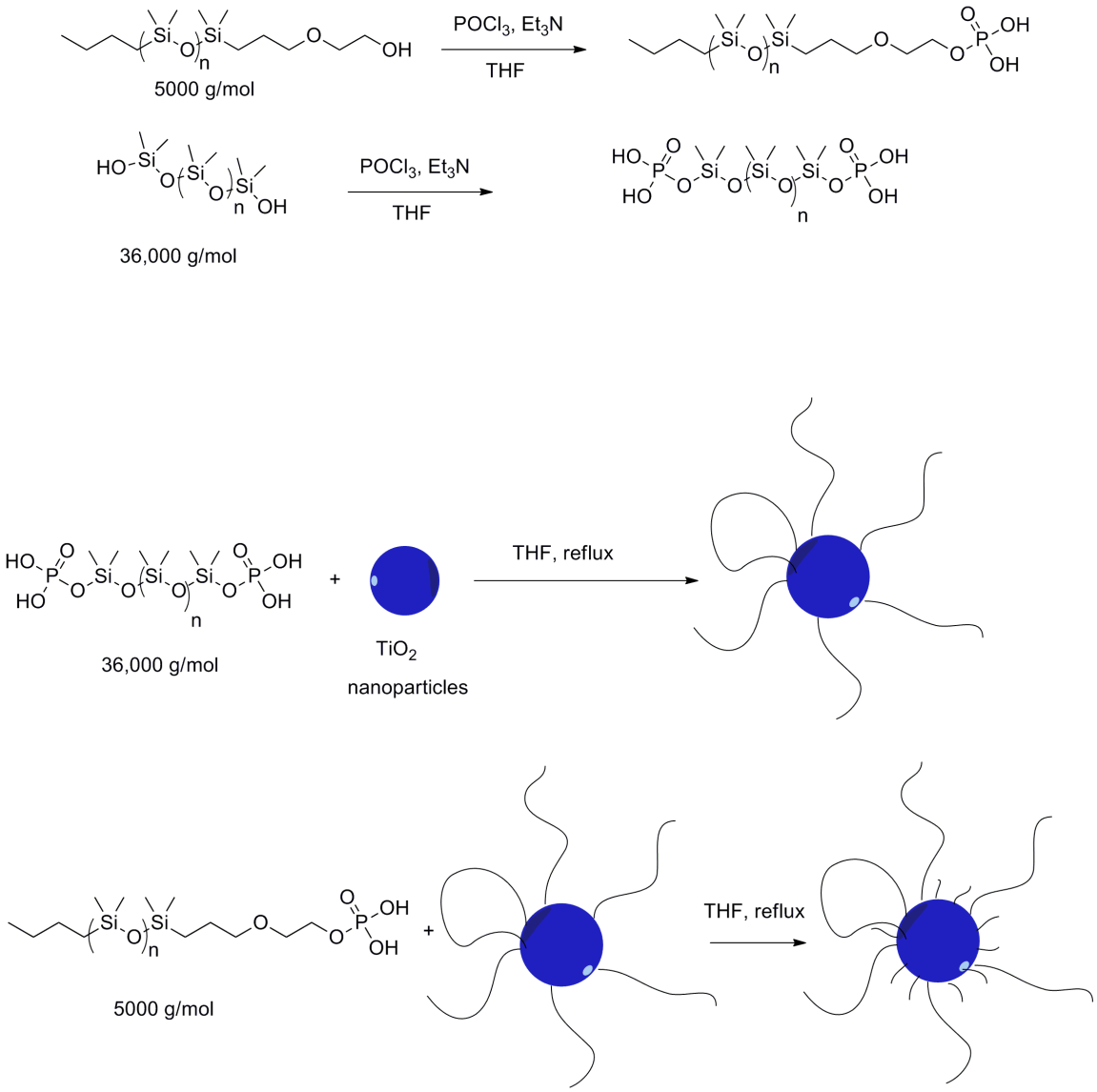


Scheme 2.4: Synthesis of monomodal and bimodal $TiO_2$-PDMS using phosphate functionalized PDMS.

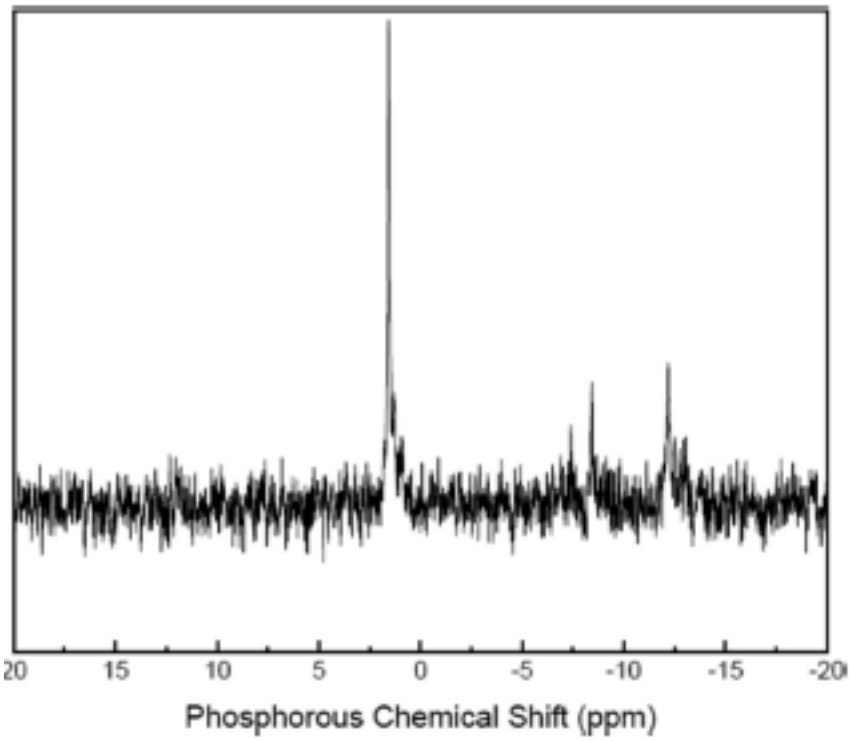


Figure 2.6: $^{31}$P NMR spectrum of phosphate modified PDMS (1000 g/mol).

### 2.3.7 Nanocomposites using ITO and $TiO_2$ NPs

The synthetic strategies for the functionalization of NPs provided an insight into the characterization tools needed for monitoring surface functionalization. However, when the polymer functionalized NPs were dispersed into the matrix, an environment of aggregation free NPs is essential for usage in the intended application. In this section, examples are shown of ITO-PGMA (grafted-to) in a commercial diglycidyl ether of bisphenol A (DGEBA) epoxy resin (Epoxy Technology, 301-1) and $TiO_2$-PDMS in 100k silicone matrix as viewed through the TEM are shown. For the PGMA grafted ITO NPs, both the low and high magnification micrographs (Figure 2.7) show that the ITO nanoparticles are homogeneously dispersed in the epoxy matrix and agglomerates are absent. Within the higher loading samples, the particles are more densely distributed. In

the case of $TiO_2$-PDMS, agglomerates are seen in the monomodal samples, and the bimodal samples display excellent dispersions (Figure 2.8). The detailed understanding behind this phenomenon was investigated and reported by Li et al.[25]

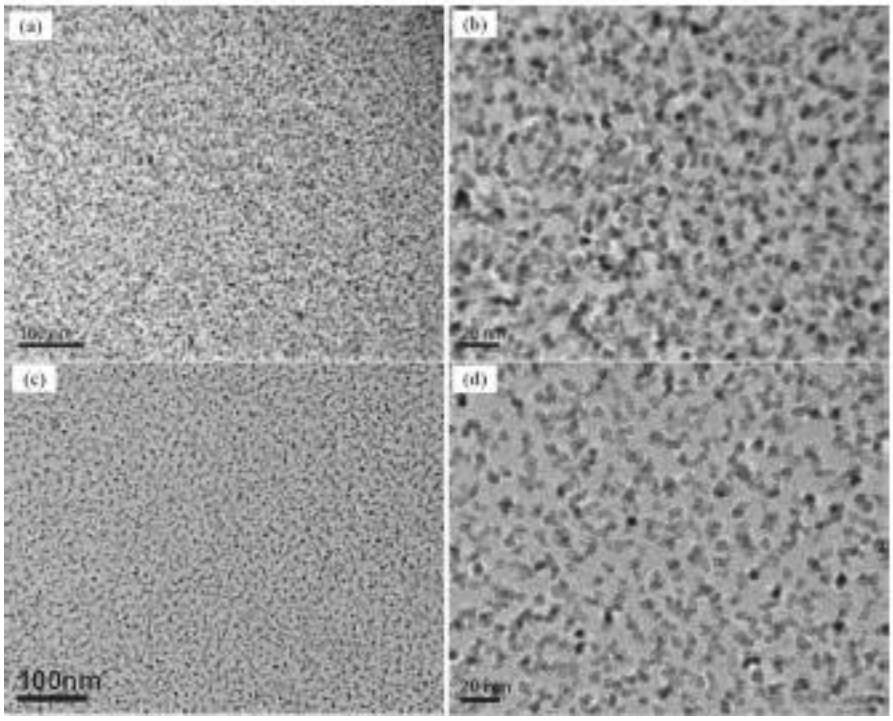


Figure 2.7: TEM image of ITO/epoxy nanocomposites with different ITO concentrations at low and high magnifications: (a, b) 35 wt %; (c, d) 20 wt %.

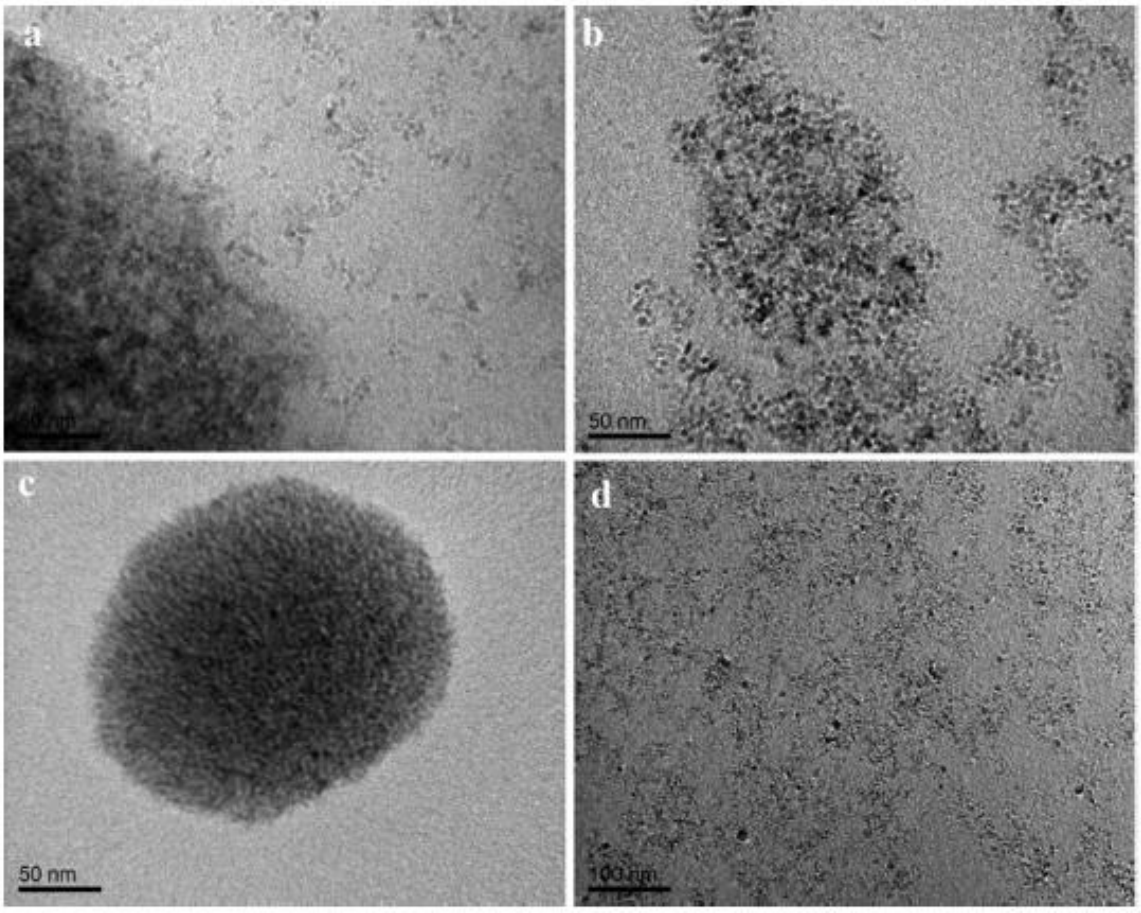


Figure 2.8: TEM images of silicone nanocomposites of 100k matrix filled with (a) 5 wt % $TiO_2$_5k NP, (b) 5 wt % $TiO_2$_10k NP, (c) 5 wt % $TiO_2$_36k NPs, and (d) 20 wt % bimodal $TiO_2$_36k_10k NPs.

## 2.4 Summary

The synthetic strategies for grafting-to and from metal oxide NPs were investigated. For effective functionalization and aggregation free nanocomposites, the choice of the ligand anchoring group is highly important. Phosphates were chosen as an appropriate ligand due to their strong binding with metal oxides. Grafting-to techniques were demonstrated on ITO NPs using an azide phosphate ligand and alkynyl poly(glycidyl methacrylate). Grafting-from was also demonstrated for the ITO system by designing a novel phosphate functional RAFT agent. Poly(methyl methacrylate) chains

were grown from the ITO surface at a grafting density of 0.5 ch/nm$^2$, and molecular weights from 87-203k with accompanying PDIs ranging from 1.77- 1.34 were obtained. In a more commercially relevant PDMS system, $TiO_2$ was modified with phosphate functional PDMS to prepare both monomodal and bimodal grafted NPs. The bimodal grafted NPs were much more successful in overcoming the strong enthalpic incompatibility of inorganic NPs than monomodal grafted chains, and were used to fabricate high volume fraction nanocomposites while maintaining optical transparencies. Overall, the synthesis and characterization tools for phosphate functional polymers and small molecules were established, which were applied to grafted NPs and their use in polymer nanocomposite applications.

## 2.5 References


(1) Hussain, F.; Hojjati, M. J.; Okamoto, M.; Gorga, R.E. *Composite Mater.* **2006**, *40*, 1511.

(2) Beecroft, L. L.; Ober, C. K. *Chem. Mater.* **1997**, *9*, 1302.

(3) Sanchez, C.; Julián, B.; Belleville, P.; Popall, M. *J. Mater. Chem.* **2005**, *15*, 3559.

(4) Schadler, L. S.; Kumar, S. K.; Benicewicz, B. C.; Lewis, S. L.; Harton, S. E. *MRS Bull.* **2011**, *32*, 335.

(5) Kumar, S. K.; Jouault, N.; Benicewicz, B.; Neely, T. *Macromolecules* **2013**, *46*, 3199.

(6) Tao, P.; Viswanath, A.; Li, Y.; Rungta, A.; Benicewicz, B. C.; Siegel, R. W.; Schadler, L. S. *MRS Proc.* **2011**, *1359*, 11.

(7) Kim, H.; Miura, Y.; Macosko, C. W. *Chem. Mater.* **2010**, *22*, 3441.

(8) Wang, H.; Zeng, C.; Elkovitch, M.; Lee, L. J.; Koelling, K. W. *Polym. Eng. Sci.* **2001**, *41*, 2036.

(9) Sen, S.; Xie, Y.; Bansal, A.; Yang, H.; Cho, K.; Schadler, L. S.; Kumar, S. K. *Eur. Phys. J. Spec. Top.* **2007**, *141*, 161.

(10) Jordan, J.; Jacob, K. I.; Tannenbaum, R.; Sharaf, M. A.; Jasiuk, I. *Mater. Sci. Eng. A* **2005**, *393*, 1.

(11) Liu, J.; Gao, Y.; Cao, D.; Zhang, L.; Guo, Z. *Langmuir* **2011**, *27*, 7926.

(12) Tao, P. Epoxy and Silicone Optical Nanocomposites Filled with Grafted Nanoparticles. Ph.D. Thesis, Rensselaer Polytechnic Institute, **2012**.

(13) Rungta, A.; Natarajan, B.; Neely, T.; Dukes, D.; Schadler, L. S.; Benicewicz, B. C. *Macromolecules* **2012**, *45*, 9303.

(14) Akcora, P.; Liu, H.; Kumar, S. K.; Moll, J.; Li, Y.; Benicewicz, B. C.; Schadler, L. S.; Acehan, D.; Panagiotopoulos, A. Z.; Pryamitsyn, V.; Ganesan, V.; Ilavsky, J.; Thiyagarajan, P.; Colby, R. H.; Douglas, J. F. *Nat. Mater.* **2009**, *8*, 354.

(15) Kuang, Q.; Wang, X.; Jiang, Z.; Xie, Z.; Zheng, L. *Acc. Chem. Res.* **2014**, *47*, 308.

(16) Mutin, P. H.; Guerrero, G.; Vioux, A. *J. Mater. Chem.* **2005**, *15*, 3761.

(17) Guerrero, G.; Mutin, P. H.; Vioux, A. *Chem. Mater.* **2001**, *13*, 4367.

(18) Queffélec, C.; Petit, M.; Janvier, P.; Knight, D. A.; Bujoli, B. *Chem. Rev.* **2012**, *112*, 3777.

(19) Li, Y.; Benicewicz, B. C. *Macromolecules* **2008**, *41*, 7986.

(20) Vosloo, J. J.; De Wet-Roos, D.; Tonge, M. P.; Sanderson, R. D. *Macromolecules* **2002**, *35*, 4894.

(21) Tao, P.; Viswanath, A.; Schadler, L. S.; Benicewicz, B. C.; Siegel, R. W. *ACS Appl. Mater. Interfaces* **2011**, *3*, 3638.

(22) Rudnick, L. R. *Lubricant Additives: Chemistry and Applications, Second Edition*; CRC Press, 2009; p. 790.

(23) Kwak, Y.; Nicolay, R.; Matyjaszewski, K. *Macromolecules* **2009**, *42*, 3738.

(24) Chong, ) Y. K.; Krstina, J.; Le, T. P. T.; Moad, G.; Postma, A.; Rizzardo, E.; Thang, S. H. *Macromolecules* **2003**, *36*, 2256.

(25) Li, Y.; Tao, P.; Viswanath, A.; Benicewicz, B. C.; Schadler, L. S. *Langmuir* **2013**, *29*, 1211.

# CHAPTER 3

## COPOLYMERIZATION AND SYNTHESIS OF MULTIPLY BINDING HISTAMINE LIGANDS FOR THE ROBUST FUNCTIONALIZATION OF QUANTUM DOTS

### 3.1. Introduction

In the past decade, considerable progress has been seen in applications of semiconductor nanocrystals (quantum dots) in areas such as light emitting diodes,[1] solar cells,[2] and bioimaging applications.[3,4] Based on the size and choice of material, the emission and absorption wavelengths of quantum dots can be tuned, allowing for narrow emission bands and high quantum yields.[5,6] The right choice of surface functional groups prevents aggregation of the quantum dots, allows for good dispersions in its environment, passivates the quantum dot surface (QD) and maintains high fluorescence quantum yield [7]. This in turn allows for its successful implementation in various high performance applications.

Hence, the need for soft functional materials that allow for quantum dots to be well dispersed in a variety of environments and facilitate stability over extended periods of time is essential. In the case of well-represented II-VI, III-V, and IV-VI compound semiconductors, colloidal quantum dots are synthesized with hydrophobic ligands such as oleic acid and trioctylphosphine; these ligands are necessary to manage precursor reactivity and colloidal stability during high-temperature growth, but lead to QDs with

low solubility in polar solvents.[7] Encapsulation with surfactants, silica shells or amphiphilic copolymers can yield stable and water-soluble QDs but adds considerably to hydrodynamic diameter.[8–10] Ligand exchange with polar molecules bearing nucleophilic anchoring groups such as thiols and amines are known to be good binders to metal chalcogenide surfaces and have shown some success in the final dispersion of quantum dots in polar solvents.[11] However, due to the limited solution stability of QDs with monodentate ligands in water,[12] several groups have explored the possibility of using polymeric ligands instead.[3,4,13] CdSe/ZnS core shell quantum dots have been ligand exchanged with polymers including poly(N,N-dimethylaminoacetyl methacrylate)[7], which presents pendant tertiary amine nucleophiles for coordination to the quantum dot surface . Another class of polymeric ligands for quantum dot functionalization include imidazole functionalized polymers, which have shown superior binding capabilities and maintenance of high quantum yields when bound to QDs.[4,14] The advantage of polymeric ligands is that they offer a tunable and scalable multiply binding system, which has shown to substantially improve the dispersion qualities of quantum dots in various environments and can provide a variety of external functional handles for subsequent derivatization.[4,15–18]

One of the challenges in designing polymeric ligands is the versatility and scalability of the complete synthetic scheme. Specifically, the factors that need to be taken into consideration include the design of polymers with multiple functionalities, versatile reaction schemes, and facile repeatability and ease in scalability. Typically, the most common source of imidazole based polymers is through the vinylimidazole monomer. However, it is difficult to perform the controlled radical polymerizations

(CRP) with vinylimidazole, and especially in conjunction with other comonomers when the radical stabilities of vinyl imidazole and other comonomers are vastly different.[19] Allen et al. have used an innovative synthetic approach to polymerize 4-vinyl imidazole through reversible-addition-fragmentation-chain transfer (RAFT) in glacial acetic acid with a high degree of control.[20] The literature on synthetic strategies for water soluble imidazole based polymers is further limited, mainly due to the difficulty in complexing histamine salts to monomers. Block copolymers with styrene and styrenic/methacrylate based imidazoles have also been described in the literature for ionic liquids, including work by Mahanthappa[21] and Segalman[22]. While such copolymers are useful in microphase separation, the presence of styrene units hinders their water solubility. In a deviation from amphiphilic block copolymers for ionic liquids, Vijayakrishna and coworkers developed a double hydrophilic copolymer with an ethylimidazolium based monomer and acrylamide using RAFT for water soluble ionic liquids.[23] The first example of imidazole based water soluble copolymers for attachment to quantum dots was provided by Liu and coworkers where they prepared copolymer ligands through a boc-protected histamine based monomer via RAFT polymerization.[3]Histamine based monomers require several synthetic steps, including protection of the imidazole amine for successful RAFT polymerization and the corresponding deprotection to access the imidazole for quantum dot attachment. Alternative strategies for obtaining imidazole bearing copolymers include a ring-opening of poly(maleic anhydride) with a mixture of histamine and an amine terminated PEG oligomer and the modification of poly(acrylic acid) with 3-aminopropyl imidazole. However, these methods offer no ability to control the placement of the copolymer residues along the chain, and the former example leaves

residual carboxylic acid side groups that can influence the overall charge of the ligand exchanged QDs. In a different approach, we report the RAFT synthesis of copolymers bearing activated esters and PEGMA units with an ability to intricately tailor the location of monomers along the polymer chain. The activated esters react quantitatively with histamine in a simple postmodification reaction to obtain water soluble multidentate histamine bearing copolymers.

The use of activated ester groups in end group modification has been widely documented, but activated ester monomers have recently become popular due to their ease of polymerization in conjunction with other monomers. Several types of activated ester monomers exist, including pentafluorophenyl[24], vinylbenzoic[25], vinylsulfonic[26] and succinimide[27] based esters. Typically, the postmodification of such polymers results in high yields, decreased side reactions and mild reaction conditions. Tew and coworkers have reported on the polymerization of N-methacryloxysuccinimide (NMS) with ATRP showing the capability to make statistical and block copolymers.[27] Wooley et al. have utilized N-acryloxy succinimide (NAS) in copolymers using NMP for biological applications.[28] The succinimide ester has also been attached to a vinyl benzoate group for the RAFT polymerization of a styrenic derivative.[26] Yanjarappa and coworkers have synthesized NMS copolymers with N-isopropylacrylamide (NIPAM) using RAFT, and have used it for modifications with peptides.[29]

Herein, we have described a simple approach for the preparation of histamine functional copolymers, and included an analysis of the kinetics of activated ester copolymerization. We have attempted to find the most convenient method for multidentate histamine copolymers, and in doing so we have identified the synthetic

method as a copolymerization of NMS and poly(ethyleneglycol) methacrylate (PEGMA), and its corresponding postmodification. These novel pseudo-gradient copolymers combine water solubility and robust attachment to QDs to provide narrow size distributions and good quantum yields. We have also explored the effect of polymer length and monomer composition on its complexation to quantum dots and display the utility of these copolymer functional materials through excellent dispersions in protic environments.

## 3.2 Experimental

### 3.2.1 Materials

All reagents were used as received from Fisher Scientific unless stated otherwise below. AIBN was purchased from Sigma Aldrich and recrystallized thrice from methanol. Poly(ethyleneglycol) methacrylate (500g/mol and 950g/mol) were obtained from Sigma Aldrich and passed through a neutral alumina column to remove inhibitors before use. 4-Cyano-4 [(dodecylsulfanylthiocarbonyl)sulfanyl]pentanoic acid was obtained from Strem Chemicals, Inc. NMS was synthesized from NHS (N-hydroxy succinimide) as described in the literature.[30]

### 3.2.2 Characterization

NMR spectra were recorded on a Varian Mercury 300 spectrometer using $CDCl_3$ or $D_2O$ as the solvent. UV-vis absorption spectra were recorded on a Perkin Elmer Lambda 4C spectrophotometer. The molecular weights and molecular weight distributions were determined using a Waters gel-permeation chromatograph equipped

with a 515 HPLC pump, a 2410 refractive index detector, three Styragel columns (HR1, HR3, HR4 in the effective molecular weight range of 100−5000, 500−30000, and 5000−500000, respectively) . Tetrahydrofuran (THF) was used as the eluent at 30°C and a flow rate of 1.0 mL/min. The GPC system was calibrated with polystyrene standards obtained from Polymer Laboratories. The detailed procedures and characterization tools used for quantum dot synthesis and analysis are discussed in detail in a separate publication.

### 3.2.3 Preparation of Poly(PEGMA-co-NMS)

In a typical copolymerization, 4-cyano-4-(dodecylsulfanylthiocarbonyl)sulfanylpentanoic acid (CDTPA) (0.0246 mmol, 0.01g), NMS (0.492 mmol, 0.0452g), PEGMA (500 g/mol, 0.246 mmol, 0.123g), trioxane (10 mg) and AIBN (0.00246 mmol, 0.004g) were dissolved in 0.246 mL of DMF. The mixture was stirred until all the reactants were dissolved, placed in a Schlenk tube and subjected to three cycles of freeze-pump-thaw. The tube was then heated at in an oil bath at 68°C for 9h. The polymerization was quenched in ice water and the mixture precipitated in ether. The mixture was centrifuged at 3000 rpm for 5 min and redispersed in 3 mL of THF. This precipitation-redispersion process was repeated twice to obtain Poly(PEGMA-co-NMS) with Mn: 10681, PDI: 1.24.

### 3.2.4 Preparation of Poly(PEG-co-imidazole)

The Poly(PEG-co-NMS) (Mn: 30,600 PDI: 1.51, 1.5 g, 3.716 mmol of NMS) was dissolved in 15 mL DMSO in a 100 mL two neck RB flask , followed by the addition of

histamine dihydrochloride (8.15 mmol, 1.5 g). The mixture was stirred for 30 min until the histamine dihydrochloride completely dissolved. The mixture was sparged with $N_2$ for 15 min, and the triethylamine (20.38 mmol, 2.84 mL) added under $N_2$. The mixture was sparged again for 20 min, and then heated at 70°C for 24 h. The reaction was cooled and the product separated through dialysis in water for 48 h. The polymer in the membrane was further purified by freeze-drying to remove excess water. $^1$H-NMR analysis illustrated that the functionalization with histamine was nearly quantitative (>96%).

### 3.2.5 Boc protection of Poly(PEG-co-imidazole)

Poly(PEGMA-co-imidazole) (Mn: 30,674, PDI: 1.35, 4.94 mmol histamine content, 1 g), was dissolved in 7 mL dichloromethane in a RB flask, followed with the addition of triethylamine (4.49 mmol, 0.313 mL). $Boc_2O$ (4.94 mmol, 0.539g) was dissolved in 3 mL DCM and added dropwise at 0˚C. The mixture was stirred overnight at 20˚C. 10 mL of $H_2O$ was added and the product was extracted into the organic layer, dried with sodium sulfate and the solvent evaporated under vacuum. The polymer was analyzed by NMR and GPC to obtain Boc protected Poly(PEGMA-co-imidazole) with Mn: 36101, PDI: 1.35.

### 3.2.6 RAFT agent removal

Poly(PEG-co-NMS) (Mn: 12,157 PDI: 1.11, 8.22 mmol RAFT, 0.1 g) was dissolved in 3 mL of THF in a RB flask, and AIBN (0.0822 mmol, 0.013 g) was added to the solution. It was then heated to 64˚C for 3 h, and then precipitated in hexanes,

centrifuged at 3000 rpm for 5 min, and then redispersed in 3 mL of THF. This precipitation-redispersion process was repeated twice to obtain a white polymer and was directly used for UV analysis.

**3.2.6 Quantum Dot Synthesis and ligand exchange** Procedures for quantum dot synthesis, purification and ligand exchange, as well as a detailed analysis of the characterization were performed by members of the Greytak research lab.

### 3.3 Results and Discussion

The homopolymerization of monomers with NHS groups via CRP has been documented in the literature extensively, with good control under mild reaction conditions. Copolymers with other monomers have also been explored, where the choice of monomer is dependent upon its reactivity ratio with NMS and the solvent conditions. Tew and coworkers have investigated the copolymerization of NMS with styrene, methyl methacrylate (MMA) and PEGMA using ATRP.[27] Alternatively, NHS based carbonates have also been introduced on the end of longer alkyl chain methacrylates and copolymerized with MMA and PEGMA.[31] N-acryloxy succinimide (NAS) and acrylamides with alkyl linkers bearing succinimide groups have been copolymerized with MMA to develop polyurethanes with soft segments.[32] For polymers incorporating organic/nonpolar side groups, PEG functional groups have been widely used to improve the water solubility for applications in the biomedicine. Fukukawa et al. have utilized a PEG based NMP initiator to polymerize NAS and DMA for core shell star copolymers for biodistribution studies.[28] NMS has also been incorporated through RAFT to make

terpolymers for similar biodistribution and imaging studies.[28] In all these cases, the succinimide group has been used for postmodification reactions to attach new functionalities to the polymer. Using a similar approach, this work demonstrates a facile synthetic strategy for the preparation of water soluble polymers and their modification with multidentate histamine ligands that can efficiently coordinate to quantum dot materials.

### 3.3.1 Copolymerization of NMS and PEGMA

For the copolymerization of NMS and PEGMA (Scheme 3.1), initially 4-cyanopentanoic acid dithiobenzoate (CPDB) was used as the RAFT chain transfer agent (Table 3.1). However, the initially pink RAFT agent suffered from a loss of color through the polymerization, suggesting the degradation of the RAFT agent as the polymerization progressed. At temperatures higher than 80°C, significant degradation was seen where the RAFT agent turned brown in color. Other RAFT agents were then investigated in order to elucidate its effects on the polymerization system. It was found that 4-cyano-4 [(dodecylsulfanylthiocarbonyl)sulfanyl]pentanoic acid (CDTPA) was a better RAFT agent for this polymerization, as no degradation of the RAFT agent was observed, with the polymer retaining the yellow color inherent to the trithiocarbonate. With lower temperatures and 0.1 eq of AIBN, lower PDIs were observed which showed controlled/living characteristics in the polymerization. Additionally, by increasing the equivalence of AIBN from 0.1 to 0.25, a large increase in the PDI was observed, which is expected when higher concentrations of radical species decrease the level of control in the polymerization. A variety of molecular weights were obtained ranging from 6.9k to

25.9k by tuning the ratio of NMS:PEG to the RAFT agent. Correspondingly, the composition of the polymer could also be altered by controlling the monomer ratios. Such a high degree of tunability is essential for applications that require specific compositions for optimal performance.

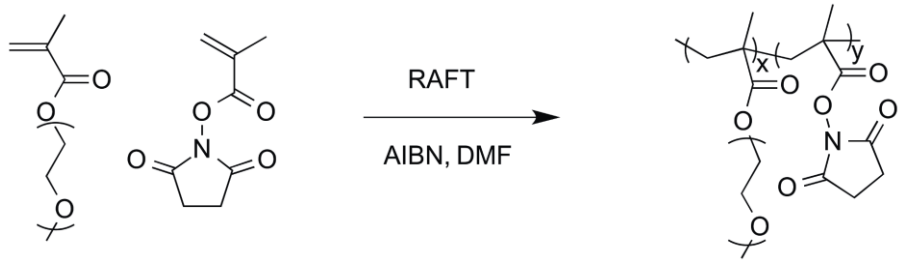


Scheme 3.1: Preparation of copolymers of NMS and PEGMA using RAFT polymerization. Copolymerizations performed in this study ranged from 65-80˚C.

Table 3.1: Summary of synthetic parameters for the RAFT copolymerizations of NMS and PEGMA with different ratios of monomers and RAFT agents in DMF. a: Polydispersity (GPC).

| Entry | RAFT agent | Ratio of NMS:PEG | Temp (˚C) | AIBN (eq) | Time (h) | PEG (%conv) | NMS (%conv) | Mn (theoretical) | Mn (GPC) | Đ[a] |
|---|---|---|---|---|---|---|---|---|---|---|
| 1 | CDTPA | 10:5 | 65 | 0.1 | 16 | 89 | 95 | 6370 | 10390 | 1.3 |
| 2 | CDTPA | 5:2.5 | 65 | 0.1 | 8 | 43 | 61.3 | 2000 | 6925 | 1.1 |
| 3 | CPDB | 20:20 | 70 | 0.1 | 17.25 | 93.76 | 91.25 | 21440 | 18580 | 1.1 |
| 4 | CPDB | 50:50 | 70 | 0.25 | 22.15 | 88.5 | 98.2 | 31400 | 38890 | 1.46 |
| 5 | CDTPA | 50:50 | 70 | 0.25 | 9.71 | 69.93 | 89.25 | 25930 | 27420 | 1.48 |

In order to measure conversion via $^{1}$H-NMR, trioxane (5.12 ppm) was used as an internal standard to compare with the PEGMA vinyl peaks at 5.85 and 6.40 ppm and the NMS vinyl peaks at 5.54 ad 6.10 ppm at various time periods. Overall, the kinetic plot of copolymerization between NMS and PEGMA (500 g/mol) with CDTPA at 80˚C is shown

in Figure 3.1, and a linear relationship is displayed between molecular weight and conversion. The polydispersity also decreases from 1.5 to 1.34 through the polymerization, showing that the polymerization occurs in a controlled manner. Copolymers ranging from 28k to 10k were obtained in this study when a ratio of 50:50:1:0.15 of NMS:PEGMA:RAFT:AIBN was used (Table 3.2). The experimental Mn (GPC) also closely relates to the theoretical Mn (NMR), although at low conversions significant deviations are seen. It must be noted that the polystyrene calibration standards used for the GPC may not display the expected Mn due to the vast difference in polymer properties (GPC curves are shown in Figure 3.2). From the Ln(Mo)/(Mt) curve, a linear relationship is also observed with time, albeit with inhibition in the polymerization initially.

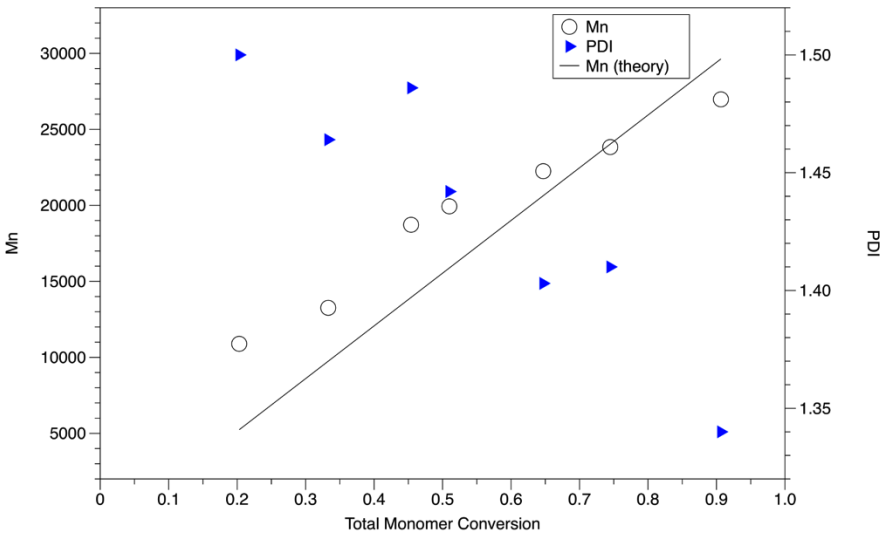

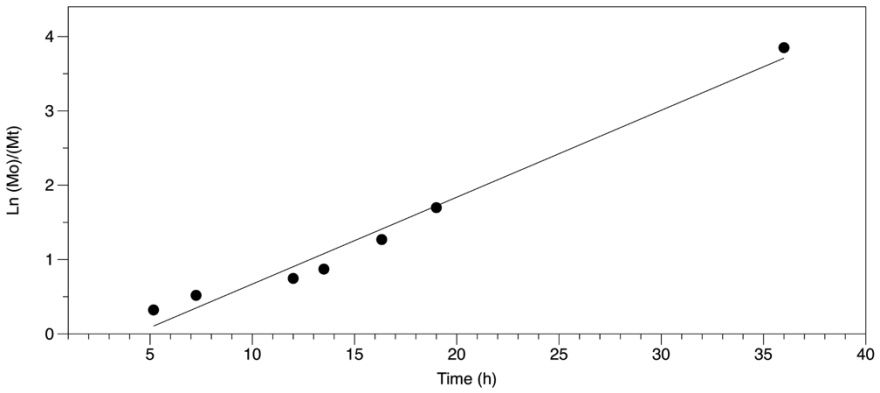


Figure 3.1: Kinetics for the RAFT polymerization of PEGMA and NMS with a monomer ratio of 50:50 using chain transfer agent CDTPA and AIBN with a ratio of 1:0.2 in DMF at 80˚C. (Top) evolution of Mn and PDI with total monomer conversion and (Bottom) semilogarithmic plot versus time.

Table 3.2: Synthetic parameters for the copolymerization of NMS and PEGMA with 0.15 eq of AIBN at 80°C in DMF.

| | Conversion (%) | | | | | Copolymer Composition (%) | |
|---|---|---|---|---|---|---|---|
| Time (h) | PEG | NMS | Mn (theoretical)[a] | Mn (GPC) | PDI | PEG | NMS |
| 5.17 | 0.15 | 0.26 | 15070 | 10890 | 1.50 | 0.37 | 0.63 |
| 7.25 | 0.23 | 0.43 | 14660 | 13260 | 1.46 | 0.35 | 0.65 |
| 12.00 | 0.31 | 0.60 | 14540 | 18725 | 1.49 | 0.34 | 0.66 |
| 13.50 | 0.37 | 0.65 | 14890 | 19940 | 1.44 | 0.36 | 0.64 |
| 16.33 | 0.53 | 0.76 | 15650 | 22250 | 1.40 | 0.41 | 0.59 |
| 19.00 | 0.68 | 0.81 | 16410 | 23840 | 1.41 | 0.46 | 0.54 |
| 36.00 | 0.85 | 0.96 | 16615 | 26975 | 1.34 | 0.47 | 0.53 |

[a] Mn theoretical = $\{[NMS]_0/[RAFT]_0 \times 183 \times Conv_{NMS}\} + \{[PEGMA]_0/[RAFT]_0 \times 500 \times Conv_{PEGMA}\}$

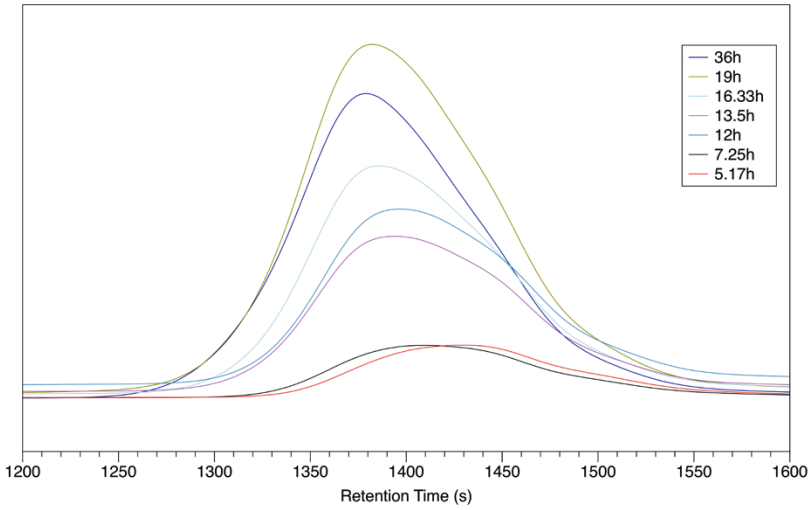


Figure 3.2: THF GPC curves illustrating the evolution of molecular weight with retention polymerization time.

### 3.3.2 Reactivity Ratios

Although an equal ratio of monomers was used, the rate of incorporation was significantly different as shown by $^{1}$H-NMR analysis. The analysis of the reactivity ratios of other monomers with NMS has been limited in the literature. Using automatic continuous online monitoring of polymerization reactions (ACOMP), Tew and coworkers determined NMS and MMA to have ratios of 0.52 and 1.35 respectively.[33] However, the reactivity ratio trend between NMS and methacrylamides is the opposite, with NMS and N-(2-hydroxypropyl)methacrylamide having ratios of 3.46 and 0.12 respectively.[29] When acrylamides are used, semi-batch methods with a separate addition of NMS are done to ensure sufficient incorporation of the acrylamide. In the case of NMS and PEGMA, the reactivity ratios study was conducted in the absence of RAFT, using a 500 g/mol PEGMA, with low conversions (<16%) of polymer and varying monomer concentrations for analysis by the Kelen-Tudos method. Table 3.3 shows the conversion data for the NMS and PEGMA copolymerization. Table 3.4 shows the mol fraction of the monomer

feed ratios used (X) and correlates the conversion data in the copolymer from Table 3.3 to obtain the functions of the Kelen-Tudos method (ξ and η).

The reactivity ratio of NMS is higher than PEGMA, where the ratios were experimentally estimated by the Kelen-Tudos method to be 0.91 for NMS and 0.69 for PEGMA (Figure 3.3). This trend is different from the MMA copolymerization, and several reactions using different RAFT agents, PEGMA lengths and monomer ratios all show the general trend that NMS is consumed at a faster rate than PEGMA. It can be postulated that the length of the PEG side chain can decrease the diffusion rate of the PEGMA towards the growing polymer chain end as compared to NMS, and hence leads to the increased consumption of NMS.

Table 3.3: Table showing the conversion and mol fraction data for NMS and PEGMA copolymers with varying monomer ratios.

| | conv PEGMA | conv NMS | mmol of PEGMA in polymer | mmol of NMS in polymer | mol fraction of NMS in polymer |
|---|---|---|---|---|---|
| 1 | 0.033 | 0.111 | 0.004 | 0.012 | 0.770 |
| 2 | 0.147 | 0.165 | 0.024 | 0.009 | 0.272 |
| 3 | 0.034 | 0.021 | 0.002 | 0.003 | 0.649 |
| 4 | 0.059 | 0.0499 | 0.008 | 0.004 | 0.336 |
| 5 | 0.115 | 0.143 | 0.0094 | 0.019 | 0.675 |

Table 3.4: Kelen-Tudos measurements for NMS and PEGMA copolymers utilizing the mol fraction data from Table 2.3. X=(Mol fraction of NMS in feed/Mol fraction of PEGMA in feed), Y= [Mol fraction of NMS in feed/(1- Mol fraction of NMS in feed)], F=X2/Y, G=X (Y-1/Y); ξ =F/a+F; η =G/a+F and a=[FM • Fm ]1/2

| | X | Y | F | G | ξ | η |
|---|---|---|---|---|---|---|
| 1 | 1 | 0.770 | 1.297 | -0.297 | 1.849 | 1.171 |
| 2 | 0.33 | 0.272 | 0.399 | -0.882 | 0.570 | 0.0246 |
| 3 | 3 | 0.649 | 13.857 | -1.619 | 19.754 | 13.168 |
| 4 | 0.6 | 0.337 | 1.070 | -1.183 | 1.525 | 0.566 |
| 5 | 1.67 | 0.675 | 4.134 | -0.806 | 5.893 | 3.791 |

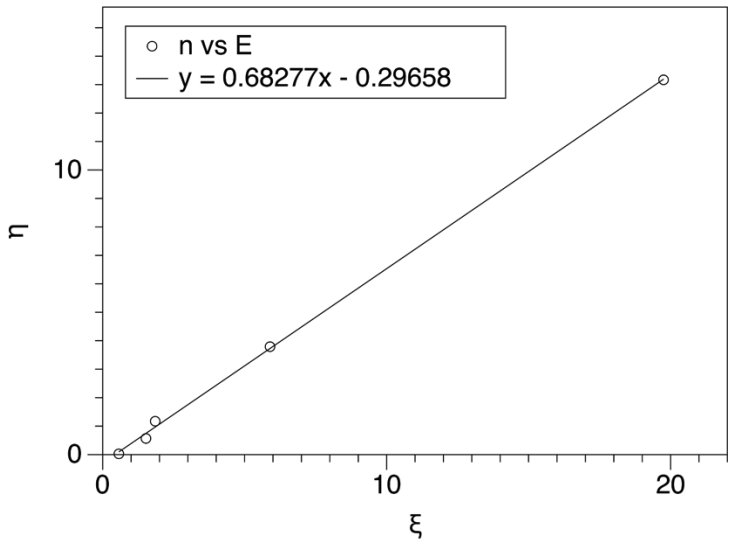


Figure 3.3: Kelen Tudos plot for low conversion poly(NMS-co-PEGMA), where $r_{NMS}$ = 0.91 and $r_{PEGMA}$ = 0.69.

Figure 3.4 illustrates conversion of the two monomers, with the initial conversion of NMS:PEG being 0.26:0.15, and the general increase in the consumption of NMS until it reaches 0.96 and PEGMA reaches 0.85. The result is more apparent in Figure 3.4

(bottom) which shows the copolymer composition throughout the polymerization. In the case of NMS, composition ranges from 0.63 to 0.53, while PEG ranges from 0.37 to 0.47. The composition of NMS decreases after 12h due to lower concentrations of NMS in solution, thus allowing for the incorporation of PEGMA. At the end of the polymerization, the composition is similar, but these results show that the composition can be intricately tuned by (i) varying the monomer ratios and (ii) stopping the reaction at different time periods. Furthermore, a pseudo-gradient copolymer is formed where the majority of the initial units include NMS, followed by the gradual inclusion of PEGMA and a tail richer in PEGMA moieties.

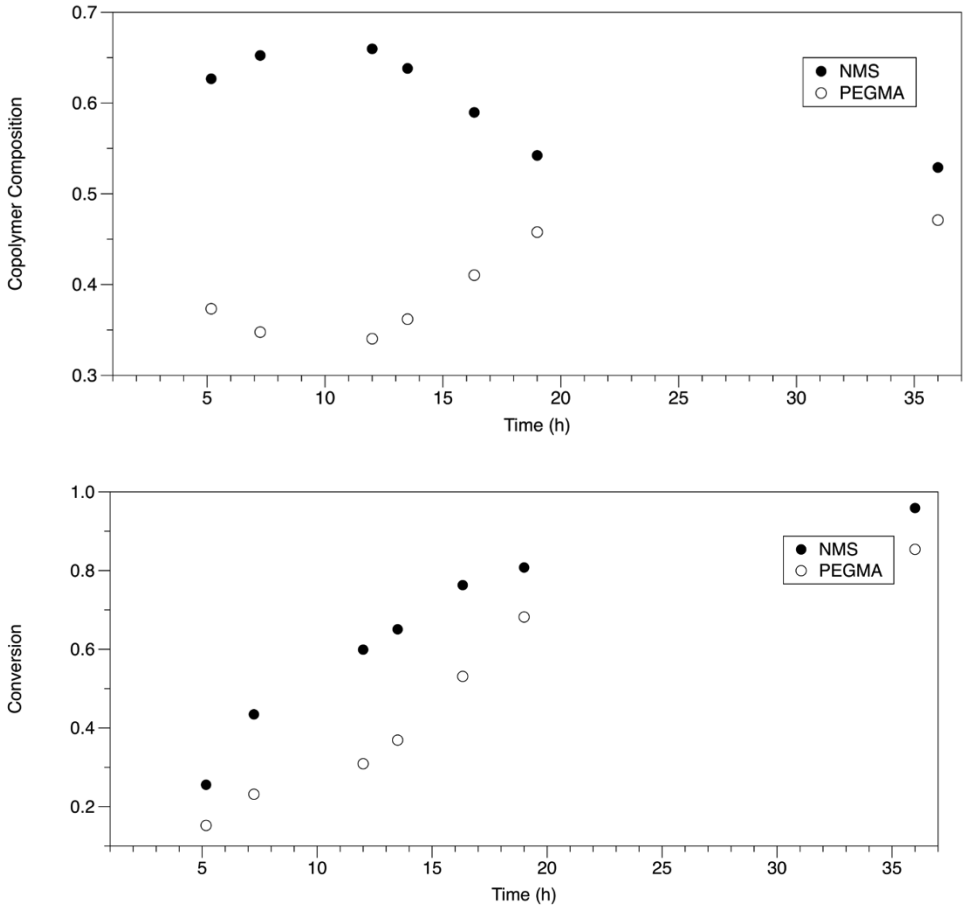


Figure 3.4: (Top) Individual monomer conversions at different reaction times in the RAFT copolymerization of PEGMA and NMS with 4-cyano-4-

(dodecylsulfanylthiocarbonyl)sulfanylpentanoic acid (CDTPA) as the chain-transfer agent. (Bottom) The copolymer composition of the copolymer at various reaction times.

### 3.3.3 RAFT removal

Several groups have demonstrated the successful substitution of RAFT end functionalized polymers with more chemically inert moieties.[34–36] Following the precipitation of the polymer in ether and redispersion in THF, the RAFT agent was removed by reaction with an excess of AIBN at 80°C for 1h. Thus, the polymer was capped with a 2-cyanoisopropyl moiety to prevent side reactions with the original trithiocarbonate end group (Scheme 3.2). This reaction was monitored by UV analysis, where the absorbance of the trithiocarbonate moiety from 290-340 nm completely disappeared after treatment with AIBN (Figure 3.5). The polymer was purified by several precipitations in ether and was redispersed in THF for subsequent use.

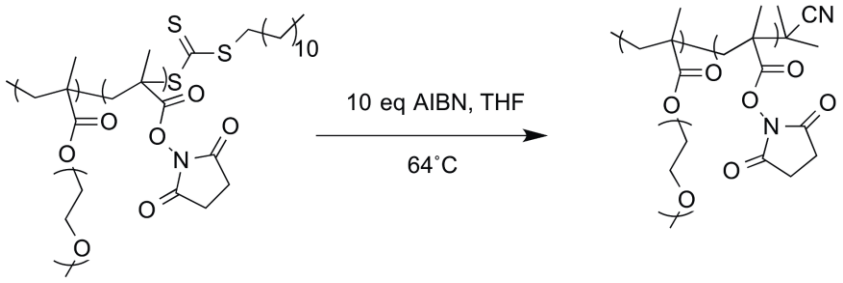


Scheme 3.2: Cleavage of the trithiocarbonate group by means of reflux in excess AIBN.

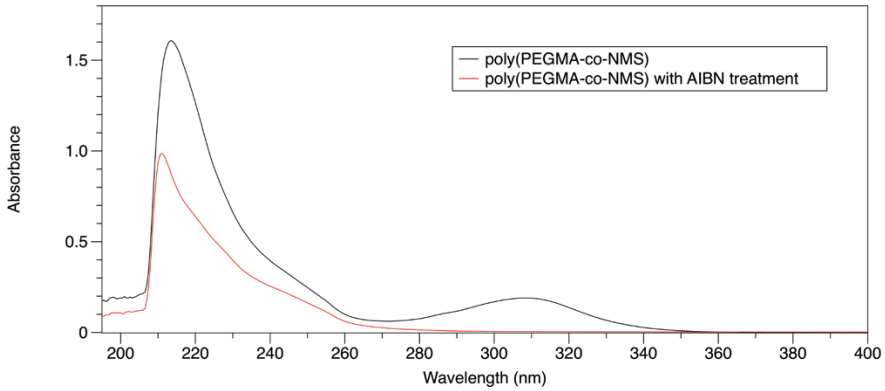

Figure 3.5: UV Absorbance spectra of Poly(PEGMA-co-NMS) both before and after AIBN treatment showing the cleavage of the RAFT agent (311 nm).

### 3.3.5 Histamine modification

The reaction of succinimide groups with small molecule amines is well documented, with the reactions usually proceeding at room temperature and resulting in high yields. Although the postmodification of polymers bearing succinimides has been successful, the main disadvantages include longer reaction times, harsher reaction conditions and lower yields as compared to reactions with monomeric succinimide esters and low molecular weight amines. However, key advantages, which include the versatility of synthetic design and easy postmodification reactions, aid this approach in cost-effectiveness and commercial viability for pilot scale production as opposed to the time intensive synthesis of unique monomer structures and characterization of their polymerization conditions and kinetics.

As mentioned before, several groups have successfully modified NMS units with small molecule amines at mild reaction conditions. However, this reaction is complicated by the limited solubility of histamine dihydrochloride in organic solvents. Several approaches were attempted in DMF, DMF/$H_2O$ mixtures with sodium bicarbonate, but the yields were poor. Even with an excess of histamine.2HCl and temperatures up to

70°C, yields were below 20%. However, several groups have reported the solubility of histamine.2HCl in DMSO.[37] Accordingly, it was dissolved with the polymer with extended stirring at 20°C, triethylamine added as the base and the mixture heated overnight at 70°C (Scheme 3.3)

The polymer was purified by dialysis for 24h, and then freeze dried to obtain the poly(PEGMA-co-imidazole). As seen in Figure 3.6, NMR analysis shows the presence of two new peaks at 7.25 and 8.65 ppm in the product, indicating the presence of the imidazole units in the polymer. The disappearance of the succinimide peaks at 2.8 ppm is difficult to follow due to the overlap of the $CH_2$ adjacent to the amide. However, by comparing the integrations of the imidazole peaks to the $CH_2$ adjacent to the amide, the reaction conversion was calculated to be 96%. The success of the reaction was attributed to the choice of an excellent solvent for all the reactants followed with a tertiary amine base catalyzing the amide formation.

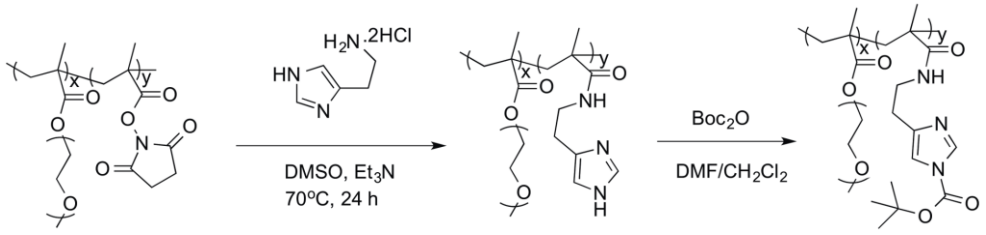


Scheme 3.3: Preparation of Poly(PEG-co-imidazole) using histamine dihydrochloride and its corresponding boc protection.

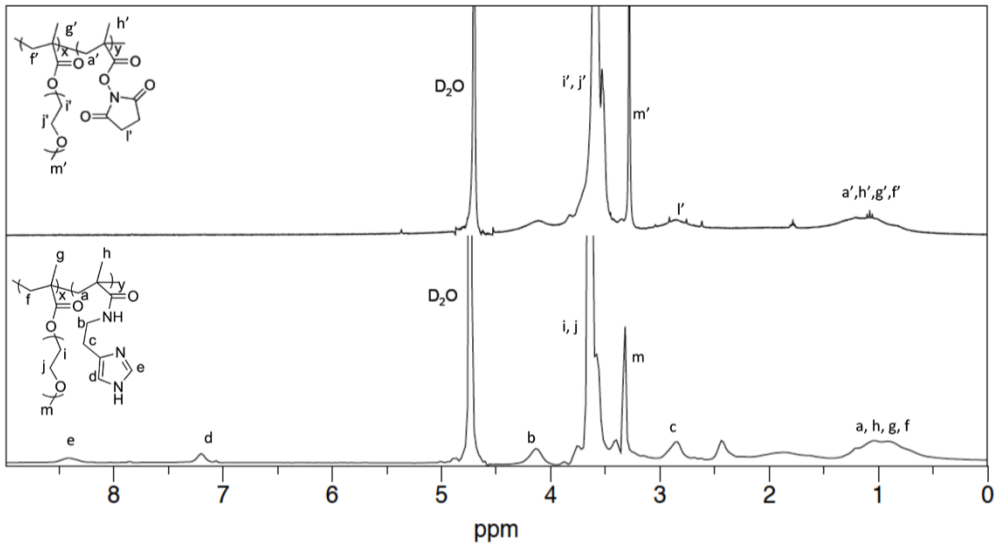


Figure 3.6: $^{1}$H-NMR spectra in $D_2O$ of (a) poly(PEGMA-co-imidazole) (Top) and poly(PEGMA-co-NMS) (Bottom).

### 3.3.4 Boc protection to tune polymer ligand solubility

The solubility of the Poly(PEGMA-co-NMS) in water was dependent on the composition of NMS in the copolymer, where compositions with NMS greater than 65% displayed poor solubility when the PEGMA was 500 g/mol. With a 950 g/mol PEGMA, poor solubilities in water were observed when the NMS composition was higher than 77%. While the poly(PEGMA-co-NMS) is soluble in THF, the poly(PEGMA-co-imidazole) is insoluble in THF, and the presence of the unprotected imidazole can cause GPC flow problems due to its affinity to the Styragel column. This hindered the latter's characterization through GPC, and the poly(PEGMA-co-imidazole) was modified with the boc protecting group to aid its solubility in THF. As expected, the boc-protected poly(PEGMA-co-imidazole) showed a slight increase in molecular weight corresponding to the boc group (Figure 3.7). This confirmed that the polymer did not degrade during the

histamine reaction, and the changes in solubility at various steps were consistent with the corresponding change in functionality.

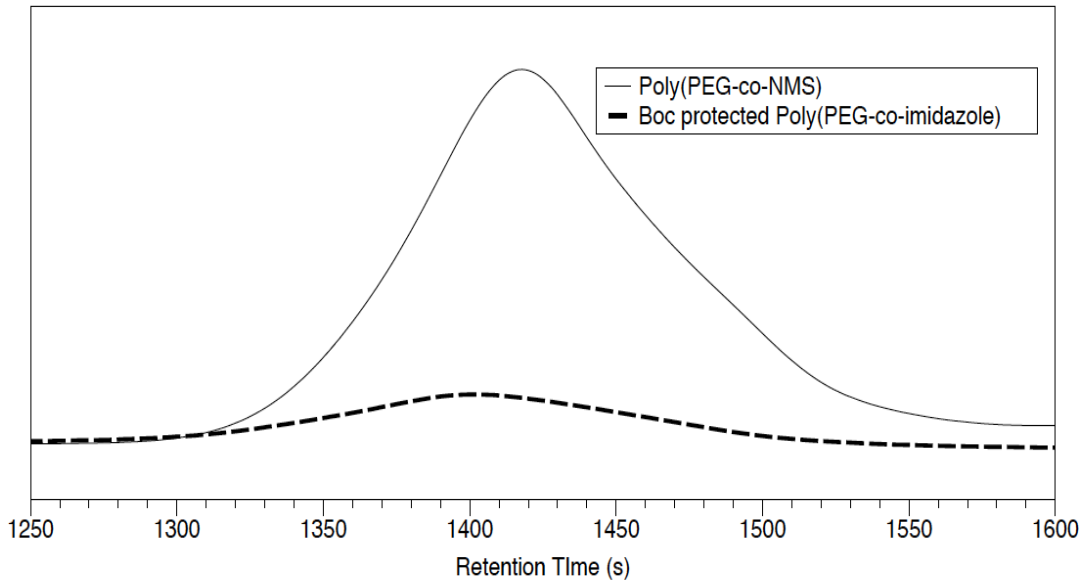


Figure 3.7: GPC curves of Poly(PEG-co-NMS) and the boc protection of Poly(PEG-co-imidazole)

**3.3.5 Ligand Exchange and Characterization of the Aqueous QDs.** After the QD purification by GPC, the ligand exchange reactions were done with 4 different molecular weight poly(PEGMA-co-imidazole) samples (11k, 18k, 30k and 50k) by using a modification of the method published previously for acrylate-based imidazoles. After the reactions, all of QDs in each sample could be well dispersed into pH=7.4 buffer to form clear solutions that remained stable for more than 1 month when stored at 4 °C. According to the absorption spectrum, there was no size change after the ligand exchange reaction. We further confirmed the monodispersity of the various polymer coated aqueous QDs by TEM and DLS analysis. Figure 3.8 shows the TEM of quantum dots

drop cast from aqueous solution, which revealed discrete inorganic cores in all samples. In C and D, where the polymers involved higher Mn and higher imidazole content (Table 3.5), the quantum dots displayed higher inter-particle separation and decreased abundance of aggregated structures compared to those seen in A and B. DLS analysis showed lower hydrodynamic radius in A and B (8-8.6 nm), indicating that the quantum dots diffuse as discrete particles in solution. We note that the higher interparticle distance and higher hydrodynamic radius in C and D (15.2-17 nm) indicate a prominent role of the chain length and imidazole content in determining dispersion. The polymer compositions were calculated via NMR, and the repeat units of imidazole ranged from 32 to 134. The 11k and 18k polymers utilized a 550 g/mol PEG side chain, while the 30k and 50k incorporated a 950 g/mol side chain. The 30k and 50k polymer both have significantly higher loadings of the imidazole (104 and 134 as compared to 32 and 44 for the 11k and 18k respectively), and may be helpful in obtaining superior dispersions. The improvement of the dispersion as the molecular weight and binding group content increases is congruent with our earlier work on functionalized polymers on various nanomaterials.[38-39] Further work in this area will focus on an investigation of understanding the effect of various molecular variables of the polymer, including molecular weight, density of chains on the quantum dot surface and histamine content on the dispersion of the functionalized quantum dots. The brightness of the QDs was also maintained after the ligand exchange reaction, with flourescenceseen under UV (Figure 2.9). The QY of these four samples was around 30%, which is suitable for applications of water-soluble QDs as fluorophores and as energy-transfer donors.

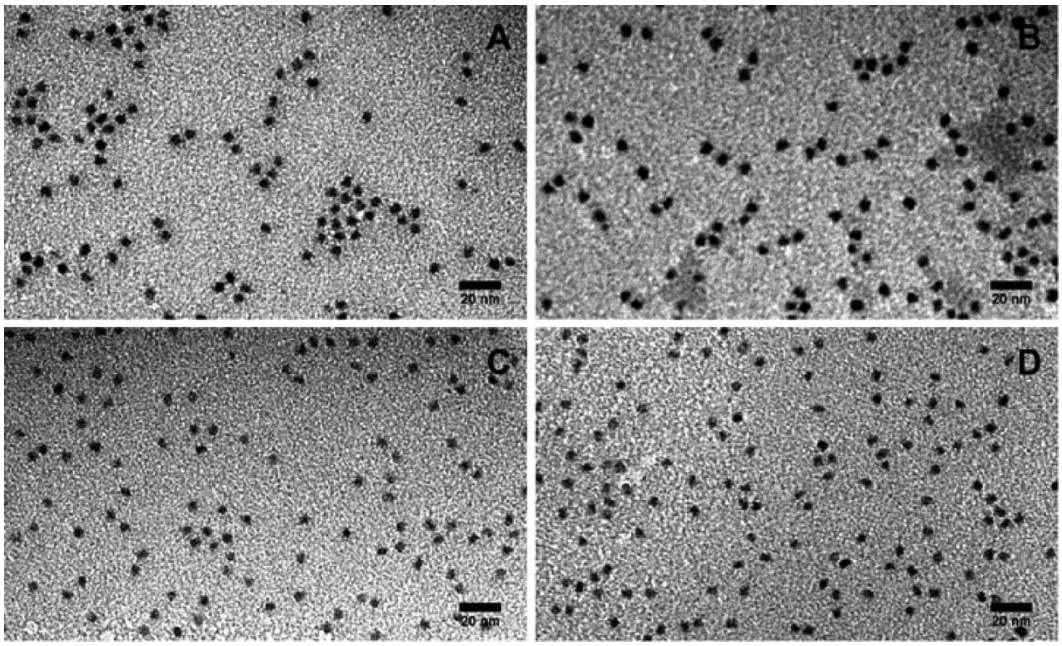


Figure 3.8: TEM images of aqueous CdSe/CdZnS QDs with different molecular weight polymeric imidazole capping ligands with molecular weight (Mn) A: 11k MW; B: 18k MW; C: 30k MW; D: 50k MW. (Scale bar – 20 nm)

Table 3.5: Polymer characteristics used for the encapsulation of QDs. Mol% and number of monomer units were calculated based on the integrations of the imidazole proton (8.32 ppm) and the terminal $CH_3$ at the end of the PEG side chain (3.21 ppm). The quantum yield and hydrodynamic radius (DLS) characterization of the PIL capped QDs are also provided. * Samples C and D utilized PEGMA with $M_n$ of 950 g/mol, while A and B involved PEGMA with $M_n$ 550 g/mol.

| Ligand Mn | PDI | Mol% Imidazole | Mol% PEGMA | # of imidazole units | # of PEGMA units | QY (%) | HR/nm |
|---|---|---|---|---|---|---|---|
| A, 10,680 | 1.24 | 54.29 | 45.71 | 32 | 9 | 36 | 8.6 |
| B, 17,950 | 1.21 | 44.10 | 55.90 | 44 | 18 | 31 | 8.0 |
| C, 30,700* | 1.35 | 61.35 | 38.65 | 104 | 12 | 34 | 15.2 |
| D, 50,550* | 1.34 | 46.95 | 53.05 | 134 | 29 | 27 | 17.0 |

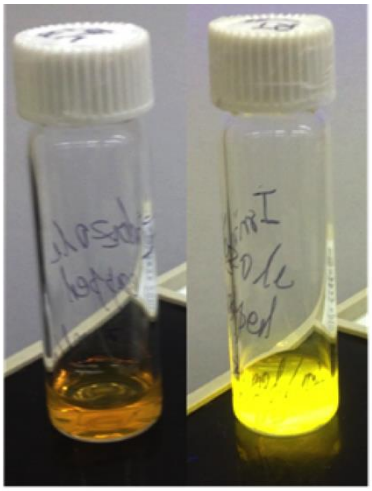


Figure 3.9: A comparison of photographs displaying the florescent properties of the quantum dots in an aqueous medium in the presence of ambient light and UV light.

### 3.4 Summary

In this work, we presented a facile copolymerization and postmodification method to prepare multidentate histamine copolymers which were shown to act as excellent ligands for CdSe/$Cd_xZn_{1-x}S$ QDs in aqueous solutions. The copolymers were synthesized with PEGMA and an activated ester (NMS) using the RAFT technique. The activated ester groups were then modified using histamine to obtain imidazole groups on the copolymer with tailored compositions based on varying the ratios of monomer and polymerization conditions. The versatility of the synthesis was demonstrated by high yields (~96%) of the postmodification reaction and its robust immobilization onto quantum dots. The ligand exchange of the quantum dots with poly(PEGMA-co-imidazole) facilitated their dispersion in aqueous media, eliminated concerns about precipitation, utilized nonspecifically bound ligands, and provided a robust system of

attachment. This method provides advantages in applications including bioimaging, drug delivery systems and biocompatible optical devices. Additionally, a study was conducted to determine the reactivity ratios of NMS with PEGMA and vales of rNMS = 0.91 and rPEGMA = 0.69 were determined using the Kelen-Tudos method. Overall, this work demonstrated a convenient and tunable method to prepare histamine based multidentate copolymers, and their corresponding functionalization of quantum dot materials.

### 3.5 References


(1) Shirasaki, Y.; Supran, G. J.; Bawendi, M. G.; Bulovic, V. *Nat Phot.* **2013**, *7*, 13.

(2) Kamat, P. V. *J. Phys. Chem. Lett.* **2013**, *4*, 908.

(3) Liu, W.; Greytak, A. B.; Lee, J.; Wong, C. R.; Park, J.; Marshall, L. F.; Jiang, W.; Curtin, P. N.; Ting, A. Y.; Nocera, D. G.; Fukumura, D.; Jain, R. K.; Bawendi, M. G. *J. Am. Chem. Soc.* **2010**, *132*, 472.

(4) Zhang, P.; Liu, S.; Gao, D.; Hu, D.; Gong, P.; Sheng, Z.; Deng, J.; Ma, Y.; Cai, L. *J. Am. Chem. Soc.* **2012**, *134*, 8388.

(5) Zimmer, J. P.; Kim, S.-W.; Ohnishi, S.; Tanaka, E.; Frangioni, J. V; Bawendi, M. G. *J. Am. Chem. Soc.* **2006**, *128*, 2526.

(6) Bruchez, M.; Moronne, M.; Gin, P.; Weiss, S.; Alivisatos, A. P. *Science* **1998**, *281* , 2013.

(7) Wang, M.; Oh, J. K.; Dykstra, T. E.; Lou, X.; Scholes, G. D.; Winnik, M. A.; Ms, C. **2006**, 3664.

(8) Yi, D. K.; Selvan, S. T.; Lee, S. S.; Papaefthymiou, G. C.; Kundaliya, D.; Ying, J. Y. *J. Am. Chem. Soc.* **2005**, *127*, 4990.

(9) Kloust, H.; Schmidtke, C.; Merkl, J.-P.; Feld, A.; Schotten, T.; Fittschen, U. E. A.; Gehring, M.; Ostermann, J.; Pöselt, E.; Weller, H. *J. Phys. Chem. C* **2013**, *117*, 23244.

(10) Schieber, C.; Bestetti, A.; Lim, J. P.; Ryan, A. D.; Nguyen, T.-L.; Eldridge, R.; White, A. R.; Gleeson, P. a; Donnelly, P. S.; Williams, S. J.; Mulvaney, P. *Angew. Chem. Int. Ed. Engl.* **2012**, *51*, 10523.

(11) Algar, W. R.; Krull, U. J. *Langmuir* **2006**, *22*, 11346.

(12) Zhan, N.; Palui, G.; Safi, M.; Ji, X.; Mattoussi, H. *J. Am. Chem. Soc.* **2013**, *135*, 13786.

(13) Aldeek, F.; Safi, M.; Zhan, N.; Palui, G.; Mattoussi, H. *ACS Nano* **2013**, *7*, 10197.

(14) Liu, W.; Greytak, A. B.; Lee, J.; Wong, C. R.; Park, J.; Marshall, L. F.; Jiang, W.; Curtin, P. N.; Ting, A. Y.; Nocera, D. G.; Fukumura, D.; Jain, R. K.; Bawendi, M. G. *J. Am. Chem. Soc.* **2010**, *132*, 472.

(15) Petryayeva, E.; Krull, U. J. *Langmuir* **2012**, *28*, 13943.

(16) Petryayeva, E.; Algar, W. R.; Krull, U. J. *Langmuir* **2013**, *29*, 977.

(17) Han, H.-S.; Martin, J. D.; Lee, J.; Harris, D. K.; Fukumura, D.; Jain, R. K.; Bawendi, M. *Angew. Chem. Int. Ed. Engl.* **2013**, *52*, 1414.

(18) Shen, L. *J. Funct. Biomater.* **2011**, *2*, 355.

(19) Shen, L.; Pich, A.; Fava, D.; Wang, M.; Kumar, S.; Wu, C.; Scholes, G. D.; Winnik, M. A. *J. Mater. Chem.* **2008**, *18*, 763.

(20) Allen, M. H.; Hemp, S. T.; Smith, A. E.; Long, T. E. *Macromolecules* **2012**, *45*, 3669.

(21) Weber, R. L.; Ye, Y.; Schmitt, A. L.; Banik, S. M.; Elabd, Y. a.; Mahanthappa, M. K. *Macromolecules* **2011**, *44*, 5727.

(22) Hoarfrost, M. L.; Segalman, R. A. *Macromolecules* **2011**, *44*, 5281.

(23) Vijayakrishna, K.; Jewrajka, S. K.; Ruiz, A.; Marcilla, R.; Pomposo, J. a.; Mecerreyes, D.; Taton, D.; Gnanou, Y. *Macromolecules* **2008**, *41*, 6299.

(24) Wiss, K. T.; Theato, P. *J. Polym. Sci. Part A: Polym. Chem.* **2010**, *48*, 4758.

(25) Nilles, K.; Theato, P. *Polym. Chem.* **2011**, *2*, 376.

(26) Nilles, K.; Theato, P. *J. Polym. Sci. Part A: Polym. Chem.* **2009**, *47*, 1696.

(27) Aamer, K. A.; Tew, G. N. *J. Polym. Sci. Part A: Polym. Chem.* **2007**, *45*, 5618.

(28) Fukukawa, K.; Rossin, R.; Hagooly, A.; Pressly, E. D.; Hunt, J. N.; Messmore, B. W.; Wooley, K. L.; Welch, M. J.; Hawker, C. J. *Biomacromolecules* **2008**, *9*, 1329.

(29) Yanjarappa, M. J.; Gujraty, K. V; Joshi, A.; Saraph, A.; Kane, R. S. *Biomacromolecules* **2006**, *7*, 1665.

(30) Batz, H.-G.; Franzmann, G.; Ringsdorf, H. *Angew. Chemie Int. Ed. English* **1972**, *11*, 1103.

(31) Cengiz, N.; Kabadayioglu, H.; Sanyal, R. *J. Polym. Sci. Part A: Polym. Chem* **2010**, *48*, 4737.

(32) Eschweiler, N.; Keul, H.; Millaruelo, M.; Weberskirch, R.; Moeller, M. *Polym. Int.* **2014**, *63*, 114.

(33) Alb, A. M.; Enohnyaket, P.; Drenski, M. F.; Shunmugam, R.; Tew, G. N.; Reed, W. F. *Macromolecules* **2006**, *39*, 8283.

(34) Boyer, C.; Bulmus, V.; Davis, T. P.; Ladmiral, V.; Liu, J.; Perrier, S. *Chem. Rev.* **2009**, *109*, 5402.

(35) Chen, M.; Moad, G.; Rizzardo, E. **2009**, 6704.

(36) Willcock, H.; O'Reilly, R. K. *Polym. Chem.* **2010**, *1*, 149.

(37) Schneider, Y.; Modestino, M. a.; McCulloch, B. L.; Hoarfrost, M. L.; Hess, R. W.; Segalman, R. A. *Macromolecules* **2013**, *46*, 1543.

(38) Tao, P.; Viswanath, A.; Schadler, L. S.; Benicewicz, B. C.; Siegel, R. W. *ACS Appl. Mater. interfaces* **2011**, *3*, 3638.

(39) Li, Y.; Tao, P.; Viswanath, A.; Benicewicz, B. C.; Schadler, L. S.*Langmuir* **2013**, *29*, 1211.

# CHAPTER 4

## SYNTHESIS OF RANDOM TERPOLYMERS BEARING MULTIDENTATE IMIDAZOLE UNITS FOR THE FUNCTIONLIZATION OF CADMIUM SULFIDE NANOWIRES

### 4.1 Introduction

Semiconductor nanowires have been extensively studied as a potential candidate for various electronic devices like photovoltaic, transistor and photo detectors because of their unique size and structure dependent optical and electronic properties.[1,2] Since these materials have high surface to volume ratios, the surface structure of nanowires (NWs) play an important role in the performance of these electronic devices.[3] Various groups have explored the properties of Cadmium Sulfide (CdS) nanomaterials by tailoring its shape (nanosheets, platelets)[4,5] and the use of ligands[6–8] that can coordinate to the nanomaterial surface. The usage of ligands to tune the optical and electronic properties of CdS nanowires is particularly appealing as it involves a one step functionalization or ligand exchange with a wide choice of ligand structures, as opposed to the challenges in controlling the architecture in the NW synthesis.

A variety of small molecule ligands have been used in the literature to coordinate to CdS surfaces, including phosphates[9], thiols[10] and carboxylic acids[11]. Recently, polymeric materials containing these functional groups have been utilized to not only tune the properties of the CdS surface, but also display robust functionalization and facilitate its dispersion into polymer matrices for commercially viable applications.[10,12]

Fewer reports discuss the use of polymer brushes to coat the CdS without the use of a polymer matrix, which are especially applicable in photoelectronic and transistor devices. For the attachment of polymeric ligands to CdS surfaces in the absence of a matrix, two challenges are prominent: choice of the appropriate ligand functionality and effective characterization of the functionalized CdS surface to ensure that the polymer is anchored to the substrate.

Regarding the choice of ligands, polymeric imidazoles have shown promise in recent reports as an efficient binder to quantum dot materials.[13–18] The interaction between the amine group in the imidazole and CdS nanowires is believed to be an ionic interaction between nitrogen and surface cadmium atoms. The development of deliberate polymer strategies to functionalize CdS NWs has not been reported, especially a tunable multidentate system, which has shown to significantly improve the dispersion qualities of the nanomaterial in various environments. Furthermore, the synthetic toolbox available for the preparation of polymeric imidazoles can provide a variety of external functional handles for further derivatization. Using the RAFT polymerization technique, imidazole monomers were copolymerized with polyethylene glycol methacrylate and boc-protected methacrylate to add water solubility and dye attachment capabilities to the polymer. The RAFT method also afforded polymers that can be intricately tailored, possessed low polydispersities and contained handles for subsequent modification. Furthermore, the unique choices of monomer structures provided a simple NMR technique to investigate kinetics and compositions which can be useful for other studies with multiple monomers. More importantly, the protocols developed herein for functionalized CdS NWs were scalable, with high yields and simplified processes for commercial viability.

The ternary copolymer (terpolymer) allows three different functions to be incorporated including binding/attachment to surface, solubility in aqueous media, and attachment of a payload, here, a fluorescent dye. We demonstrate the utility of a methacrylate-based terpolymer by testing whether the imidazole binding motif used to prepare water-soluble nanocrystals (NCs) via ligand exchange can also spontaneously associate to chalcogenide NW surfaces prepared by vapor deposition. Essentially, a successful binding of terpolymer ligand on the nanowire surface has been shown. It has also been shown than fluorescence microscopy can be a good technique to illustrate ligand binding on nanowire surface using a dye. This has been accomplished by labeling the terpolymer with a rhodamine dye, and binding the terpolymer on CdS nanowire surface using imidazole units in the terpolymer.

## 4.2 Experimental

### 4.2.1 Materials

All reagents were used as received from Fisher Scientific unless stated otherwise below. AIBN was purchased from Sigma Aldrich and recrystallized thrice from methanol. Poly(ethyleneglycol) methacrylate (500 g/mol) was obtained from Sigma Aldrich and passed through a neutral alumina column to remove inhibitors before use. 4-Cyano-4 [(dodecylsulfanylthiocarbonyl)sulfanyl]pentanoic acid was obtained from Strem Chemicals, Inc. NMS (N-methacryloxy succinimide) was synthesized from NHS (N-hydroxy succinimide) as described in the literature.[19]

### 4.2.2 Instrumentation

NMR spectra were recorded on a Varian Mercury 300 spectrometer using $CDCl_3$ or $D_2O$ as the solvent. The molecular weights and molecular weight distributions were determined using a Waters gel-permeation chromatograph equipped with a 515 HPLC pump, a 2410 refractive index detector, three Styragel columns (HR1, HR3, HR4 in the effective molecular weight range of 100−5000, 500−30000, and 5000−500000, respectively). Tetrahydrofuran (THF) was used as the eluent at 30°C and a flow rate of 1.0 mL/min. The GPC system was calibrated with polystyrene standards obtained from Polymer Laboratories. FT-IR spectra were recorded on a Perkin Elmer Spectrum 100 using an attenuated total reflection diamond cell attachment.

### 4.2.3 Synthesis of Boc protected methacrylamide monomer (MAMboc)

To a solution of 2,2' (ethyleneglycol) bis (ethylamine) (50.00 g, 337.38 mmol) in DCM (100 mL) di-tert-butyl dicarbonate (14.73 g, 67.48 mmol) in 25 mL of DCM was added dropwise at 4 °C. The solution was allowed to warm to room temperature (RT) and stirred overnight. The solution was washed with water (3 × 100 mL) to remove the unreacted diamine. The organic layer was dried over sodium sulfate and solvent removed via rotary evaporation. The crude product (7.13 g, 28.76 mmol) was dissolved in a mixture of 0.3 M sodium bicarbonate solution (40 mL) and DMF (30 mL). NMS (6.06 g, 33.08 mmol) was dissolved in a solution of DMF (10 ml) and was then added to the crude product mixture dropwise at 4 °C. The reaction was warmed to room temperature and stirred for 1 hour. Water (80 mL) was added to the mixture and the mixture was extracted with DCM (3 X 125 mL). The combined organic layers were then dried with sodium

sulfate and the resulting oil was obtained after rotary evaporation. The crude product was purified by column chromatography (5% methanol/ethyl acetate) to provide the product as a clear oil (4.51g, 22% yield). $^{1}$H NMR (300 MHz, CDCl3): δ (ppm) 6.3 (t, 1H), 5.7 (s, 1H), 5.33 (s, 1H), 4.99 (t, 1H), 3.6-3.44 (m, 10H), 3.3 (t, 2H), 1.96 (s, 3H), 1.43 (s, 9H).

### 4.2.4 Preparation of poly(NMS-PEGMA-MAMboc)

In a typical copolymerization, 4-cyano-4-(dodecylsulfanylthiocarbonyl)sulfanylpentanoic acid (CDTPA) ( 0.01g, 0.0123 mmol), NMS (0.0675g, 0.369 mmol), PEGMA (500 g/mol, 0.185g, 0.369 mmol), MAMboc (0.117g, 0.369 mmol) trioxane (18.4 mg) and AIBN (0.00246 mmol, 0.004g) were dissolved in 1.35 mL of THF. The mixture was stirred until all the reactants were dissolved, placed in a Schlenk tube and subjected to three cycles of freeze-pump-thaw. The tube was then heated at 65C for 20h. The polymerization was quenched in ice water and the mixture precipitated in ether. The mixture was centrifuged at 3000 rpm for 5 min and redispersed in 3 mL of THF. This precipitation-redispersion process was repeated twice to obtain poly(NMS-PEGMA-MAMboc) with Mn: 19,865, PDI: 1.29.

### 4.2.5 Preparation of poly(imid-PEGMA-MAMboc)

The poly(NMS-PEGMA-MAMboc) (0.5 g, 0.369 mmol of NMS content) was dissolved in 10 mL THF in a 50 mL two neck RB flask , followed by the addition of 3-aminopropyl imidazole (0.046g, 0.372 mmol) and triethylamine (0.056g, 0.558 mmol) at room temperature. The mixture was sparged with $N_2$ for 15 min, and then heated at 70C overnight. The reaction was cooled and the polymer was precipitated in ethyl ether (30

mL). The mixture was then centrifuged at 3000 rpm for 5 min to separate out the unreacted imidazole, and the polymer redispersed in THF (10 mL). The precipitation-centrifugation-redispersion process was repeated twice more to ensure complete removal of the free imidazole and obtain the purified poly(imid-PEGMA-MAMboc) (0.48g). $^{1}$H-NMR analysis illustrated quantitative consumption (>98%) of the succinimide to imidazole units.

### 4.2.6 Preparation of poly(imid-PEGMA-MAMamine)

Poly(imid-PEGMA-MAMboc) (0.275g, 0.25 mmol of boc content) was dissolved in DCM (3 mL) and cooled to 0C. Trifloroacetic acid (TFAA) (2mL) was added dropwise to the stirring mixture. The mixture was allowed to warm to room temperature and stirred for 12h. The mixture was precipitated in ether to recover the boc deprotected polymer, and the solvent was removed under vacuum. The polymer was dissolved in methanol (5 mL) and a solution of NaOH in methanol was added dropwise until the pH of the solution adjusted to 7-9. The methanol was evaporated to yield a white solid of poly(imid-PEGMA-MAMamine) (0.2g). Using $^{1}$H-NMR analysis of the boc methyl protons of the starting material at 1.43 ppm, 100% deprotection of the boc group was observed.

### 4.2.7 Conjugation of terpolymer with rhodamine dye

Commercially available 5-(and-6)-Carboxy-X-Rhodamine succinimidyl ester (5 (6)-ROX, SE） was dissolved in dry DMSO to make a stock solution of dye. The known amount of polymer was dissolved in 0.1M $NaHCO_3$ solution. 10 equivalents of

dye (per polymer chain) was mixed with polymer solution and was continuously vortexed for 2 hours to achieve polymer-dye conjugation. Excess dye was removed by dialysis with bicarbonate buffer using 10K MW cutoff centrifugal filters; centrifugal dialysis was continued until eluent was clear. The total concentration of dye in the final product was calculated using UV-Vis. Assuming no polymer was lost during dialysis and transferring, the average number of dyes to 1 polymer was calculated to be 0.25. The detailed procedures and characterization of the CdS NWs and the polymer attachment were performed by members of the Greytak research lab.

### 4.2.8 Characterization of terpolymer functionalized CdS NWs

#### 4.2.8.1 Fluorescence Microscopy

Confirmation of binding of polymer dye ligand on NW surface was performed using fluorescence microscopy. The dark field and corresponding fluorescence image were taken. The emission peak of the NWs is at 510nm, and the dye emission peak is at 590nm. The fluorescence microscopy setup has an excitation wave with wavelength higher than the emission peak of nanowires (510nm) in order to avoid the collection of the NW emission. The emission filter is a 590 nm long pass filter.

## 4.3 Results and Discussion

Controlled radical polymerization has seen a surge in various applications to access new opportunities in the area of functionalized nanomaterials.[20–22] In particular, this is due to its high degree of control over various molecular variables and the ability for subsequent functionalization. The ability to perform post-modification reactions to

incorporate new functionalities on the polymer broadens the scope of applicability of the polymer system. Using conventional polymerization methods, it is difficult to maintain low polydispersity and control of the composition when multiple monomers are present in the polymerization mixture. Large variations in the molecular weight distributions can impose problems in postmodification reactions, and in applications where the modified polymer is utilized as a ligand, challenges in effective functionalization to the substrate arise. Using RAFT polymerization, our group has demonstrated the synthesis of highly functional polymers for the functionalization of various substrate materials. In this project, the synthetic approach builds on earlier strategies for the development of multifunctional copolymers that can (i) coordinate to a CdS substrate, (ii) display water solubility and (iii) extend its usage in optical applications through coordination with organic dyes. This is accomplished by synthesizing a terpolymer with succinimide ester, PEG and boc protected monomers in the first step. The succinimide group is then cleaved in a nucleophilic attack to attach the imidazole ligand in the second step, followed by a boc deprotection in the final step, which enables dye coordination via the amine. The finer details of the synthetic strategy and the appropriate choice of monomer units will be discussed in the following sections.

### 4.3.1 RAFT polymerization of poly(NMS-PEGMA-MAMboc)

In this strategy, an activated succinimide ester was directly copolymerized along with PEGMA and the MAMboc monomer (Scheme 4.1). Several reports have investigated the use of an imidazole bearing monomer, but this has disadvantages including degradation of the RAFT agent by the nucleophilic imidazole and limited

solubility parameters of the polymer (especially for analysis by GPC).[23] Accordingly, the NMS monomer allows for postmodification to obtain the imidazole group, enables solubility in many common organic solvents, and maintains the integrity of the RAFT agent. The boc protected monomer (MAMboc) (synthesis shown in Scheme 4.2) enables the polymerization of a protected amine monomer. Again, using a simple postmodification, the amine can be accessed for attachment to dyes. PEGMA (500 g/mol) was chosen to supply water soluble characteristics to the terpolymer, as the reaction of the polymer with the CdS NWs is performed in aqueous media.

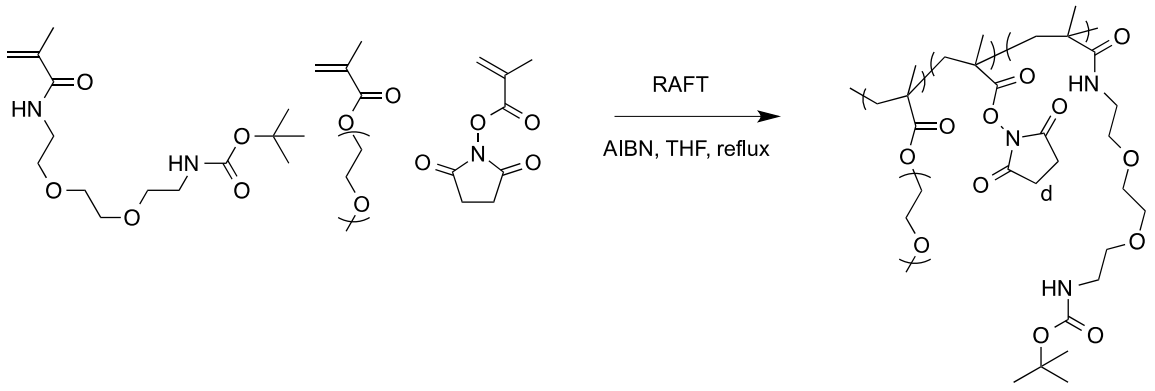


Scheme 4.1: Preparation of terpolymers of NMS, PEGMA and MAMboc using RAFT polymerization.

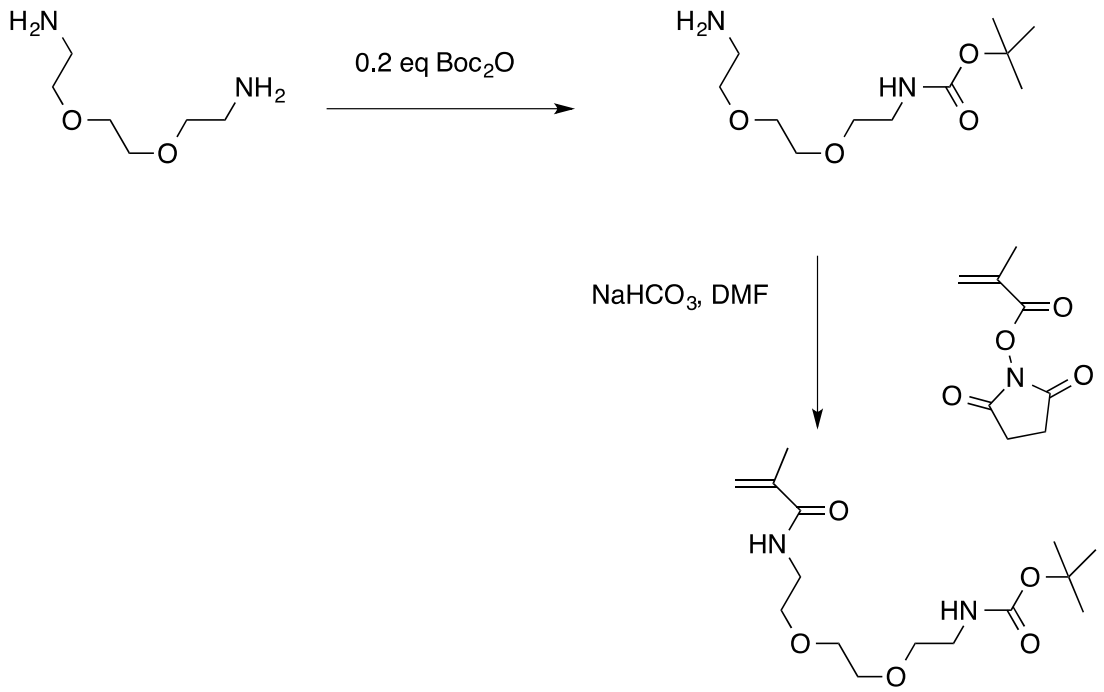


Scheme 4.2: Synthetic scheme for the preparation of the MAMboc monomer.

Additionally, the monomer functionalities present in the copolymerization mixture include a methacrylate (PEGMA), methacrylamide (MAMboc) and a methacrylate derivative (NMS). Due to the difference in electronegativities of the functional groups next to the vinyl bonds in the monomers, the vinyl terminal $CH_2$ signals are discrete for each monomer in the $^1$H-NMR spectrum (Figure 4.1). Typically, comonomer mixtures have overlapping vinyl signals, which makes the analysis of individual monomer conversions difficult. In many cases, block copolymerization has been attempted to solve this issue.[24] However, through a random copolymerization strategy, the individual monomer conversions and composition in the copolymer can be analyzed in detail via measuring the integrations of the monomer signals compared to that of 1,4-trioxane. As seen in Figure 4.2, the decrease in monomer signal intensity is seen as the polymerization progresses at reflux when 0.15 eq of AIBN is used. The kinetics of the polymerization can then be analyzed by removing a small sample under

nitrogen for analysis by $^{1}$H-NMR. This approach is unique as such a method for kinetic analysis has not been reported previously for a random terpolymerization method, mainly due to complications in the vinyl signal overlap in the various monomers.

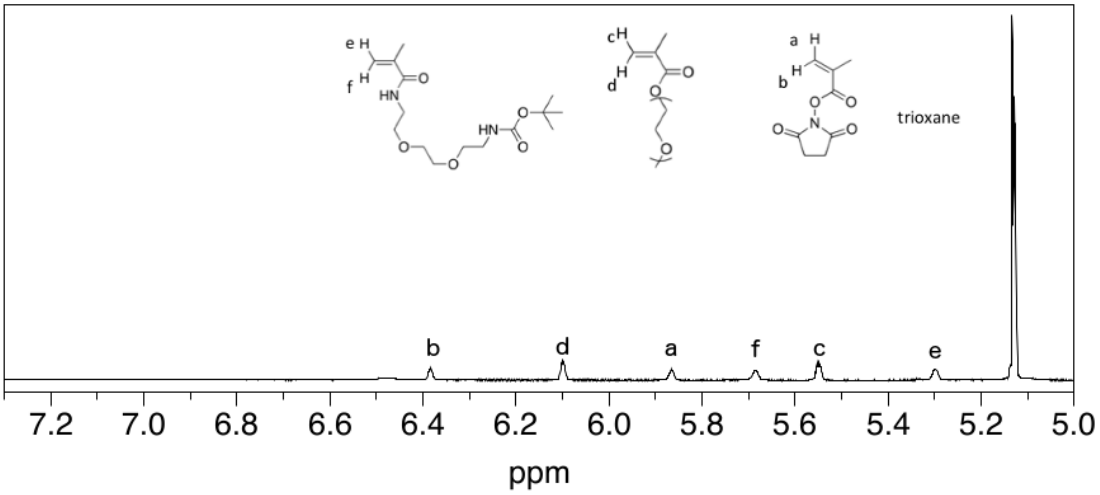


Figure 4.1: $^{1}$H-NMR spectrum of the polymerization mixture in $CDCl_3$ showing the discrete monomer signals. An equimolar ratio (50:50:50:1 of NMS:PEGMA:MAMboc:RAFT) is used, along with 0.15 eq of AIBN. Trioxane (5.13 ppm) is also present as an internal standard.

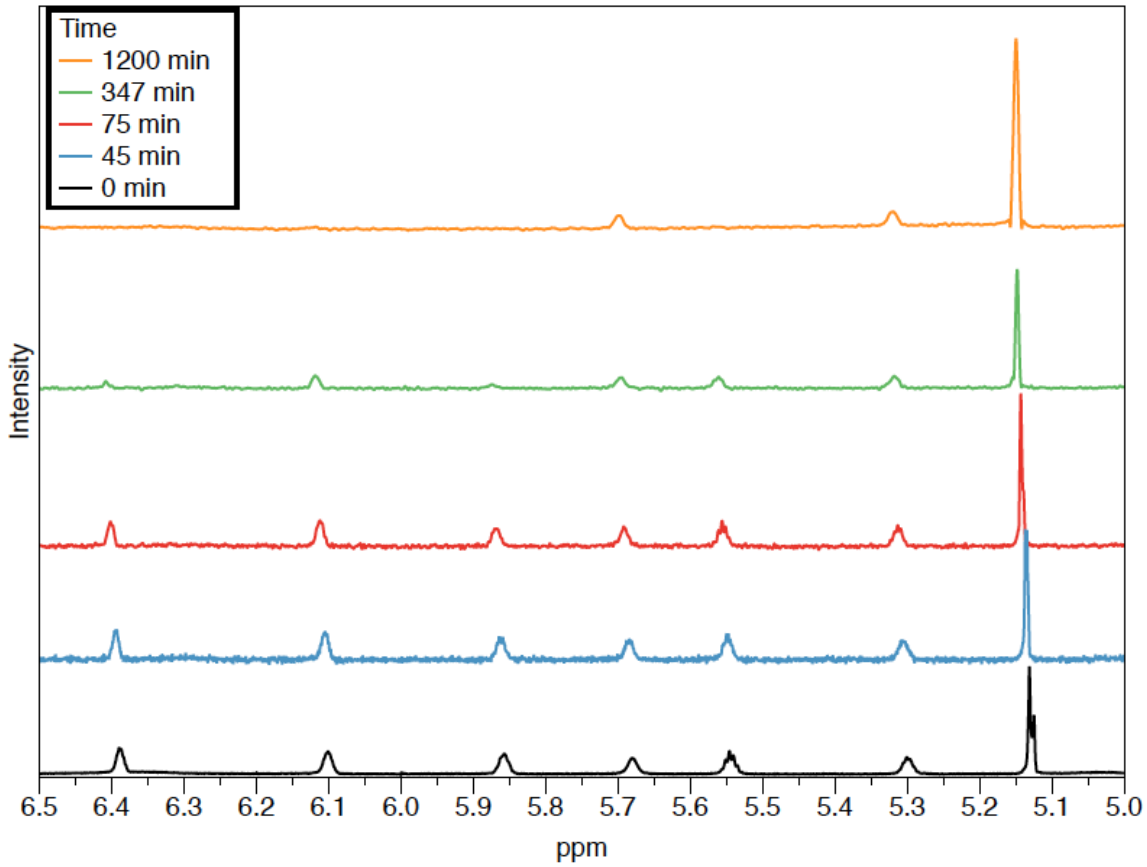


Figure 4.2: $^{1}$H-NMR spectrum of the polymerization mixture in $CDCl_3$ at various polymerization times showing an inverse relationship between monomer signal intensity and polymerization.

Furthermore, the overall kinetics of the random copolymerization was followed. A linear relationship was seen in the total monomer conversion with time, suggesting the controlled growth of polymer chains over time (Figure 4.3). The polymers at various conversions also displayed low polydispersities and a gradual decrease in polydispersity over time, and this points to the control coordinated by the RAFT polymerization technique. Further evidence is also provided by Figure 4.3, where a linear relationship between ln([Mo]/[Mt]) and time is displayed. [Mo] is the initial monomer concentration and [Mt] is the final monomer concentration at various times in the polymerization. This supports the theory of control in RAFT where the concentration of the growing species remains constant and the first-order kinetics is achieved.

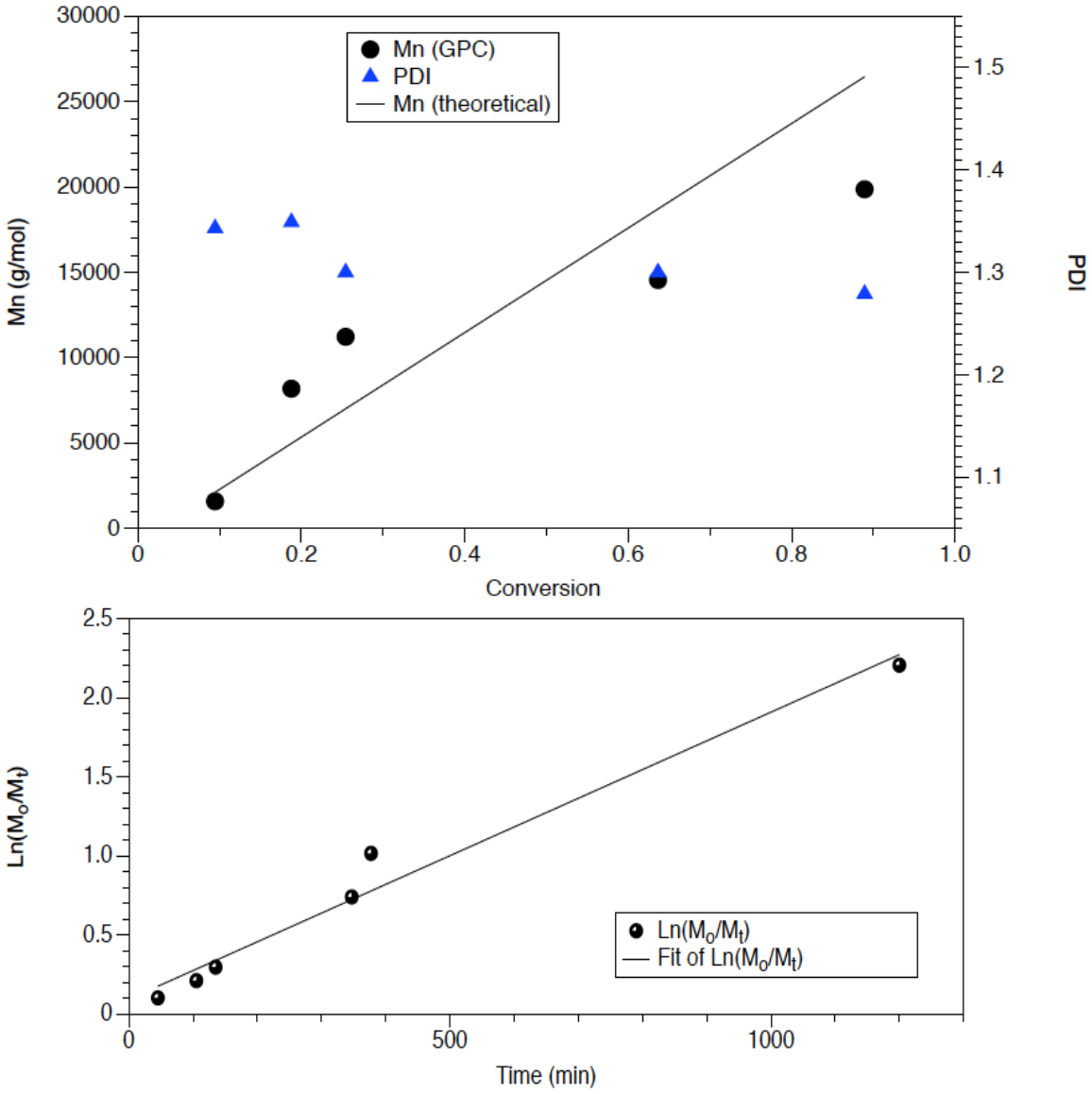


Figure 4.3: Kinetic curves for the RAFT polymerization of NMS, PEGMA and MAMboc with a monomer ratio of 50:50:50 using chain transfer agent CDTPA and AIBN with a ratio of 1:0.15 in DMF at 80˚C. (Top) evolution of Mn and PDI with total monomer conversion and (Bottom) semilogarithmic plot versus time.

Although the kinetic curves provided an overview of the total monomer consumption with time, there was a need to study the individual monomer conversions to investigate the exact composition of the polymer at various reaction times. This can be

important in cases where the composition of the polymer can affect performance, e.g. when lower amounts of the PEG can inhibit water solubility characteristics. As seen in Figure 4.4 and Table 4.1, the NMS monomer displayed an increased propensity to be consumed during the polymerization as compared to the other monomers. This behavior was also observed in other copolymerizations, including with butyl acrylate[25] and N-(2-hydroxypropyl) methacrylamide (HPMA)[26]. As seen in Figure 4.4, the trend for the reactivity of monomers is NMS>PEGMA>MAM-boc. It is interesting that MAMboc is not fully consumed in the polymerization, while the other two monomers are able to achieve 100% conversion. Another interesting aspect is that NMS and PEGMA both tend to react faster than the MAMboc, and this observation correlates well with other studies in the literature, where NMS and methacrylate based polymers tend to have higher reactivity ratios than the corresponding methacrylamides. The relationship between NMS and methacrylates has not been extensively looked in the literature, but work on their dual copolymerization revealed a higher reactivity ratio for NMS compared to PEGMA (Chapter 3). Thus, the reactivity trends seen in Figure 4.4 can be understood by analyzing the fundamental reactivity relationships of the different monomer pairs.

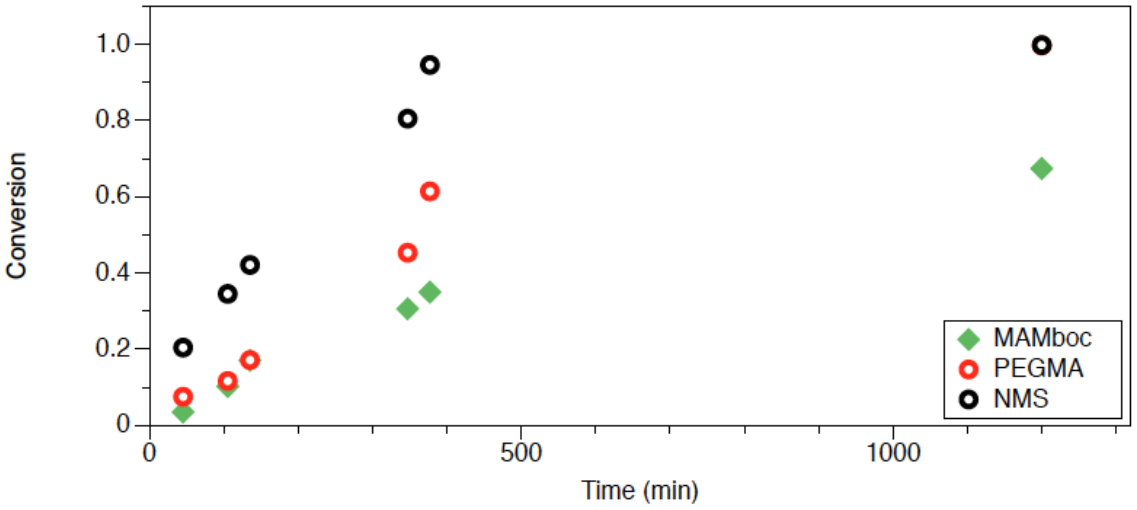
Conversion
1.0
0.8
0.6
0.4
0.2
0
0
500
1000
Time (min)
MAMboc
PEGMA
NMS

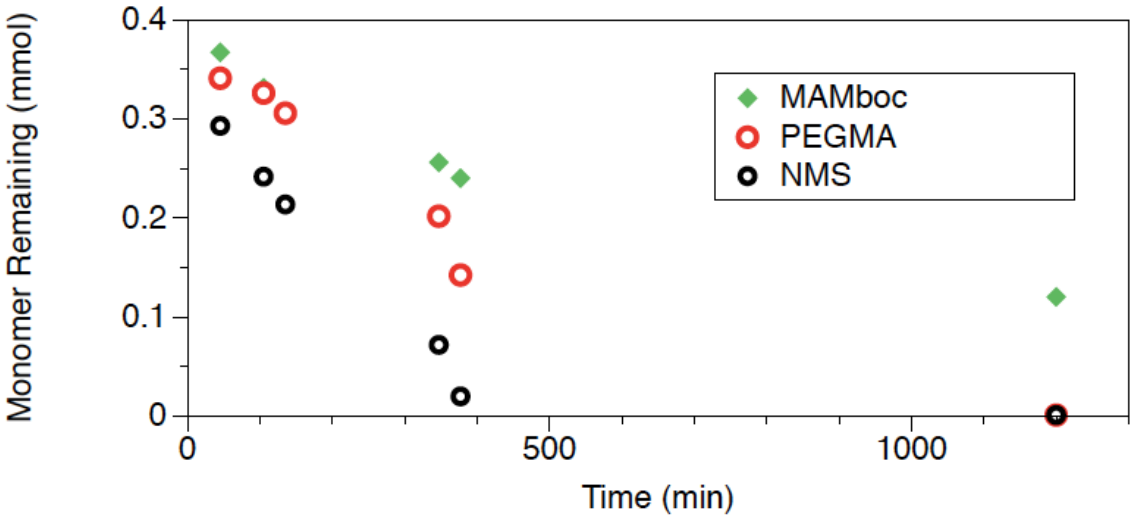
Monomer Remaining (mmol)
0.4
0.3
0.2
0.1
0
0
500
1000
Time (min)
MAMboc
PEGMA
NMS

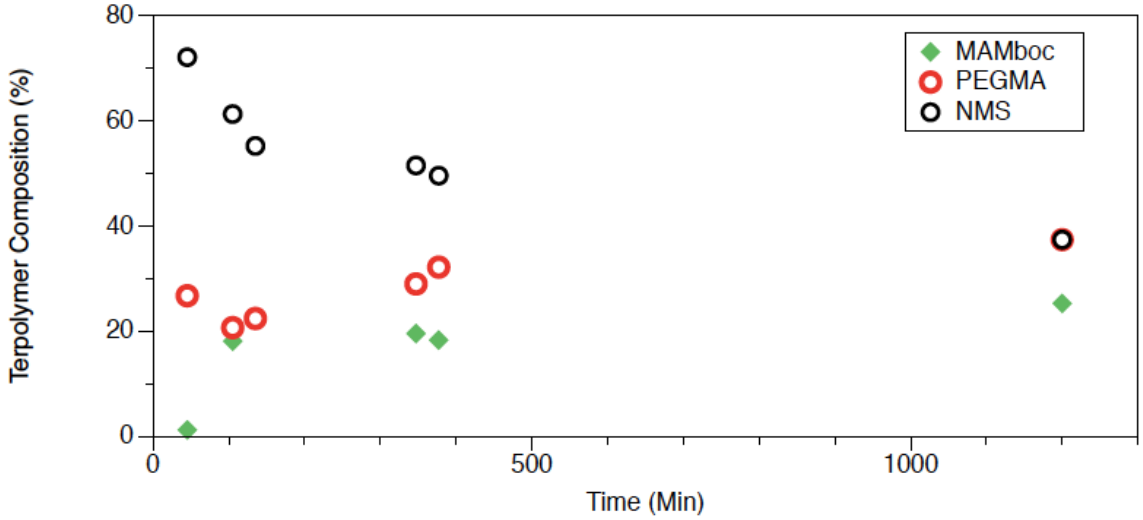
Terpolymer Composition (%)
80
60
40
20
0
0
500
1000
Time (Min)
MAMboc
PEGMA
NMS

Figure 4.4: (Top) Individual monomer conversions at different reaction times in the RAFT copolymerization of NMS, PEGMA and MAMboc with a ratio of 50:50:50 in the presence of CDTPA and AIBN (1:0.15 eq). (Middle) The monomer remaining in the copolymerization mixture with varying reaction time. (Bottom) Total terpolymer composition at different reaction times.

Table 4.1: Table showing individual monomer conversions, Mn and PDI results at varying times in the copolymerization of NMS, PEGMA and MAMboc (50:50:50) with using CDTPA and AIBN (1:0.15 eq) at reflux in THF.

| Time (min) | MAM Conv. (%) | PEG Conv. (%) | NMS Conv. (%) | Total monomer conversion (%) | Theoretical Mn (g/mol) | Mn (GPC) (g/mol) | PDI |
|---|---|---|---|---|---|---|---|
| 45 | 2.75 | 2.31 | 4.32 | 3.1 | 965 | 4030 | 1.225 |
| 67 | 10.5 | 16.31 | 54 | 26.9 | 4675 | 9898 | 1.309 |
| 85.5 | 27.34 | 32.54 | 61.41 | 40.4 | 7630 | 11307 | 1.3 |
| 257 | 45.33 | 64.39 | 99.47 | 69.7 | 13350 | 19880 | 1.3 |

Ideally, reactivity ratio studies can be performed for dual monomer systems using established methods such as the Kelen-Tudos or Fineman-Ross, but terpolymer reactivity ratio calculations require the use of ternary plots and are limited in the literature. A viable alternative to obtain a quick understanding of the relative reactivities is provided through these studies. Essentially, the growing chain is richer in NMS units initially, and due to the more drastic decrease in concentration of NMS, the polymers chains start to incorporate additional PEGMA units, leaving the tail end of the polymer heavily composed with MAM-boc units (Figure 4.4 bottom). The trend in reactivity seen with the monomers confirms the presence of a pseudo gradient polymer. The randomization of monomer units also avoids complications related to the solubility if prepared by a block

copolymerization method. It was observed that NMS homopolymers tended to precipitate out of the solvent, and a large amount of PEGMA units was needed for water solubility. This can have implications for CdS functionalization, and a random method was hence preferred.

### 4.3.1 Synthesis of poly(imid-PEGMA-MAMboc)

Using a simple postmodification strategy of cleaving succinimide with amines, the poly(NMS-PEGMA-MAMboc) was dissolved in THF, followed by the addition of triethylamine (catalyst) and the imidazole (Scheme 4.3). After the reaction, the polymer precipitated into diethyl ether, followed by centrifugation to purify the polymer. Typically, the imidazole used for such polymers involve hydrochloride salts, for e.g. histamine salts. Ionic imidazoles are often incompatible for reactions in organic media, and when polymeric reactions are done in water, the product has to undergo a time-consuming dialysis process in water, followed by an expensive lyophilization step (to remove the water while preserving the polymer functionality) to remove the excess imidazole. Furthermore, the imidazole used herein (3-amino propyl imidazole) has shown to be useful as a coordinating ligand in quantum dots, and is significantly less expensive than other commercially available imidazole based amine linkers. The reaction of the succinimide is known to have characteristics of the click reaction, with high yields and mild reaction conditions. The characterization of this reaction is further discussed in section 4.3.4.

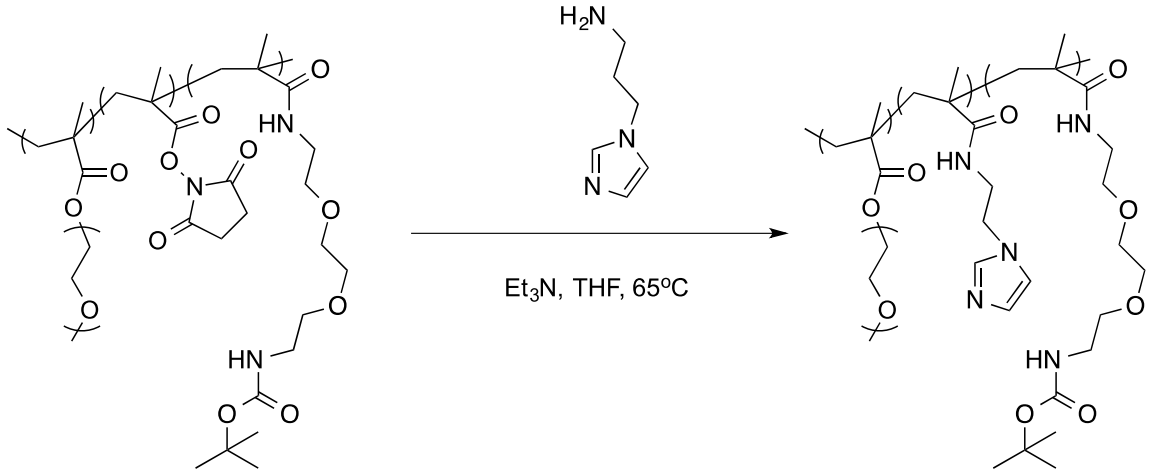


Scheme 4.3: Preparation of poly(imid-PEGMA-MAMboc) using 3-amino propyl imidazole.

### 4.3.3 Synthesis of poly(imid-PEGMA-MAMamine)

The boc deprotection of polymers typically involves a reaction with conc HCl solution. However, the boc deprotection of poly(imid-PEGMA-MAMboc) was not successful with various HCl solutions (0.3 – 1M) and increased temperatures (20-40˚C). However, trifloroacetic acid (TFAA) proved to be an efficient deprotection agent (Scheme 4.4), where the boc peak is completely removed (see section 3.3.4). In this reaction, the TFAA protonates tert-butyl carbamate followed by decarboxylation and releases the amine product. The polymer undergoes precipitation in ether to remove any starting material, and excess TFAA is removed under vacuum. The pH of the polymer is adjusted to 7-8 to neutralize any TFAA salts in the mixture.

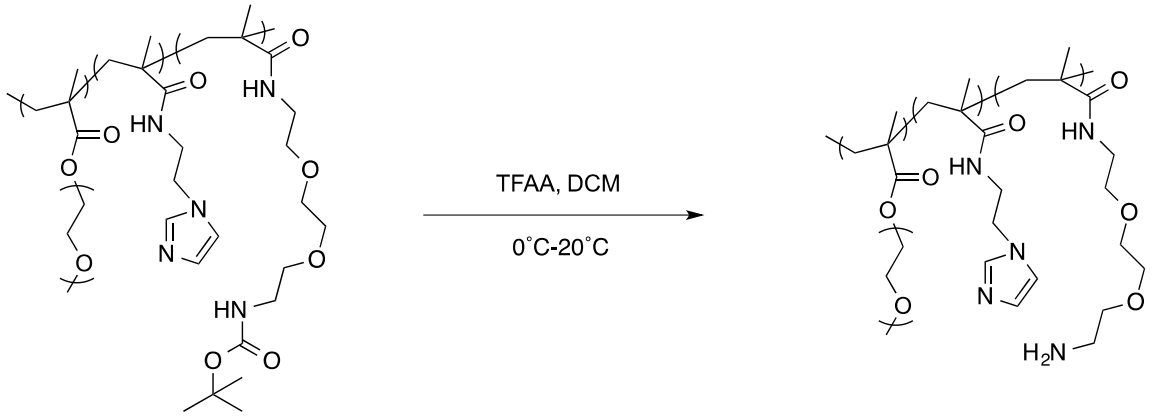


Scheme 4.4: Boc deprotection of poly(imid-PEGMA-MAMboc) with TFAA.

### 4.3.4. NMR and IR characterization of the terpolymers

The reaction of poly(NMS-PEGMA-MAMboc) with the imidazole was monitored by $^{1}$H-NMR, where the product displayed characteristic peaks from the imidazole from 6.8 ppm to 6.95 ppm and at 7.35 ppm (Figure 4.5). The succinimide peaks of the starting material (expected to be a broad peak at 2.75-2.85 ppm) were overshadowed by the $CH_2$ next to the imidazole unit, and was difficult to calculate the conversion of the imidazole in this manner. The PEGMA peaks (3.7-3.85 ppm) and the boc methyl peaks (1.43 ppm) from the MAMboc units were retained without degradation in the product, which illustrated the relatively mild conditions used for the imidazole attachment reaction. The replacement of the succinimide units by the imidazole was also confirmed through IR analysis, where the C=O in the succinimide clearly showed a significant decrease in intensity at 1700 $cm^{-1}$ (Figure 4.6). The presence of the imidazole units could not be confirmed by IR, as the imidazole signals (at 1130 and 1484 $cm^{-1}$) were obscured by broader peaks corresponding to the C-N stretches from the succinimide in the poly(NMS-PEGMA-MAMboc). For the removal of the boc group in poly(imid-PEGMA-MAMboc),

the boc peak at 1.43 ppm was monitored with $^{1}$H-NMR, and the complete disappearance of the boc peak was displayed after the reaction with TFAA. The terminal amine signal could not be confirmed with $^{1}$H-NMR, and was confirmed via a ninhydrin stain method, where a purple stain was obtained (the starting material poly(imid-PEGMA-MAMboc) gave a pale yellow stain in the ninhydrin test). It must also be noted that a shift in the imidazole signals was also seen, with the CH peaks on the imidazole ring broadening at 7.1-8 ppm, and may be the result of the imidazole amine coordinating with the TFAA salts.

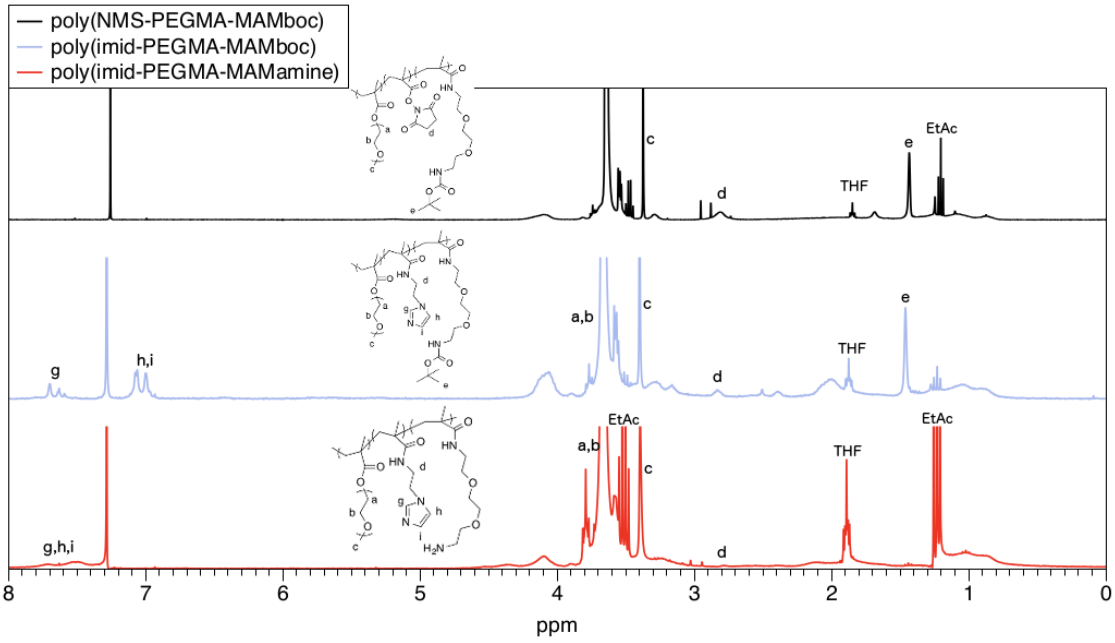


Figure 4.5: $^{1}$H-NMR spectrum of poly(NMS-PEGMA-MAMboc), poly(imid-PEGMA-MAMboc) and poly(imid-PEGMA-MAMamine) in $CDCl_3$.

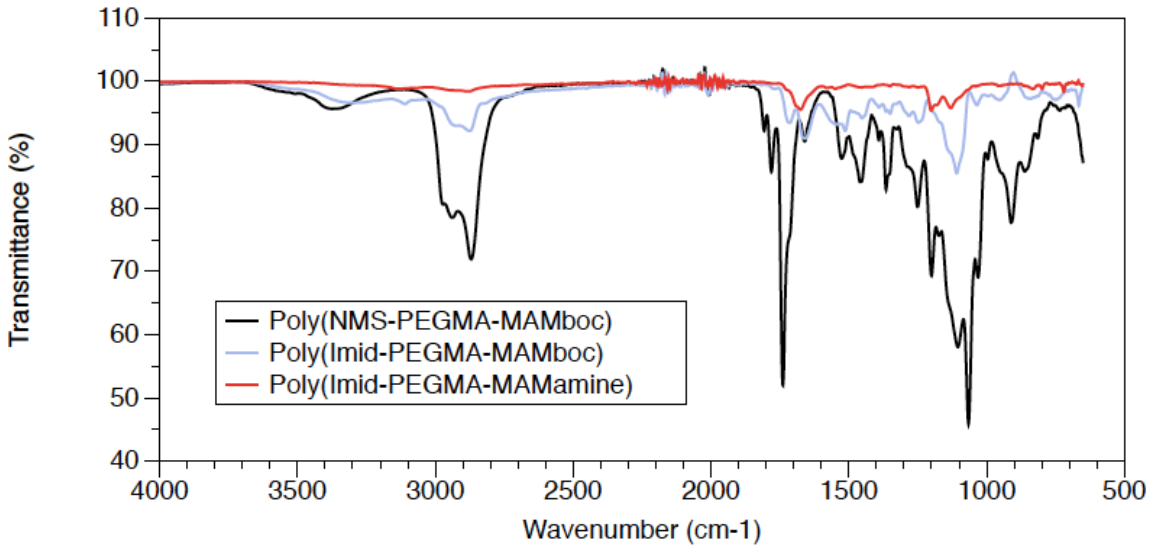


Figure 4.6: IR spectrum showing the changes in functionality at various points in the synthetic route.

### 4.3.5 CdS NWs and polymer attachment

In order to confirm the attachment of the dye-functionalized polymer to the NW substrate, the fluorescence microscopy was used to analyze the CdS NWs with a free rhodamine dye and with the dye functionalized polymer. The NW emission peak is at 510nm, and dye emission peak is at 590nm. The darkfield image displays the signal seen for the emission at 510 nm, and the fluorescence mode shows that at 590 nm. The fluorescence mode setup ensures that any signal seen is only from emission at 590 nm. Hence, in fluorescence mode, if the dye is attached to the NW, then the NW can be seen in the fluorescence image.

Figure 4.7 shows the darkfield and fluorescence mode of the free dye functionalized NWs. The darkfield image clearly shows the presence of the NW, but in fluorescence mode, the signal is very noisy and no NWs are visible. This suggests that the free dye is incapable of complexing with the NW surface. Comparatively, Figure 4.8 illustrates the darkfield and fluorescence mode of the terpolymer-dye functionalized

NWs. Again, the NWs are visible in darkfield mode, and are also clearly visible in fluorescence mode. The fluorescence mode signal (red) has a clean signal, demonstrating the presence of the dye on the NW surface. These images also signify the effect of the terpolymer ligand units in being able to complex with the NWs, as well as being able to attach the dye payload. These experiments confirm the hypothesis that a terpolymer with three discrete functionalities is capable of CdS nanowire functionalization, and paves the path for new opportunities in the optoelectronic field.

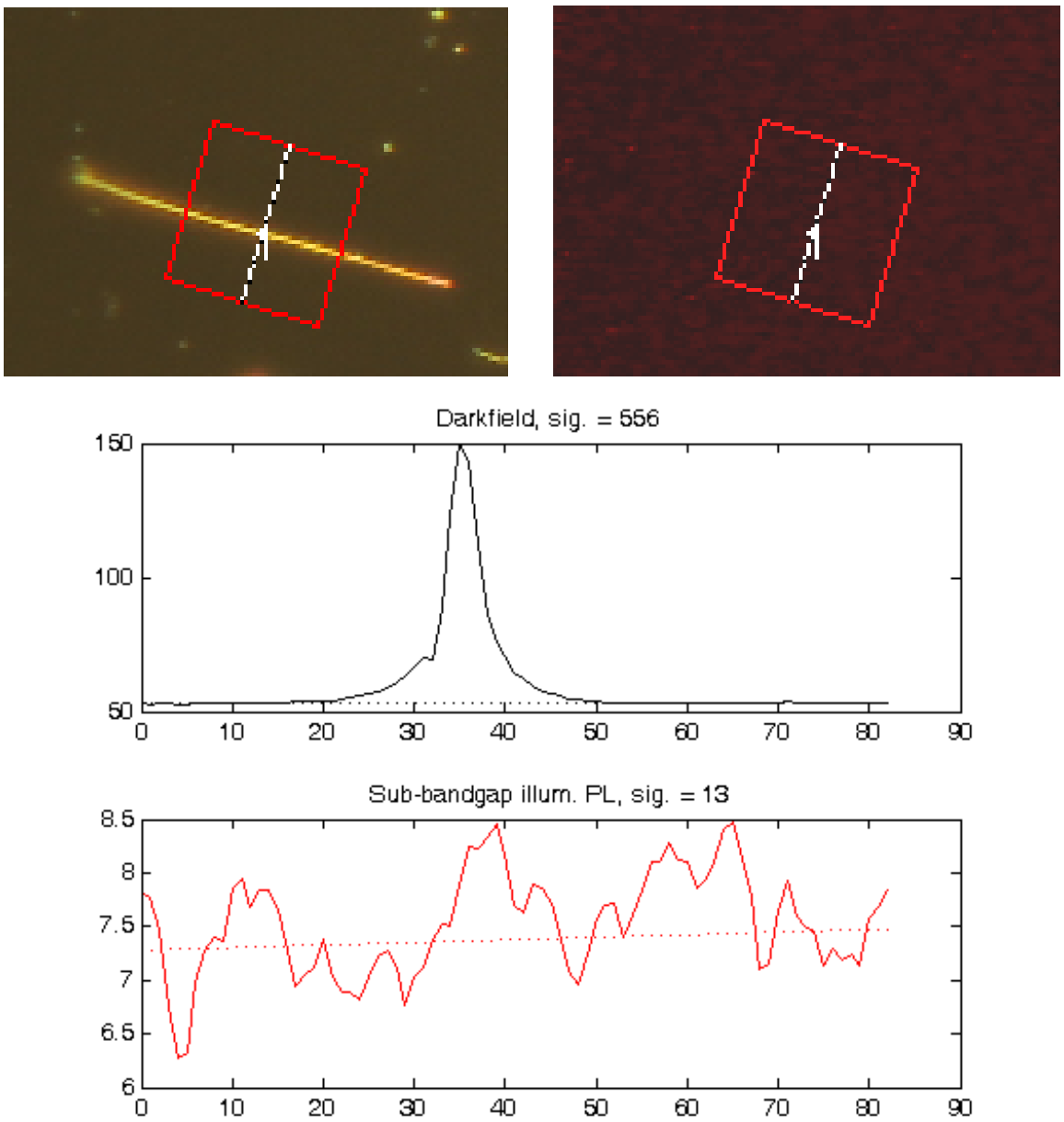


Figure 4.7: Fluorescence microscopy images of free dye attached NWs. (Top Left) NW in dark field mode and (Top Right) NWs in fluorescence mode. The corresponding darkfield signal (black) and fluorescence mode signal (red) is also shown.

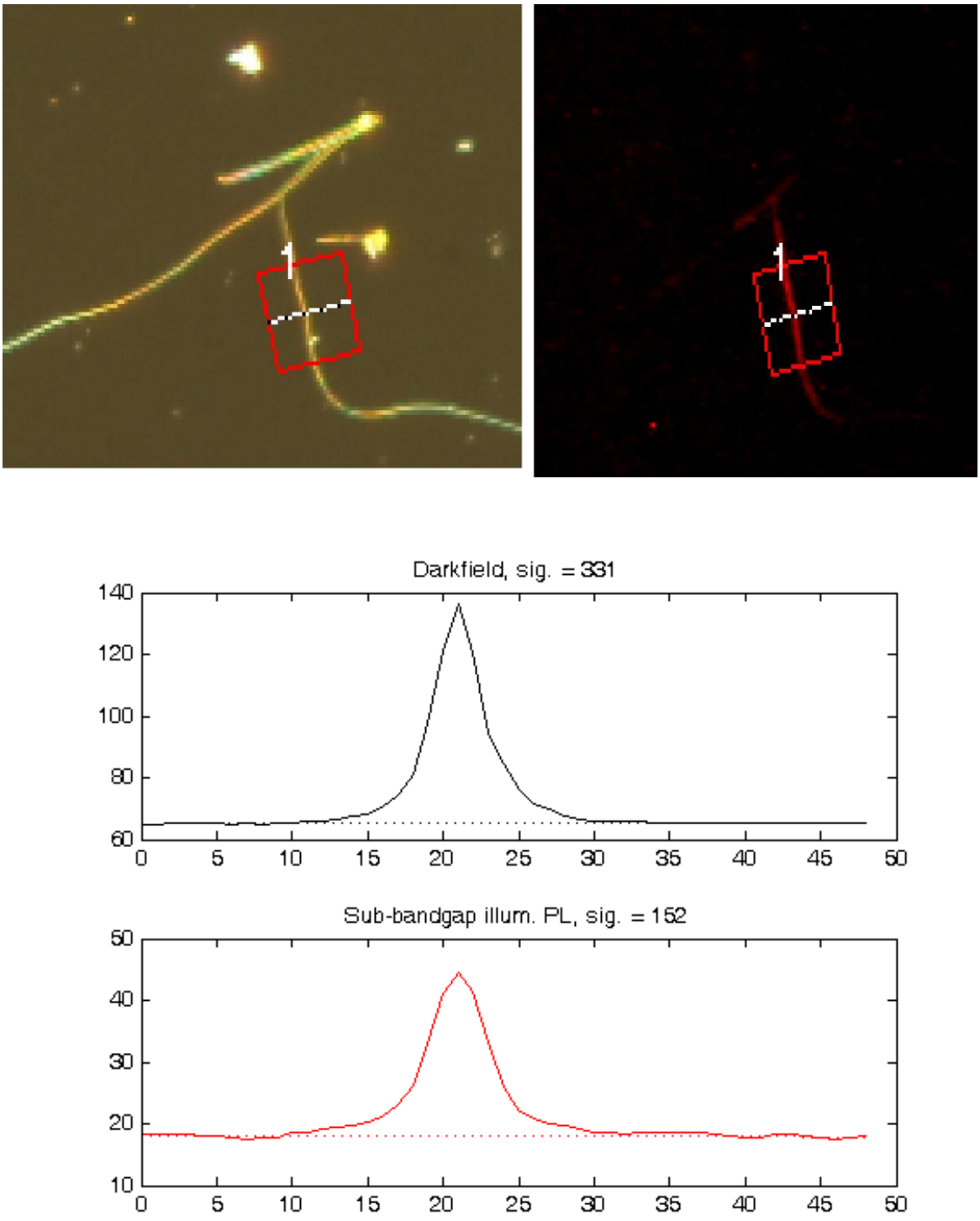


Figure 4.8: Fluorescence microscopy images of terpolymer-dye functionalized NWs. (Top Left) NW in dark field mode and (Top Right) NWs in fluorescence mode. The corresponding darkfield signal (black) and fluorescence mode signal (red) is also shown.

## 4.4 Summary

A synthetic route for the preparation of random copolymers bearing imidazole, PEG and amine groups was developed for the optical confirmation of the functionalization of CdS NWs. The versatile route of using activated esters in copolymerization was shown to incorporate unique methods of measuring copolymer composition and synthesizing a pseudo-gradient copolymer. The kinetics of the polymerization were scrutinized in detail to reveal differences in reactivities of the monomers, which play a large role in copolymer composition. Additionally, the postmodification of the succinimide groups on the terpolymer with an organic imidazole proved to be a simple and scalable synthetic method. In the final step, cleavage of the boc groups provided amines capable of attaching to rhodamine dyes. The hypothesis of terpolymer-dye based ligands being able to functionalize CdS NW surfaces was also tested and confirmed via fluorescence microscopy. The development of polymers with a high degree of control and functionality may open up new opportunities in optoelectronic applications, and lead to a better understanding of the kinetics of binding various ligand structures to nanowire substrates.

## 4.5 References


(1) Hochbaum, A. I.; Yang, P. *Chem. Rev.* **2010**, *110*, 527.

(2) Law, M.; Goldberger, J.; Yang, P. *Annual Review of Materials Research* **2004,** *34***,** 83.

(3) Duan, X.; Lieber, C. M. *Adv. Mater.* **2000**, *12*, 298.

(4) Gao, T.; Wang, T. *Cryst. Growth Des.* **2010**, *10*, 4995.

(5) Prudnikau, A.; Chuvilin, A.; Artemyev, M. *J. Am. Chem. Soc.* **2013**, *135*, 14476.

(6) Ning, Z.; Molnár, M.; Chen, Y.; Friberg, P.; Gan, L.; Ågren, H.; Fu, Y. *Phys. Chem. Chem. Phys.* **2011**, *13*, 5848.

(7) Widmer-Cooper, A.; Geissler, P. *Nano Lett.* **2014**, *14*, 57.

(8) Rajendran, V.; Lehnig, M.; Niemeyer, C. M. *J. Mater. Chem.* **2009**, *19*, 6348.

(9) Ma, N.; Sargent, E. H.; Kelley, S. O. *Nat. Nanotechnol.* **2009**, *4*, 121.

(10) Chen, S.; Zhu, J.; Shen, Y.; Hu, C.; Chen, L. *Langmuir* **2007**, *23*, 850.

(11) Li, X.; Nichols, V. M.; Zhou, D.; Lim, C.; Pau, G. S. H.; Bardeen, C. J.; Tang, M. L. *Nano Lett.* **2014**, *14*, 3382.

(12) Jang, W.; Koo, P.; Bryson, K.; Narayanan, S.; Sandy, A.; Russell, T. P.; Mochrie, S. G. *Macromolecules* **2014**, *47*, 6483.

(13) Zhang, P.; Liu, S.; Gao, D.; Hu, D.; Gong, P.; Sheng, Z.; Deng, J.; Ma, Y.; Cai, L. *J. Am. Chem. Soc.* **2012**, *134*, 8388.

(14) Liu, W.; Greytak, A. B.; Lee, J.; Wong, C. R.; Park, J.; Marshall, L. F.; Jiang, W.; Curtin, P. N.; Ting, A. Y.; Nocera, D. G.; Fukumura, D.; Jain, R. K.; Bawendi, M. G. *J. Am. Chem. Soc.* **2010**, *132*, 472.

(15) Petryayeva, E.; Krull, U. J. *Langmuir* **2012**, *28*, 13943.

(16) Greytak, A. B.; Allen, P. M.; Liu, W.; Zhao, J.; Young, E. R.; Popović, Z.; Walker, B. J.; Nocera, D. G.; Bawendi, M. G. *Chem. Sci.* **2012**, *3*, 2028.

(17) Hoarfrost, M. L.; Segalman, R. A. *Macromolecules* **2011**, *44*, 5281.

(18) Petryayeva, E.; Algar, W. R.; Krull, U. J. *Langmuir* **2013**, *29*, 977.

(19) Shunmugam, R.; Tew, G. N. *J. Polym. Sci. Part A Polym. Chem.* **2005**, *43*, 5831.

(20) Li, Y.; Tao, P.; Viswanath, A.; Benicewicz, B. C.; Schadler, L. S. *Langmuir* **2013**, *29*, 1211.

(21) Tao, P.; Li, Y.; Rungta, A.; Viswanath, A.; Gao, J.; Benicewicz, B. C.; Siegel, R. W.; Schadler, L. S. *J. Mater. Chem.* **2011**, *21*, 18623.

(22) Akcora, P.; Liu, H.; Kumar, S. K.; Moll, J.; Li, Y.; Benicewicz, B. C.; Schadler, L. S.; Acehan, D.; Panagiotopoulos, A. Z.; Pryamitsyn, V.; Ganesan, V.; Ilavsky, J.; Thiyagarajan, P.; Colby, R. H.; Douglas, J. F. *Nat. Mater.* **2009**, *8*, 354.

(23) Allen, M. H.; Hemp, S. T.; Smith, A. E.; Long, T. E. *Macromolecules* **2012**, *45*, 3669.

(24) Luo, C.; Liu, Y.; Li, Z. *Soft Matter* **2012**, *8*, 2618.

(25) Alb, A. M.; Enohnyaket, P.; Drenski, M. F.; Shunmugam, R.; Tew, G. N.; Reed, W. F. *Macromolecules* **2006**, *39*, 8283.

(26) Yanjarappa, M. J.; Gujraty, K. V; Joshi, A.; Saraph, A.; Kane, R. S. *Biomacromolecules* **2006**, *7*, 1665.

# CHAPTER 5

# POLYMER ANCHORED SILICA PARTICLES: SYNTHESIS AND USAGE IN ENVIRONMENTALLY FRIENDLY FRACTURING FLUIDS

## 5.1 Introduction

Hydraulic fracturing, or fracturing, has recently seen a surge in its application to newly minted oil and gas fields. Although the technology has been known for several decades, recent improvements in the technology has made it economically feasible to extract oil and gas "horizontally", as opposed to the more common vertical drilling for oil recovery. Its adoption is more pronounced in U.S., where more than 1.1 million active oil and gas wells span across 36 states.[1] There are, however, several difficulties in oil recovery, and in particular, the location of the gas in the shale deposits at depths of several thousand feet.[2]

A hydraulic fracture is created when fluids are pumped for short period (2-3 hours), and the resulting high pressure (high viscosity of the mixture) exceeds the rock formation strength and a fracture is created.[3] Materials known as proppants (small particles or sand) are pumped into the fractures as a component of the fracturing fluid. The high viscosity of the mixture ensures that no settling behavior of the proppant occurs, which is important for the prevention of fines, or clogged networks.[4] The proppant remains in the fracture as permeable networks to keep the fracture open for oil recovery.

The conductive pathways formed allow the oil in the opened shale formations to flow into the wellbore, which enables oil recovery at high rates.[5] One issue of concern is the leftover fracturing fluid - it needs be evacuated from the established networks after oil recovery is completed.[6,7] Typically, established methods involve chemical or thermal decomposition, followed by its recovery into the well. However, the cleanup procedures vary between drilling companies, and effective methods of monitoring this step are uncertain.

Fracturing fluids typically contain a variety of additives that essentially aid the following properties: (a) enable fracture formation, (b) carry the proppants to the fracture zone and (c) maintain good conductivity such that the networks formed do not collapse/clog. These additives include viscosifiers (high molecular weight polymers), biocides, corrosion inhibitors, crosslinkers, friction reducers, gelling agents, scale inhibitors, surfactants and pH control agents.[8] The exact recipe for the fracturing fluid varies depending on the type and depth of the shale formation, borehole geometry and the amount of recoverable gas as well. However, two main ingredients are an absolute necessity: friction reducers and proppant materials.

The amount of friction reducing materials, typically high molecular weight (MW) polymers range from 0.05-1% of the fracturing fluid mixture; these materials are often known to impart ‘slickwater’ characteristics to the fluid.[9] Friction exists between the fluid and the contact surface of the steel pipe and in the water itself (turbulence) when the fluid is pumped. Extra pressure can overcome this friction, and friction reducers are added to the water to maintain non-turbulent flow during the pumping step.[8] In the absence of the friction reducer, the surface pressure would be higher than needed to reach the required

pump rate, and can increase operational costs. Friction reducers typically involve a high molecular weight polyacrylamide polymer. In the presence of water, the polyacrylamide hydrates and its hydrodynamic radius increases, resulting in the lack of turbulence in the moving water. Polyacrylamides are generally available as a dry powder, and are mixed with a mineral oil base fluid for stabilization of the mixture prior to its addition to the water for pumping. This water-soluble polymer does not degrade easily and its monomer unit (acrylamide) is known as a toxic contaminant (neurotoxin) when found in ground water.[10]

Proppants are solid materials (treated sand or ceramic structures) that can aid in keeping the fracture open during the operation. The type and structure of sand used can play a large role in maintaining flow of the fluids through the fractures. Untreated sand can cause significant fines to be generated (due to crushing of the sand at high pressure), which are smaller particulates that do not maintain the fracture opening.[11,12] There has been a shift towards chemically treated sand, especially where sands can be treated to be both lightweight (to prevent settling) and high strength (to avoid being crushed).

Given the surge in the adoption of fracturing as a vital source of energy, there has been a spotlight on the environmental concerns related to its operation. Once the pressure is released after pumping, about 60% of the fluid returns to the wellbore and can be consequently reused.[13] It has also been noted that more of the fluid can be obtained slowly over a period of weeks. Since close to 4 million gallons of fluid is used per well, several thousand gallons of chemical fluid remains in the fracture strata.[14] Additionally, it must be noted that these retained fluids can slowly migrate to the surface though other channels, and may pose a significant environmental problem.[8,9,13] More importantly, the

chemical additives in the fluid can leak into the water table, and pose an alarming environmental concern.[9,13,15,16] The EPA is currently investigating several sites and water sources close to the drilling area, and there is a lot of controversy whether chemical leakage from fracturing fluids is possible. Nevertheless, if any potential leakage occurs, the treatment of water becomes significantly more complicated if needed for human consumption. Hence, it is in the interest of the industry to have solutions that directly address this issue and minimize the risk in a cost-effective manner.

Addressing the concern of chemical leakage of polymeric additives in the fracturing fluid with the development polymer functionalized substrates, we proposed a potential solution that utilized both the polymeric additives and the proppant (silica) in fracturing fluids. By anchoring the polymeric additive to a large substrate, we hypothesized that this would hinder any potential migration of the polymer in the rock strata. As the proppants are silica based materials, our hypothesis provides the development of an optimized proppant where the chemically treated sand is further modified with the polymeric additive. Essentially, the concept to be tested is simple - will the polymer functionalized proppant prevent migration of the polymer as opposed to the free polymer through a layer of soil?

The following sections will discuss the synthetic methods for the development of polymer functionalized silica particles (5.5 um). A variety of functionalization methods were tested including grafting from/to, varying types of polymers and controlled radical polymerization/free radical methods. The migration of the polymers was also analyzed through retention efficiency tests, and revealed the crucial role played by effective surface functionalization methods.

## 5.2 Experimental

### 5.2.1 Materials

All reagents were used as received from Fisher Scientific unless stated otherwise below. AIBN was purchased from Sigma Aldrich and recrystallized thrice from methanol. Poly(ethyleneglycol) methacrylate (500 g/mol) was obtained from Sigma Aldrich and passed through a neutral alumina column to remove inhibitors before use. 4-Cyano-4 [(dodecylsulfanylthiocarbonyl)sulfanyl]pentanoic acid (CDTPA) and 2-(Dodecylthiocarbonothioylthio)-2-methylpropanoic acid (DTDMA) were obtained from Strem Chemicals, Inc. NMS (N-methacryloxy succinimide) was synthesized from NHS (N-hydroxy succinimide) as described in the literature. Silica Particles (Syloid FP 244, ~5.5 um) were obtained from W. R. Grace & Co. Acrylamide was recyrstallized from acetone, and acrylic acid was purified by passing through a neutral alumina column prior to use. Activated 4-cyanopentanoic acid dithiobenzoate (CPDB) was prepared according to established procedures in the literature.[17] 3-Aminopropyldimethylethoxysilane was purchased from Gelest and used as received.

### 5.2.2 Characterization

NMR spectra were recorded on a Varian Mercury 300 spectrometer using $CDCl_3$ or $D_2O$ as the solvent. UV-vis absorption spectra were recorded on a Perkin Elmer Lambda 4C spectrophotometer.

### 5.2.3 Synthesis of Activated CDTPA

4-Cyano (dodecylsulfanylthiocarbonyl)sulfanylpentanoic acid (1 g, 2.48 mmol), 2-mercaptothiazoline (0.295 g, 2.48 mmol), and dicyclohexylcarbodiimide (DCC) (0.613 g, 2.97 mmol) were dissolved in 20 mL of dichloromethane. (Dimethylamino)pyridine (DMAP) (30 mg, 0.25 mmol) was added slowly to the solution under ice, which was stirred at room temperature overnight under nitrogen. The solution was filtered to remove the salt. After removal of solvent and silica gel column chromatography (5:4 mixture of hexane and ethyl acetate), activated trithiocarbonate, was obtained as a yellow oil (68% yield). $^{1}$H-NMR (300 MHz, $CDCl_3$): δ (ppm) 4.59 (t, 2H), 3.57 (t, 2H), 3.33 (t,2H), 2.57-2.67 (quin, 2H) 2.43-2.53 (t, 2H), 2.05 (s, 3H), 1.65-1.74 (m, 2H), 1.23-1.29 (m, 16H), 0.88 (t, 3H).

### 5.2.4 Synthesis of activated DTDMA

2-(Dodecylthiocarbonothioylthio)-2-methylpropanoic acid (1g, 2.743 mmol) 2-mercaptothiazoline (0.326 g, 2.743 mmol), and dicyclohexylcarbodiimide (DCC) (0.679 g, 3.291 mmol) were dissolved in 15 mL of dichloromethane. (Dimethylamino)pyridine (DMAP) (33.5 mg, 0.274 mmol) was added slowly to the solution under ice, which was stirred at room temperature overnight under nitrogen. The solution was filtered to remove the salt. After removal of solvent and silica gel column chromatography (1:1 mixture of hexane and ethyl acetate), activated DTDMA, was obtained as a yellow oil (0.85g, 66.5% yield). $^{1}$H-NMR (300 MHz, $CDCl_3$): δ (ppm) 4.59 (t, 2H), 3.58 (t, 2H), 3.26 (t, 2H), 2.57-2.67 (quin, 2H), 2.05 (s, 3H), 2.03 (s, 3H), 1.23-1.4 (m, 18H), 0.89 (t, 3H).

### 5.2.5 Preparation of Amino-functionalized Syloid

A suspension of syloid particles (2.0 g) in THF (20 ml) was added to a three-necked round-bottom flask with 3-aminopropyldimethylethoxysilane (0.60 µl) and THF (80 mL). The reaction mixture was heated under an oil bath temperature of 75˚C with $N_2$ protection overnight and then cooled to room temperature. The reaction mixture was precipitated into a large amount of hexanes (500 mL, ACS Reagent). The particles were recovered by centrifugation at 3000 rpm for 15 min. The particles were then redissolved in 20 mL of THF and reprecipitated in 100 mL of hexanes. The centrifugation-redispersion step was repeated once more, and the amino functionalized particles were dispersed directly into 50 mL of THF and used directly for the next modification.

### 5.2.6 Preparation of Syloid-CDTPA

A THF solution (20 mL) of the high surface density amino-functionalized syloid (1.8 g, 0.319 mmol of anime groups) was added dropwise to a THF solution (10 mL) of activated 4-cyano-4 [(dodecylsulfanylthiocarbonyl)sulfanyl]pentanoic acid (CDTPA) (0.18 g, 0.351 mmol) at 0˚C. After complete addition, the solution was stirred overnight at room temperature under nitrogen. The reaction mixture was then precipitated into a large amount of 4:1 mixture of cyclohexane and ethyl ether (200 mL). The particles were recovered by centrifugation at 3000 rpm for 15 min. The particles were then redissolved in 20 mL of THF and reprecipitated in 4:1 mixture of cyclohexane and ethyl ether. This dissolution-precipitation procedure was repeated another two times until the supernatant layer after centrifugation was colorless. The syloid particles were dried under vacuum at

room temperature for 1 hr and subjected to analysis by UV. The particles had a grafting density of 36.26 μmol/g.

### 5.2.7 Preparation of Syloid-DTDMA

A THF solution (100 mL) of the high surface density amino-functionalized syloid (2g, 0.266 mmol of anime groups) was added dropwise to a THF solution (10 mL) of activated DTDMA (0.136 g, 0.2926 mmol) at 0˚C. After complete addition, the solution was stirred overnight at room temperature under nitrogen. The reaction mixture was then precipitated into a large amount of hexanes (200 mL). The particles were recovered by centrifugation at 3000 rpm for 15 min. The particles were then redissolved in 20 mL of THF and reprecipitated in hexanes (200 mL). This dissolution-precipitation procedure was repeated another two times until the supernatant layer after centrifugation was colorless. The yellow syloid particles were dried under vacuum at room temperature for 1 hr and subjected to analysis by UV. The particles had a grafting density of 40.8 μmol/g.

### 5.2.8 Acrylamide Graft Polymerization from CDTPA Anchored Syloid

CDTPA agent anchored syloid (0.050 g, 36.36 μmol/g), DMSO (3 mL), acrylamide (0.5 g, 6.94 mmol) and trioxane (25 mg, internal standard) were added to a 15 mL Schlenk tube followed by sonication and addition of AIBN (69 μL of 10 mM DMSO solution). The tubes were subjected to three cycles of freeze-pump-thaw to remove oxygen. They were then placed in an oil bath preset to 70 °C for various intervals. The polymerizations were stopped by quenching the tubes in ice water, and the polymerization mixtures were precipitated into acetone. The polymer was collected by centrifugation of the acetone mixture at 3000 rpm for 5 min. NMRs of the reaction

mixture were taken both prior to and directly after the polymerization to calculate conversion. A monomer conversion of 34% was reached after 23 h.

### 5.2.9 Acrylamide polymerization using free DTDMA in solution

DTDMA (0.01 g, 0.0274 mmol), DMSO (3.948 mL), acrylamide (0.987 g, 13.7 mmol) were added to a 25 mL Schlenk tube followed the addition of ACVA (822 µL of 10 mM DMSO solution) and trioxane (25mg). The tubes were subjected to three cycles of freeze-pump-thaw to remove oxygen. They were then placed in an oil bath preset to 70 °C for various intervals. The polymerizations were stopped by quenching the tubes in ice water, and the polymerization mixtures were sampled for NMR analysis, followed by precipitation into acetone. The polymer was collected by centrifugation of the acetone mixture at 3000 rpm for 5 min.

### 5.2.10 General Procedures for Cleaving Grafted Polymer from Syloid

Polyacrylamide (PAM) grafted syloid particles (100 mg) was dissolved in 3 mL of DMSO. Aqueous HF (49%, 0.2 mL) was added, and the solution was allowed to stir at room temperature overnight. The solution was poured into a PTFE Petri dish and allowed to stand in a fume hood overnight to evaporate the volatiles.

### 5.2.11 Preparation of CPDB Anchored Syloid

Activated CPDB was prepared as outlined in the literature,[17] and was attached in a similar fashion as described in procedure 5.2.5. Grafting densities of CPDB on the syloid particles ranged from 60-142 µmol/g.

### 5.2.12 Graft Polymerization of Acrylic Acid from CPDB anchored Syloid

In a dried Schlenk tube, CPDB anchored syloid (0.50 g, 30.56 μmol/g) was dissolved in DMF (14 mL) along with a minimal amount of trioxane (5 wt% of monomer). Acrylic acid (13.84 mL) and AIBN (152 μL, 0.01M in DMF) were then added to the tube. The mixture was degassed by three freeze-pump-thaw cycles, back filled with nitrogen, and then placed in an oil bath preset at 65˚C. The polymerization was quenched by submersion of the reaction vessel in ice water. The polymer solution was precipitated into ether, and redispersed in DMF. The precipitation-redispersion process was repeated once more to obtain poly(acrylic acid) functionalized syloid.

### 5.2.13 Polymerization of poly(NMS-PEGMA)

In a dried Schlenk flask, CDTPA (0.005 g, 0.0124 mmol) was dissolved in DMF (0.127 mL). To this solution was added N-methacryloxy succinimide (NMS) (0.034g, 0.186 mmol), PEGMA (Mn: 500 g/mol, 0.093g, 0.1858 mmol) and AIBN (310 μL, 0.01M in DMF). The mixture was degassed by three freeze-pump-thaw cycles, back filled with nitrogen, and then placed in an oil bath preset at 65$^{o}$C. The polymerization was quenched by submersion of the reaction vessel in ice water. The polymer solution was precipitated into ether, and redispersed in DMF. The precipitation-redispersion process was repeated once more to obtain poly(NMS-PEGMA) with Mn: 17687 g/mol and PDI of 1.27.

### 5.2.14 Grafting-to Procedure for PEG Functionalized Syloid

Amine functionalized syloid (82.5 mg, 136.6 μmol/g) was dispersed in THF (2 ml) in a round bottom flask, followed by the addition of triethylamine (17.1 mg, 0.17

mmol). The mixture was purged with nitrogen for 10 min, and the poly(NMS-PEGMA) (17687 g/mol, 0.186 mmol of NMS) in 1 ml THF was added via a syringe. The flask was attached to a condenser, purged for 10 min, and then stirred at a 70˚C oil bath overnight. The mixture were diluted with THF (10 ml) and then centrifuged at 3000 rpm for 5 min. The particles were recovered and then dried under vacuum for 2 h to obtain PEG functionalized syloid.

### 5.2.15 Preparation of activated ACVA

4,4′-Azobis(4-cyanovaleric acid) (20g, 35.679 mmol) was dissolved in 400 ml of 1,4-dioxane in a 1000 ml round bottom flask. 2-Mercaptothiazoline (22.58g, 188.38 mmol) and 4-dimethyl aminopyridine (0.5g, 4.07 mmol) were added and the mixture was stirred until complete dissolution of the mixture was observed. The mixture was cooled to 0˚C, and in a separate 500 ml beaker, N,N'-dicyclohexylcarbodiimide (34g, 164.84 mmol) was stirred in 100 ml of 1,4-dioxane until a cloudy suspension was observed. The carbodiimide solution was added dropwise to the mixture in the round bottom flask at 0˚C via a seperatory funnel. The mixture was stirred overnight, and then filtered, followed by removal of the solvent through rotary evaporation. The yellow solid was then purified through recrystallization in a 70% hexane/ethyl acetate mixture (31.5g, 91.6% yield). $^{1}$H-NMR (300 MHz, $CDCl_3$): δ (ppm) 4.59 (t, 2H), 3.30 (t, 2H), 3.12-3.63 (m, 2H), 2.41-2.64 (m, 2H), 1.75 (s, 3H).

### 5.2.16 Preparation of azo-functionalized Syloid

A THF solution (50 mL) of the bare syloid particles (0.5 g) was mixed in a 200 ml round bottom flask and stirred for 10 min. 3-Aminopropylsilane (50µl, 0.265 mmol) was

added to the mixture and the flask was equipped to a condenser and purged with $N_2$. The mixture was refluxed overnight under $N_2$. The mixture was diluted with 100 ml of THF and then centrifuged at 3000 rpm for 5 min. The particles were isolated and suspended in 50 ml of THF. The centrifugation-redispersion process was repeated two more times, and in the final step, the isolated particles were stored as a dichloromethane (DCM) solution (20 ml).

Activated ACVA (0.128g, 0.266 mmol) was dissolved in THF (7 ml) added to the amino functionalized Syloid in DCM (20 ml) at 0˚C. After complete addition, the solution was stirred overnight at room temperature under nitrogen. The reaction mixture was then diluted into a large amount of THF (100 mL). The particles were recovered by centrifugation at 3000 rpm for 15 min. The particles were then resuspended in 100 mL of THF. This centrifugation-dilution procedure was repeated another two times until the supernatant layer after centrifugation was colorless. The yellow azo functionalized syloid particles were then dried in the oven for 1h, and then stored in the freezer in an air-tight container.

### 5.2.17 Polymerizations using azo functionalized Syloid

In a dried Schlenk tube, azo anchored syloid (0.05 g) was dissolved in THF (2 mL). Methyl methacrylate (MMA) (2 mL) was then added to the tube. The mixture was degassed by three freeze-pump-thaw cycles, back filled with nitrogen, and then placed in an oil bath preset at 65˚C. The polymerization was quenched by submersion of the reaction vessel in ice water. The polymer solution was precipitated into hexanes, and

redispersed in THF. The precipitation-redispersion process was repeated once more to obtain poly(methyl methacrylate) functionalized syloid.

For the polymerization of styrene, the above reaction was used with the same ratio of reactants, but MMA was substituted with styrene (2 mL). The polymer solution was precipitated into methanol, and redispersed in THF. The precipitation-redispersion process was repeated once more to obtain poly(styrene) (PSt) functionalized syloid. The polymer functionalized syloid was then subjected to cleavage of the polymers according to the procedure in 5.2.10. GPC analysis of the cleaved PMMA provided Mn: 342k, PDI: 2.12 and that of the cleaved PSt with Mn: 681k, PDI: 2.81.

### 5.2.18 Filtration Procedure

Filter columns were made with a plug of cotton, sand (1 mm) and filter material (4 cm) in a Fisherbrand$^{TM}$ Disposable Borosilicate Glass Pasteur Pipette (length: 5.75 in., 146 mm). Filter materials used include Syloid particles, silica gel (70-200 um), and diatomaceous earth. A typical method involved the dissolution of the sample (14-78 mg) in water (1 ml) and its addition to the column to be filtered into a vial. The vial was then freeze-dried to calculate the mass of its contents. All experiments involved three sets of samples including the control (1 ml of water), free polymer (for PAA, Mn: 1800 g/mol) and Syloid-polymer. Retention efficiencies were calculated based on the amount of Syloid-polymer and free polymer had passed through the column compared to the original amounts of each used. A retention efficiency of 0% for the free polymer indicated that all of the free polymer had passed through the column. Conversely, a retention efficiency of 100% for the Syloid-polymer indicated that none of the Syloid-

polymer had passed through the column. All filtration tests were accompanied with a control test, where water (1 mL) was passed through the same mass of the filter material in a separate piptette. As some of the filter material managed to pass through the cotton plug, the mass of the filter material in the vial (after freeze-drying) was calculated and compared with the run with syloid-polymer/polymer. This control test was used to recalculate an adjusted retention efficiency, which accounts for any filter material that passes through the cotton plug.

### 5.2.19 Filtration Procedure (Extended Wash)

In order to simulate real world conditions, extended washing procedures were tested to see the retention efficiency after several additions of water to the column. In this procedure, samples were dissolved in water (2 ml), passed through the column, and followed up with two separate additions of water (1 ml) each. Similar to the procedure outlined above, each experiment included a control (2 ml of water), and the free polymer and syloid-polymer respectively.

## 5.3 Results and Discussion

The controlled radical polymerization of poly(acrylic acid) on silica particles has been well documented[18], but comparative examples with poly(acrylamide) are limited in the literature. One of the main reasons includes difficulty in handling of the poly(acrylamide), as it is soluble only in water and in select cosolvent mixtures. Poly(acrylic acid) can be postmodified using the acid functionality to enable solubility in a variety of solvents. As both polymers have usage as components in fracturing fluids, there was a need to develop procedures for their functionalization onto silica particles.

The functionalization of the silica was performed based on procedures developed by our group for Nissan silica particles.[17] As the silica used in the fracturing application required larger sizes to behave as proppant materials, Syloid FP 244 (Grace) was chosen as an appropriate substrate. The syloid had several advantages over other commercial silica particles, including porosity (lower density and solvent absorption), ease in handling (good dispersion in solvent without clumping) and the presence of hydroxyl groups on the surface to enable further modification of the syloid. Untreated crystalline silica, for e.g. MIN-U-SIL® (U.S. Silica) did not permit chemical modification of the surface using silanes.

Although several groups have investigated the attachment of poly(acrylic acid) and poly(acrylamide) on substrates[18–20], the usage of such techniques to investigate their usage for "greener" fracturing fluids has not been reported. Furthermore, a comprehensive study for the functionalization of silica using both grafting-to and grafting-from methods for the purpose of measuring migration of free polymer versus that of the substrate anchored polymer was essential for the goals of this work. Hence, the following sections provide an analysis of the synthetic steps needed for polymer functionalization, as well as the migration studies of the polymer in materials similar to the fracture zone.

### 5.3.1 Anchoring of the RAFT agent to Syloid particles

The attachment of RAFT agents to the particle surface enables the synthesis of polymer functionalized silica through the grafting-from method. Two different RAFT agents were used for surface functionalization, including a dithiocarbonate (CPDB) and a

trithiocarbonate (CDTPA). Both RAFT agents are similar in the nature of the R group, but differ in the Z group structure. CPDB has a phenyl group for stabilization of the C=S bond, as compared to the S-alkyl group for CDTPA. The additional sulfur group in CDTPA is reported to provide improved control (lower polydispersities) and less significant retardation in the polymerization of acrylamides as compared to CPDB.[21] When free CPDB was utilized for the polymerization of acrylamide at 65˚C, degradation of the pink CPDB to an orange color was seen, which suggested the formation of intermediate thiol based compounds. Furthermore, the decomposition of the RAFT agent was accompanied with a lack of polymerization in the reaction mixture. It has been established that acrylamides can decompose to form ammonia, which can play a role in the decomposition of CPDB.[21] Usage of the trithiocarbonate (CDTPA) alleviates this problem due to its higher hydrolytic stability. In this study, CPDB was utilized for its ability to polymerize acrylic acid, and CDTPA was used for the preparation of acrylamide based polymers due to its improved control over that monomer system.

The commercially available CPDB and CDTPA with acid functionalities were converted to an activated group using mercaptothiazoline via DCC coupling. Amino functional syloid was prepared by refluxing the syloid with aminosilane, followed by its reaction with the activated RAFT agents (Scheme 5.1 shows the reaction with activated CPDB). This reaction with CPDB has been well established by our group using silica nanoparticles. As the C=S bond of the CPDB absorbs in the UV at ~300 nm, calibration curves from previous procedures[17] were used to calculate the grafting density, and ranged from 60-142 μmol/g.

The reaction of the amino functionalized syloid with activated CDTPA was similar to that with activated CPDB, where the activated CDTPA is added dropwise to a stirring mixture of the amino-syloid (Scheme 5.2). However, for the syloid-CDTPA system, the C=S displayed an absorbance (max) peak at 308 nm (Figure 5.1). Hence, a new calibration curve for CDTPA was designed by analyzing the absorbance characteristics for the free CDTPA at various concentrations (Figure 5.2). Using the calibration curve in Figure 5.3, grafting densities were calculated ranging from 36-128 µmol/g.

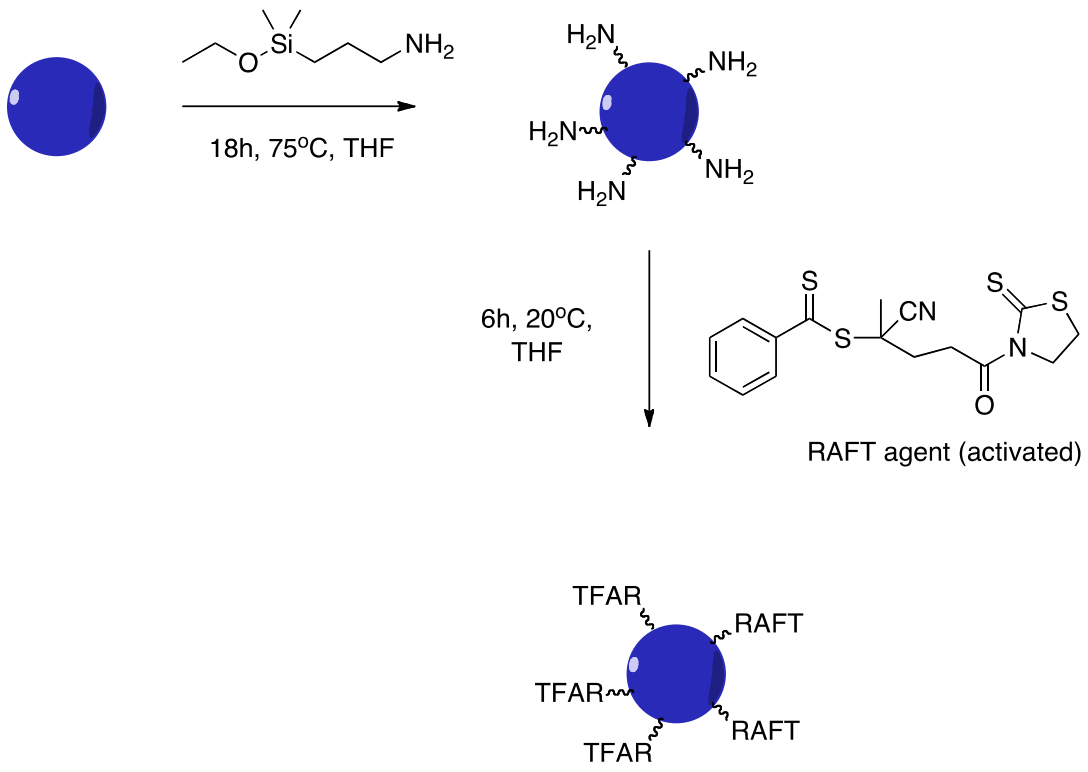


Scheme 5.1: Preparation of amine functionalized syloid particles and its corresponding modification with activated CPDB.

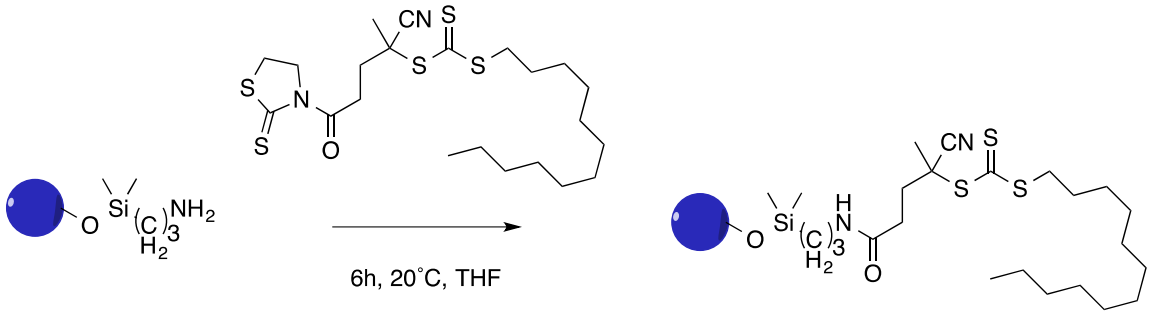


Scheme 5.2: Preparation of CDTPA functionalized syloid particles using activated CDTPA.

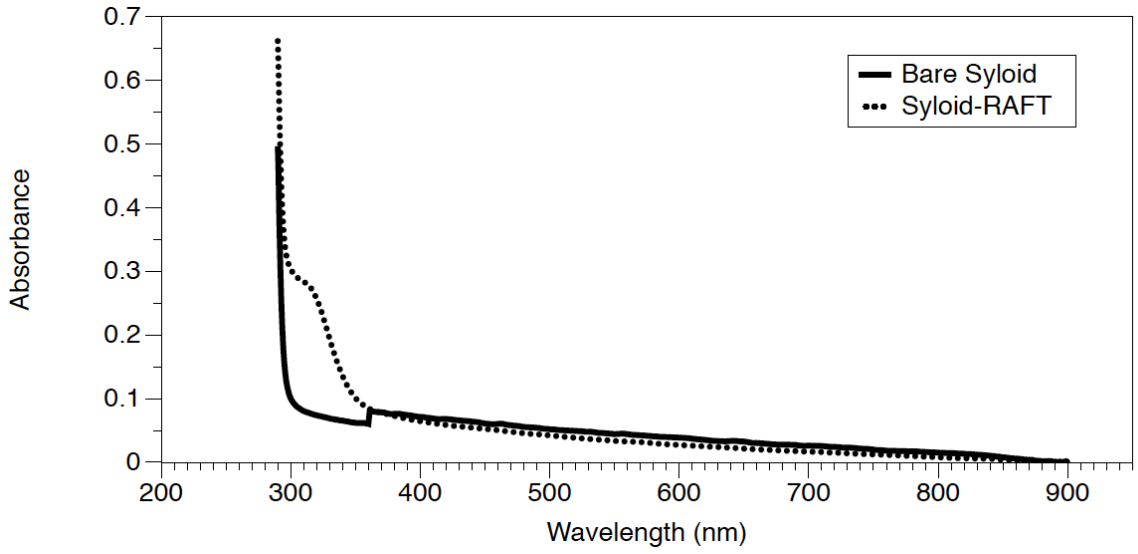


Figure 5.1: UV absorption spectra of the bare syloid and Syloid-CDTPA showing the presence of RAFT at 308 nm.

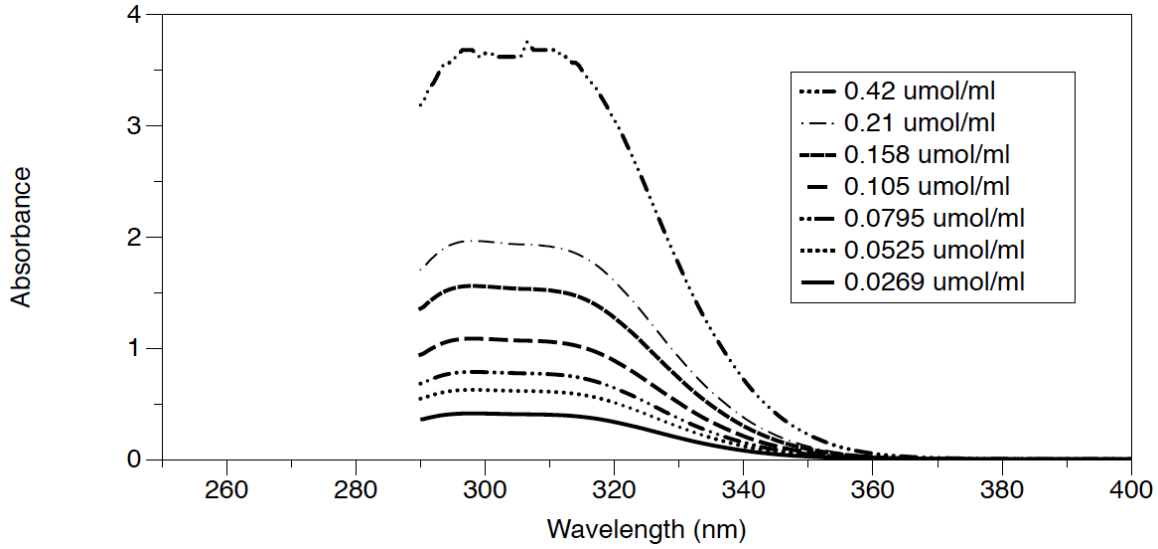


Figure 5.2: UV absorption curves of CDTPA at various concentrations.

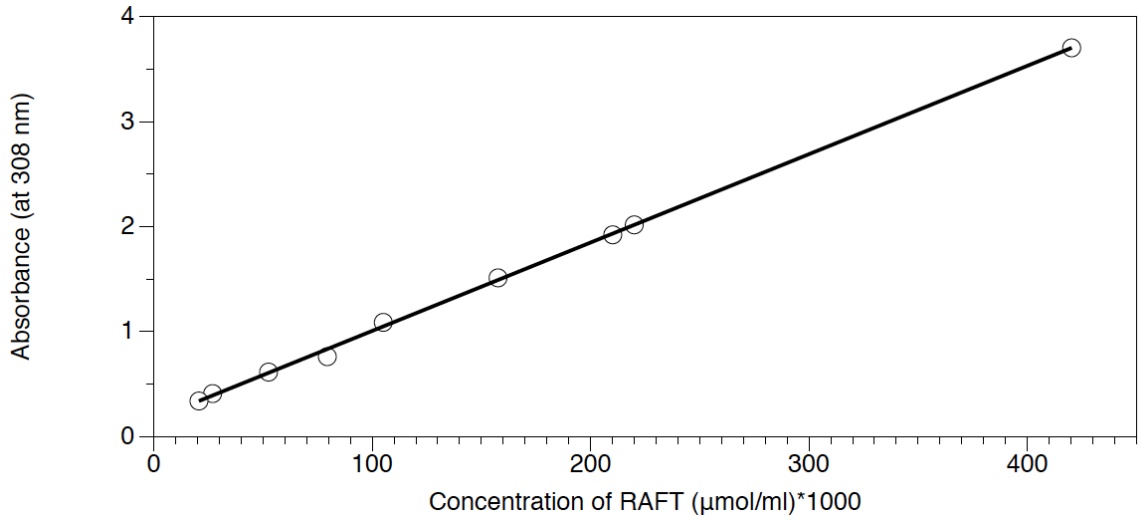


Figure 5.3: UV calibration curve of CDTPA for the calculation of grafting densities.

### 5.3.2 Polymerizations using RAFT functionalized Syloid

For polymerizations involving acrylic acid and acrylamide, trioxane was added as an internal standard in order to measure conversions. This provided a convenient method to calculate conversion for the syloid-anchored polymerizations. The trioxane peak

occurs at 5.13 ppm, and an NMR of the polymerization mixture at t=0 is obtained which integrations from 5.1-5.2 ppm and the monomer peak range. At various times, the NMR of the polymerization mixture is obtained and the exact integration as done in t=0 is performed. The comparison of integrations of the monomer regions relative to the trioxane peak before and after polymerization allows for the calculation of conversion. The GPC analysis of these polymers could not be measured due to the limited solubility of these polymers in THF using the existing GPC setup. Thus, conversions measured by NMR provided a means to calculate the conversions by comparing the vinyl peaks of acrylic acid and acrylamide with that of trioxane before and after the polymerization.

For the polymerization of acrylic acid using CPDB, this has been extensively documented in other studies.[22] Molecular weights ranging from 120k-200k were obtained by tuning the polymerization time and the CPDB: acrylic acid ratio (Table 5.1 and Scheme 5.3).

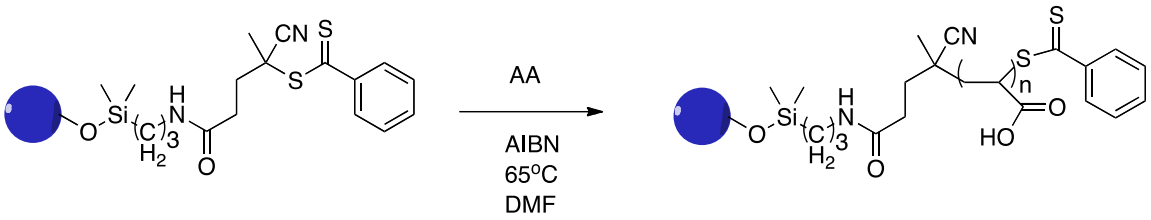


Scheme 5.3: Polymerization of Syloid-CPDB to obtain Syloid-Poly(Acrylic acid).

Table 5.1: Polymerizations of Syloid-CPDB using acrylic acid at various reaction conditions and grafting densities.

| Time (h) | Conv (%) | Temp. (˚C) | Monomer | Graft density (umol/g) | Monomer (eq) | Solvent | Mn (NMR) |
|---|---|---|---|---|---|---|---|
| 41.5 | 10.6 | 68 | AA | 102.99 | 20000 | DMF | 120k |
| 30.5 | 21.68 | 70 | AA | 138.01 | 12800 | DMF | 200K |
| 24 | 13.1 | 70 | AA | 138.01 | 15000 | DMF | 140k |

Acrylamide polymerizations were performed with the CDTPA functionalized silica, and molecular weights were measured by NMR using trioxane as the internal standard. Ideal conditions involved polymerizations at 70-75˚C with DMSO as the solvent for polymerization (Table 5.2 and Scheme 5.4). Although examples of syloid-PAM were demonstrated using CDTPA, one issue of concern related to the inability in control in the polymerization. Reaction times below 17h for a graft density of 36.26 μmol/g did not provide any conversion, while those above resulted in very high conversions. It must also be noted that the R group of CDTPA is not particularly optimized for acrylamides as the cyano alkyl group is not a good homolytic leaving group with respect to the propagating radical.[21] Carboxylated alkyl R groups are known to be better at mediating acrylamide polymerizations,[21,23] and the usage of this RAFT agent (DTDMA) is discussed in the following section.

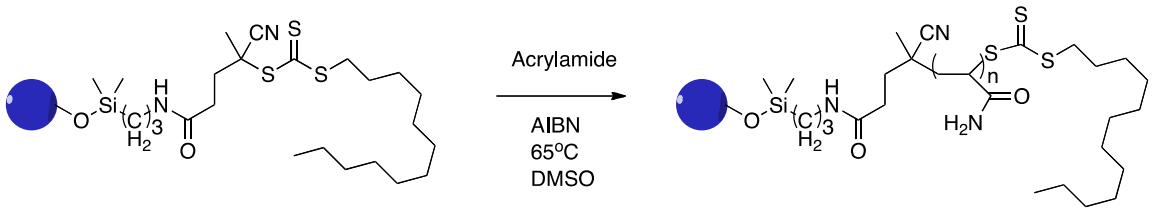


Scheme 5.4: Polymerization of Syloid-CTD to obtain Syloid-Poly(Acrylamide).

Table 5.2: Polymerizations of Syloid-CDTPA using acrylamide at various reaction conditions and grafting densities.

| Time (h) | Conv (%) | Temp. (˚C) | Monomer | Graft density (umol/g) | Monomer (eq) | Solvent | Mn (NMR) |
|---|---|---|---|---|---|---|---|
| 23 | 100 | 75 | AM | 36.26 | 3827 | DMSO | 272k |
| 17 | 62 | 70 | AM | 36.26 | 5000 | DMSO | 223k |

### 5.3.3 Synthesis of poly(acrylamide) in solution with DTDMA

As there was a need for better control over the RAFT polymerization of acrylamide, DTDMA was used in solution to ascertain its potential for syloid anchored polymerizations. Polymerizations with DTDMA were performed with at 70˚C using ACVA as the initiator in DMSO (Table 5.3). Conversions were measured by NMR using trioxane as an internal standard. The semi-logarithmic plots revealed a linear relationship between molecular weight and time, suggesting a controlled growth of polymer chains (Figure 5.4). The molecular weights could not be measured by GPC as polyacrylamide does not dissolve in typical organic solvents such as THF and DMF. A linear relationship is also seen from the graph of molecular weight (measured by NMR) over time, although

a tendency for the molecular weight to plateau at longer polymerization times was observed (Figure 5.5). This suggested a role of the high viscosity of the polymer playing a role in polymerization kinetics, where the monomer may have difficulty in diffusing to the growing chain end.

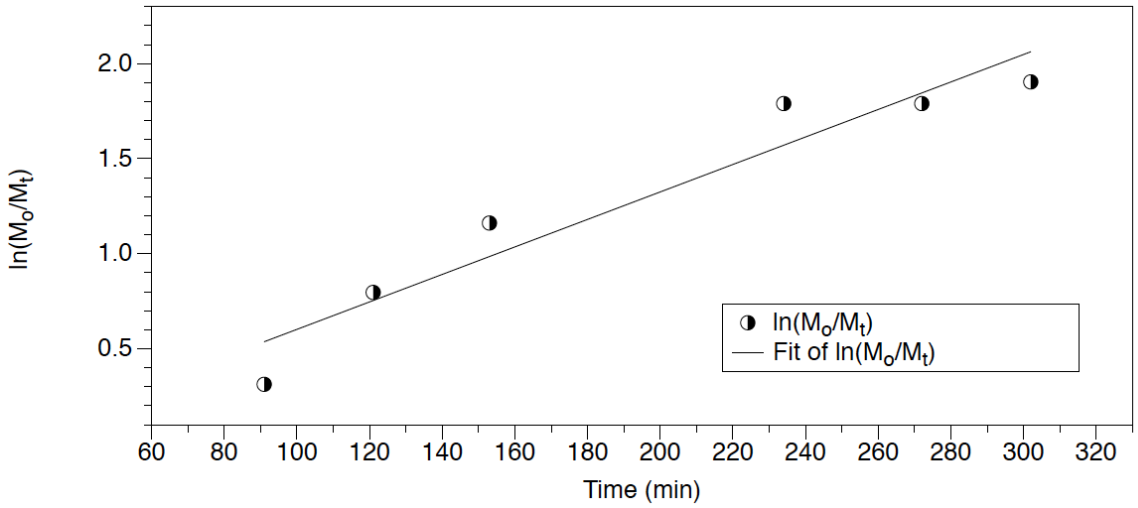


Figure 5.4: Semi-logarithmic plot of the kinetics of acrylamide polymerization. DTDMA: acrylamide: ACVA ratios of 1:13.7: 0.3 were used in DMSO at 70˚C.

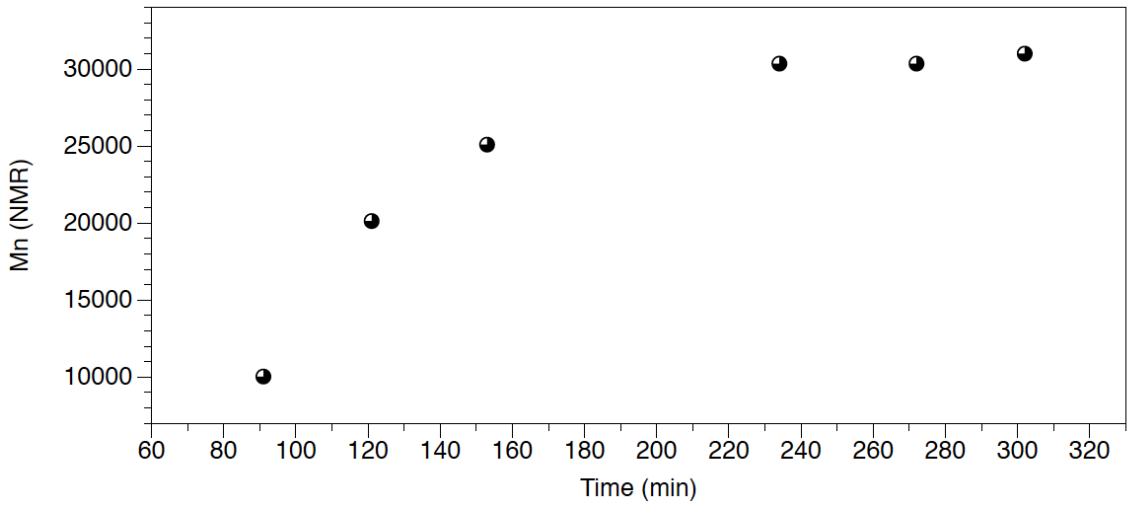


Figure 5.5: Kinetics of poly(acrylamide) polymerization using DTDMA showing the evolution of Mn (NMR) over polymerization time. DTDMA: acrylamide: ACVA ratios of 1:13.7: 0.3 were used in DMSO at 70˚C.

Table 5.3: Conversions and Mn (NMR) of poly(acrylamide) polymerization using DTDMA. DTDMA: acrylamide: ACVA ratios of 1:13.7: 0.3 were used in DMSO at 70˚C.

| # | Time (min) | Conversion | Mn (NMR) |
|---|---|---|---|
| 1 | 91 | 0.2685 | 10032 |
| 2 | 121 | 0.549 | 20131 |
| 3 | 153 | 0.6869 | 25096 |
| 4 | 205 | 0.858 | 31257 |
| 5 | 234 | 0.833 | 30357 |
| 6 | 272 | 0.833 | 30357 |
| 7 | 302 | 0.851 | 31005 |

Correspondingly, activated DTDMA was synthesized to anchor this RAFT agent to the syloid particles. As both CDTPA and DTDMA have similar UV absorption characteristics, the calibration curve in section 5.3.1 was used to calculate a grafting density of 40.8 μmol/g for the syloid-DTDMA. Further tests need to be performed to demonstrate the controlled polymerization of acrylamide on the syloid using DTDMA.

### 4.3.3 Grafting-to on Syloid particles

As a comparative test method for the grafting-from examples in retention efficiency testing, grafting-to methods were also investigated on the silica particles. In these methods, the silica-amine was reacted with polymers being activated esters (Scheme 5.5). Syloid-NH2 with a grafting density of 136.6 μmol/g was used for the grafting-to example. The grafting density was calculated by reacting a small portion of the syloid-NH2 (0.165 g, 0.0489 mmol of maximum amine content) with act. CPDB

(0.021g, 0.0539 mmol) and stirred for 6h. After the washing and drying process, the graft density of the syloid-CPDB was determined to be 136.6 μmol/g. As this reaction with the activated CPDB is correlates to the amount of reactive amine groups, this grafting density was used for the reaction of the syloid-amine with poly(NmS-PEGMA). Similar to the thiazoline group in terms of being a cleavable moiety, the succinimide ester was used as a monomer with N-methacryloxy succinimide (NMS) and PEGMA with a ratio of 1:15:15 (RAFT:NMS:PEGMA) at 65˚C in DMF to generate poly(NMS-PEGMA) with Mn: 17687 and PDI: 1.27. The advantage of such copolymer systems with the NMS monomer allowed for the calculation of individual monomer conversions, and in this example was a 100% conversion of NMS and 97% conversion of PEGMA. The reaction of this polymer with the syloid-amine was performed in THF at 70˚C (Scheme 5.5). Triethylamine was used as a catalyst to facilitate the nucleophilic attack of the amine, and several groups have reported the high conversions with small molecule amines.[24–26] For the poly(PEGMA-NMS) system, it was found that these copolymers were soluble in THF and DMF and the resulting syloid-PEG (after complete consumption of the succinimide units) was able to be suspended well in THF, without any signs of clumping or aggregation.

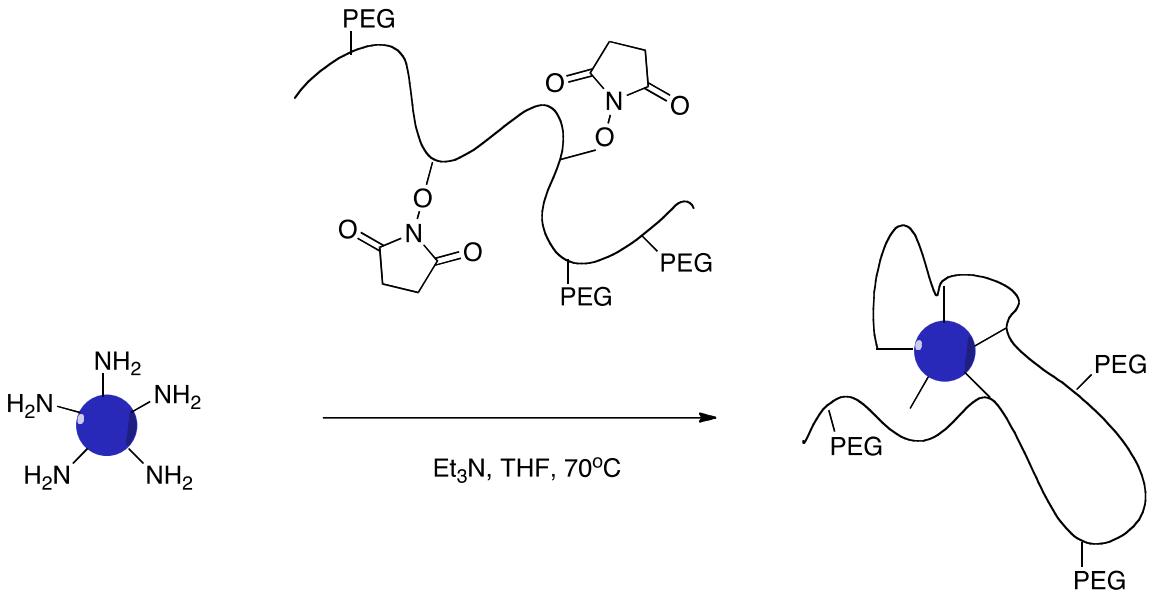


Scheme 5.5: Grafting-to procedure to obtain Syloid-PEG using poly(NMS-PEGMA).

### 5.3.4 Preparation of the Activated Azo and Azo functionalized Syloid

In several industrial applications involving polymeric materials, the significance of high yields, optimized processes and cost efficiency of the materials needed cannot be understated. Typically, industrial polymers are synthesized using condensation, free radical and anionic polymerization methods. RAFT and other CRP methods encounter limited stability of the chain transfer agents, air-free conditions and slower rates of polymerization, which limit their large-scale use in industry today. To truly facilitate this method of using polymers on silica surfaces at scale in the fracturing industry, a difunctional free radical initiator was synthesized. Typically, free radical polymerization has several advantages, including tolerance to low $O_2$ concentrations, very fast polymerization kinetics and inexpensive initiator compounds. 4,4′-Azobis(4-cyanovaleric acid), a commercially available free radical initiator was modified on both of its

carboxylic acid functional groups  using mercaptothiazoline in a reaction similar to the modification of RAFT agents (Scheme 5.6). The synthetic process for this technique allowed for recrystallization of the product, due to the unique nature of the azo functionality to precipitate in hexane solvents. This avoided the use of column chromatography, which is an expensive and time-consuming purification step.

Furthermore, the dual activation provides thiazoline groups on both ends of the azo, and the substitution can vary depending on the ratio of amines on the silica to the difunctional azo. In the case where the ratio of amines is higher than the azo, both ends of the azo are attached to single/multiple silica particles. In cases where the ratio of azo is higher, one of the terminal ends of the attached azo is available for further reactions. In the latter scenario, this aspect becomes important as during polymerization, untethered units result in significant amounts of free polymer. This becomes a problem in applications where the presence of inseparable free polymer can lead to complications. However, as the goal of this study was to show the proof of concept of azo functionalization, a 1:1 ratio of amines: activated azo was used to investigate whether azo groups could be attached. After the reaction, the azo functionalized syloid appeared as yellow particles (after several washes), demonstrating that the activated azo starting material (yellow) could be attached.

In order to further test the proof of concept for the free radical polymerization, several polymerizations were performed with styrene and methyl methacrylate without the presence of any free initiator (Table 5.4). In all cases where the ratio of monomer to solvent was 1:1 (mL), the polymerization proceeded very quickly and gelled composites were obtained. The composites were dissolved in THF and then subject to HF to cleave

the polymers for analysis by GPC. GPC traces revealed high MW polymers and high polydispersities (2.12-2.81), both relating to the uncontrolled characteristics of the free radical polymerization. Further studies pertaining to the calibration curves for the azo-functionalized syloid will permit a complete understanding of the graft densities of azo groups on the syloid.

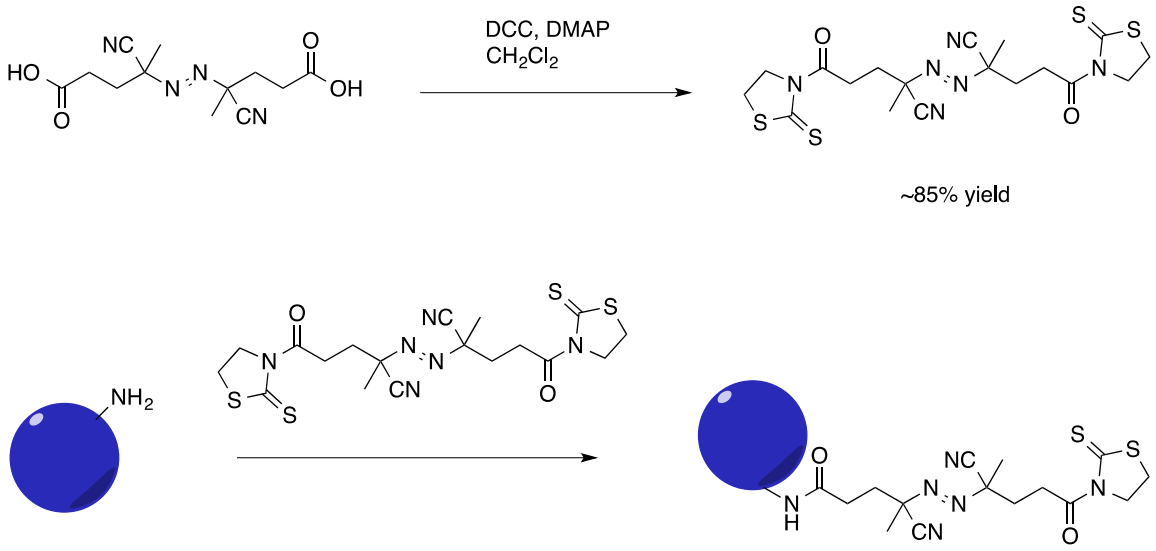


Scheme 5.6: Synthesis of activated ACVA and its functionalization on syloid particles.

Table 5.4: Polymerizations with styrene and MMA in THF (2 mL) at 65˚C using the syloid-azo showing the presence of polymer in the absence of free initiator.

| Syloid-azo (g) | Monomer | Time (h) | Mn (GPC) | PDI |
|---|---|---|---|---|
| 0.05 | MMA (2mL) | 2.22 | 342k | 2.12 |
| 0.05 | Styrene (2 mL) | 2.1 | 681k | 2.81 |

### 5.3.5 Retention studies

In order to perform a simple test to investigate the migration of free polymers versus syloid-anchored polymers, a retention efficiency test method was developed. In these tests, a pipette filled with a filter material (silica gel or diatomaceous earth) was designed in order to pass samples of polymer/syloid anchored polymer (14-78 mg) solutions in water (1 mL). Simultaneously, a control with water (1 mL) only was passed through the pipette. The solutions passed through the pipette were collected in a vial and then freeze-dryed to remove the water. With the polymer/syloid anchored polymer samples, the mass of the migrated material after freeze drying were compared with the amount of starting material to calculate the retention efficiency. Additionally, the mass of any filter material that passed through in the control experiments were subtracted from the amount recovered in the polymer/syloid anchored polymer samples to give an adjusted retention efficiency. In the following discussion, use of extended wash methods, where an additional amount of water (2 mL) was used following the polymer/syloid anchored polymer addition to simulate conditions in the field.

The results for the retention efficiency tests are tabulated in Tables 5.15-5.10. In these experiments, retention efficiency (RE) was calculated based on the amount of composite obtained after the filtration as compared to the amount of composite used for the filtration. Therefore, a retention efficiency of 100% equates to all of the material being retained in the column, while 0% means that the material was able to pass through the pores of the filter material. As the silica particle is relatively large (~4.5 um) compared to the free polymer (in the nm range for hydrodynamic radius), it was expected

that the polymer functionalized silica would have a higher retention efficiency that the free polymer.

In Table 5.5 and 5.6, normal wash conditions (2 ml solution of material passed through the filter) for the PAA system are displayed. The RE of the free PAA ranged from 53.3-65.9% based on the Mn of the PAA, with a higher RE obtained for the 200k as compared to the 140k. In comparison, the syloid-PAA displayed RE ranging from 95-100%, clearly displaying the ability of the composite to maintain the polymeric linkages. However, the RE of the free PAA was observed to be higher than expected, although the free polymer was expected to pass through the filter in a facile manner. In order to simulate real world conditions, extended washing procedures were tested to investigate the RE after several additional amounts of water to the column. In this procedure, samples were dissolved in water (2 ml), passed through the column, and followed up with two separate additions of water (1 ml) each. Similar to the procedure outlined above, each experiment included a control (2 ml of water), and the free polymer and Syloid-polymer respectively. For the silica-PAA system, as seen in Table 5.7 and 5.8, the free PAA displayed a RE of 3.8-6.4%, while the syloid-PAA had a RE of 83.7-88.5%. This definitively supported the hypothesis where the larger silica with anchored polymers displayed a greater propensity to remain in the filter material without leakage.

The grafting-to method with syloid-PEG was also tested with the extended wash method, and here the free poly(NMS-PEGMA) had an RE of 27.8% (Table 5.9). The syloid-PEG displayed an RE of 98.5%, showing that the grafting-to method also agreed with the hypothesis of increased RE for the polymer functionalized syloid. Finally, the extended wash method was also performed for the PAM grafted from the syloid (Table

5.10), where the free PAM had a significantly high RE of 72.4%. The syloid-PAM had a slightly higher RE of 84.1%. It must be noted that the free PAM (180k) was very viscous, and this could be a reason behind its high RE where more washes may be needed to completely remove the PAM from the filter material.

Overall, the RE test methods showed that the polymer functionalized syloid had higher REs for all cases, including various grafting methods and different polymer systems. This validates the proof-of-concept that grafting methods provide a robust attachment to particles, and further demonstrates the use of this property for use in the fracturing industry. The presence of free polymers in the water table can pose a significant environmental concerns with respect to human consumption and complications in the removal of such polymers. The emergence of the syloid-polymers with high RE further validates their usage in various applications where the loss of free polymers becomes a major concern.

Table 5.5: Syloid-PAA (Mn : 140k g/mol), water (1 ml), Filter (Diatomaceous Earth)poly(acrylic acid)of 140k g/mol on Syloid silica particles prepared by grafting-from techniques was tested by the procedures outlined in section 5.2.12. The adjusted efficiency data showed that 53.3% of the free polymer was retained in the column, as compared to 100% retention of the Syloid-polymer in the diatomaceous earth.

| | Amount Used (mg) | Amount Filtered (mg) | Efficiency (%) | Adjusted Efficiency (%) |
|---|---|---|---|---|
| Control | - | 1 | | |
| PAA | 15 | 1 | 46.7 | 53.3 |
| Syloid-PAA | 15 | 8 | 93.3 | 100 |

Table 5.6: Syloid-PAA (Mn : 200,000 g/mol), water (1 ml), Filter (Diatomaceous Earth). Poly(acrylic acid) of 200,000 g/mol on Syloid silica particles prepared by grafting-from techniques was tested by the procedures outlined in section 5.2.12. The adjusted efficiency data showed that 65.9% of the free polymer was retained in the column, as compared to 95.4% retention of the Syloid-polymer in the diatomaceous earth.

| | Amount Used (mg) | Amount Filtered (mg) | Efficiency (%) | Adjusted Efficiency (%) |
|---|---|---|---|---|
| Control | - | 0.05 | | |
| PAA | 22 | 8 | 63.63 | 65.9 |
| Syloid-PAA | 22 | 1.5 | 93.1 | 95.4 |

Table 5.7: Syloid-PAA (Mn : 140,000 g/mol), water (2 ml), Extended wash with water (2 ml), Filter (Diatomaceous Earth). Poly(acrylic acid) of 140k g/mol on Syloid silica particles prepared by grafting-from techniques was tested by the procedures outlined in section 5.2.12. The adjusted efficiency data showed that 6.4% of the free polymer was retained in the column, as compared to 88.46% retention of the Syloid-polymer in the diatomaceous earth.

| | Amount Used (mg) | Amount after filtration (mg) | Retention Efficiency (%) | Adjusted Efficiency (%) |
|---|---|---|---|---|
| Control | - | 0.5 | | |
| PAA | 14 | 13.6 | 2.85 | 6.4 |
| Syloid-PAA | 13 | 2 | 84.6 | 88.46 |

Table 5.8: (Diatomaceous Earth). Poly(acrylic acid) of 200k g/mol on Syloid silica particles prepared by grafting-from techniques was tested by the procedures outlined in section 5.2.12. The adjusted efficiency data showed that 3.75% of the free polymer was retained in the column, as compared to 83.7% retention of the Syloid-polymer in the diatomaceous earth.

| | Amount Used (mg) | Amount Filtered (mg) | Retention Efficiency (%) | Adjusted Efficiency (%) |
|---|---|---|---|---|
| Control | - | 0.1 | | |
| PAA | 16 | 15.5 | 3.1 | 3.75 |
| Syloid-PAA | 16 | 2.7 | 83.1 | 83.7 |

Table 5.9: Syloid-PEG (Grafted–to. Mn: 17,687 g/mol, PDI : 1.27), poly(NMS-PEGMA) (Mn: 38,888, PDI: 1.46), water (2 ml), Extended wash with water (2 ml), Filter (Diatomaceous Earth). PEG of 17,687 g/mol on Syloid silica particles prepared by grafting-to techniques was tested by the procedures outlined in section 5.2.14. The adjusted efficiency data showed that 27.8% of the free polymer was retained in the column, as compared to 98.5% retention of the Syloid-polymer in the diatomaceous earth.

| | Amount Used (mg) | Amount after filtration (mg) | Retention Efficiency (%) | Adjusted Efficiency (%) |
|---|---|---|---|---|
| Control | - | 1.7 | | |
| PEG-co-NMS | 78 | 58 | 25.64 | 27.8 |
| Syloid-PEG | 20 | 2 | 90 | 98.5 |

Table 5.10: Syloid-PAM (Grafted–from. Mn: 180,000 g/mol), Free PAM (Mn: 310,000 g/mol), water (2 ml), Extended wash with water (2 ml), Filter (Diatomaceous Earth). Polyacrylamide of 180,000 g/mol on Syloid silica particles prepared by grafting-from techniques was tested by the procedures outlined in section 5.2.8. The adjusted efficiency data showed that 72.4% of the free polymer of 310,000 g/mol was retained in the column, as compared to 84.1% retention of the Syloid-polymer in the diatomaceous earth.

| | Amount Used (mg) | Amount after filtration (mg) | Retention Efficiency (%) | Adjusted Efficiency (%) |
|---|---|---|---|---|
| Control | - | 1.8 | | |
| PAM | 25 | 8.7 | 65.2 | 72.4 |
| Syloid-PAM | 34 | 7.2 | 78.8 | 84.1 |

## 5.4. Summary

Given the significant environmental concerns related to the use of additives in fracturing fluids, the development of solutions that prevent leakage of such additives into the water table is essential. In this project, the hypothesis of anchoring polymeric additives to proppants (silica, an essential component in fracturing fluids) to prevent polymer migration is investigated. A variety of methods, including grafting-from and grafting-to procedures are developed for the attachment of polymers to large-sized (5.5

μm) syloid silica particles. RAFT agents are designed for the surface attachment of poly(acrylic acid), poly(acrylamide) and poly(ethylene glycol) on the syloid particles. In order to optimize the use of this technology for industry, cost-effective synthetic strategies have also been developed for surface attachment using free radical polymerization. More importantly, the hypothesis of additive anchored proppants having reduced migration of the additives in soil compositions were analyzed using retention efficiency tests. For all the strategies and polymeric systems in a variety of different filter materials, the polymer anchored syloid displayed highly reduced migration compared to the free polymer. This study combines a foundation in synthetic surface functionalization with an insightful migration test to illustrate its potential as vital components in environmentally fracturing fluids.

## 5.5 References


(1) Auch, T. Hydrocarbon Industrial Complex Map In Detail - FracTracker Alliance http://www.fractracker.org/2014/01/us-hydrocarbon-map/ (accessed Oct 22, 2014).

(2) Yew, C. H. *Mechanics of Hydraulic Fracturing*; Elsevier, 1997; pp. 1–29.

(3) *Modern Shale Gas Development in the United States: A Primer | Department of Energy*; 2009.

(4) Raimbay, A.; Babadagli, T.; Kuru, E.; Develi, K. In *SPE/CSUR Unconventional Resources Conference – Canada*; Society of Petroleum Engineers, 2014.

(5) Holloway, M. D.; Rudd, O. *Kirk-Othmer Encyclopedia of Chemical Technology*; John Wiley & Sons, Inc.: Hoboken, NJ, USA, 2000.

(6) Aldhous, P. *New Sci.* **2012**.

(7) Karisny, S. *Wayne Law Rev.* **2011**, *57*.

(8) Beemster, B.; Beemster, R. *Report on the effects of shale gas extraction by means of hydraulic fracturing in the Republic of Ireland.*; 2011; pp. 1–59.

(9) Jackson, R. E.; Gorody, A. W.; Mayer, B.; Roy, J. W.; Ryan, M. C.; Van Stempvoort, D. R. *Ground Water 51*, 488.

(10) Seybold, C. A. *Commun. Soil Sci. Plant Anal.* **1994**, *25*, 2171.

(11) Gidley, J. L.; Penny, G. S.; McDaniel, R. R. *SPE Prod. Facil.* **2013**, *10*, 20.

(12) Reinicke, A.; Rybacki, E.; Stanchits, S.; Huenges, E.; Dresen, G. *Chemie der Erde - Geochemistry* **2010**, *70*, 107.

(13) Benicewicz, B. C.; Calundann, G. W. Shale oil and gas fracturing fluids containing additives of low environmental impact. US20140090850 A1, 2014.

(14) Zoback, M.; Kitasei, S.; Copithorne, B. *Addressing the environmental risks from shale gas development*; Worldwatch Institute, 2010; Vol. 21.

(15) Howarth, R. W.; Ingraffea, A.; Engelder, T. *Nature* **2011**, *477*, 271.

(16) Myers, T. *Ground Water* **2012**, *50*, 872.

(17) Li, C.; Han, J.; Ryu, C. Y.; Benicewicz, B. C. *Macromolecules* **2006**, *39*, 3175.

(18) Radhakrishnan, B.; Ranjan, R.; Brittain, W. J. *Soft Matter* **2006**, *2*, 386.

(19) Heikkinen, J. J.; Heiskanen, J. P.; Hormi, O. E. O. *Polym. Adv. Technol.* **2006**, *17*, 426.

(20) Ranjan, R.; Brittain, W. J. *Macromolecules* **2007**, *40*, 6217.

(21) Barner-Kowollik, C. *Handbook of RAFT Polymerization*; John Wiley & Sons, 2008; p. pg. 245.

(22) Pelet, J. M.; Putnam, D. *Macromol. Chem. Phys.* **2012**, *213*, 2536.

(23) Lai, J. T.; Filla, D.; Shea, R. *Macromolecules* **2002**, *35*, 6754.

(24) Aamer, K. A.; Tew, G. N. *J. Polym. Sci. Part A Polym. Chem.* **2007**, *45*, 5618.

(25) Tew, G. N.; Aamer, K. A.; Shunmugam, R. *Polymer (Guildf).* **2005**, *46*, 8440.

(26) Shunmugam, R.; Tew, G. N. *J. Polym. Sci. Part A Polym. Chem.* **2005**, *43*, 5831.

# SUMMARY AND CONCLUSIONS

The synthetic toolbox of the RAFT technique relating to the surface modification of inorganic substrates was explored in this thesis, resulting in the functionalization of a variety of substrates. One of the challenges involved the functionalization of metal oxides such as titania and indium tin oxide (ITO), and phosphate based RAFT agents and polymers were used to graft-to and from these surfaces. Poly(glycidyl methacrylate) was synthesized with a RAFT agent bearing a terminal alkyne group, followed by its click reaction with azide-phosphate functionalized ITO. In order to facilitate the grafting from method, a phosphate functionalized RAFT agent was synthesized to anchor to ITO nanoparticles (NPs). Poly(methyl methacrylate) was then grafted from the surface, and the kinetics of polymerization from the surface were analyzed. Poly(dimethyl siloxane) bearing a terminal phosphate group was also designed to attach to titania NPs. All examples of nanoparticle-polymer were further tested for use in nanocomposites by mixing with polymer matrices. Good dispersions were obtained by optimizing the molecular variables and type of attachment, further confirming the crucial role played by effective surface functionalization through the phosphate ligand.

Some of the major challenges in quantum dot-polymer mixtures include the stability of the dots and its dispersability in aqueous media for bioapplications. To address these issues, imidazole functionalized poly(ethylene glycol) random copolymers were designed to attach to quantum dots. In this synthetic method, N-methacryloxy

succcinimide (NMS) was used as a monomer to introduce activated esters into the polymer chain. This was followed by a postmodification reaction with histamine to introduce imidazole units in the copolymer. Upon attachment to quantum dots, the functionalized dots displayed water solubility and good quantum yields. Furthermore, an analysis of the TEMs of the dots revealed excellent dispersions of the dots that were functionalized with polymers that had a higher imidazole content as well as a higher molecular weight.

Building on the synthetic approach using activated esters, terpolymers of poly(NMS-PEGMA-MAMboc) were synthesized, where a boc-protected methacrylamide (MAMboc) was added to the random copolymerization. This provided an additional property of dye loading capabilities upon deprotection of the boc group. The kinetics of the copolymerization was analyzed using a unique NMR technique, and the reactivities of the monomers were in the order: NMS>PEGMA>MAMboc. The succinimde units were postmodified to include imidazole groups, followed by the boc deportection to load a rhodamine based dye. The dye modified polymer was the used to functionalize CdS nanowires, and the successful functionalization was investigated using florescence spectroscopy.

Due to the recent expansion in horizontal drilling (fracking), there have been concerns regarding the environmental safety of the fracturing fluids used. Polymeric additives are used in conjunction with silica as a component of these fluids, and a simple method to reduce the risk of the additives leaking into the water table is via the robust functionalization of the polymers to the silica particles. The silica surface was modified with amines, followed by the anchoring of the RAFT agent. Poly(acrylamide) and

poly(acrylic acid) were grafted from the silica surface with RAFT polymerization. The silica-polymer samples were then tested for the tendency of the attached polymer to migrate through diatomaceous earth and silica gel. The silica-polymer samples displayed high retention efficiencies (low migration of the polymer) compared to high migrations of the free polymers through the filter materials. Overall, a simple functionalization and grafting-from method was used to display the potential of polymer anchored silica in environmentally friendly fracturing fluids.

# FUTURE WORK

Based on the results of this work, the two concepts shown to be significant are: (a) appropriate ligand for the substrate functionalization and (b) tailoring of the molecular variables of the polymers using RAFT. As a result, this section addresses potential avenues for future work for further understanding of the ligand binding and synthetic manipulations for optimization in the application.

For the use of phosphate-based ligands in the modification of metal oxides, the exact binding strength of phosphates to metal oxides is controversial in the literature. Binding/Desorption studies would be instrumental in improving the long-term stability of the metal oxide nanocomposites. In terms of characterization of the phosphate functionalized oxides, TGA was shown to provide a rough measurement of the grafting density. A more accurate measurement technique, such as UV-vis, is needed for the analysis of grafting density, particularly for the small molecule functionalization. As metal oxides absorb heavily in the 250-400 nm range, phosphate-dyes that can absorb in the 400-500 nm range can be a simple solution to this issue.

In this dissertation, there was a significant discussion of the synthesis of imidazole functionalized polymers for their attachment to semiconductor nanomaterials. Similar to the phosphate-metal oxide attachment, there is a need for a fundamental analysis of the binding strength of the polymeric imidazole to CdSe/CdS materials.

Furthermore, this analysis should also investigate the binding strength of the imidazole small molecules as opposed to their polymeric counterparts. Although it is believed that the polymeric imidazoles provide better stability to the functionalized quantum dot, further studies to substantiate this claim will aid in future bio/optical applications.

Additionally, the synthetic method was limited to the random copolymerization in the research work. An interesting alternative is a block copolymer or terpolymer, where the terminal ends of the polymer chain are rich in imidazole content. It was noted in the TEM results in the third chapter where a difference was seen in the dispersion quality of the quantum dot with changes in the molecular weight and imidazole content of the copolymer. Potentially, by controlling the location of the imidazole in the polymer chain to be highly populated in certain regions, it is possible to control the level of functionalization, and hence control the stability or quantum yield of the functionalized semiconductor. In particular, given the recent interest in quantum dots by several industrial companies as components in LEDs, this level of tunability can be useful in dictating various product lines in the LED market.

With regards to the polymer anchored silica for fracturing fluids, this work provides the proof of concept with synthetic methods and retention efficiency testing for a new approach to potentially safer and more effective additives. In order to be amenable to application in the field, further migration tests need to be performed in the presence of high pressures and temperatures to simulate field conditions. Additionally, polymeric additives in fracturing fluids, especially viscosity modifiers such as poly(acrylamide) require molecular weights to be greater than 800k. In this case, alternatives to RAFT,

such as the activated azo compounds are more promising due to its ability to generate high molecular weight polymers in a short period of time (albeit without control of chain length). The characterization of azo anchored silica is lacking in terms of grafting densities, and the azo goup is known to absorb in the 300-350 nm region in the UV. With a calibration curve for the azo group, the grafting densities can be accurately measured. Finally, the data for the poly(acrylamide) and poly(acrylic acid) reported in this work are not accurate as GPC characterization could not be performed. Other techniques, including the use of Mark-Houwink coefficients can be utilized to obtain an improved measurement of the molecular weights for the polymers.

# BIBLIOGRAPHY


(1) Chiefari, J.; Chong, Y. K. (Bill); Ercole, F.; Krstina, J.; Jeffery, J.; Le, T. P. T.; Mayadunne, R. T. A.; Meijs, G. F.; Moad, C. L.; Moad, G.; Rizzardo, E.; Thang, S. H. *Macromolecules* **1998**, *31*, 5559.

(2) Moad, G.; Rizzardo, E.; Thang, S. H. *Aust. J. Chem.* **2009**, *62*, 1402.

(3) Barner-Kowollik, C. *Handbook of RAFT Polymerization*; John Wiley & Sons, 2008; p. pg. 245.

(4) Kango, S.; Kalia, S.; Celli, A.; Njuguna, J.; Habibi, Y.; Kumar, R. *Prog. Polym. Sci.* **2013**, *38*, 1232.

(5) Kumar, S. K.; Jouault, N.; Benicewicz, B.; Neely, T. *Macromolecules* **2013**, *46*, 3199.

(6) Olivier, A.; Meyer, F.; Raquez, J.-M.; Damman, P.; Dubois, P. *Prog. Polym. Sci.* **2012**, *37*, 157.

(7) Minakuchi, H.; Nakanishi, K.; Soga, N.; Ishizuka, N.; Tanaka, N. *Anal. Chem.* **1996**, *68*, 3498.

(8) Mutin, P. H.; Guerrero, G.; Vioux, A. *J. Mater. Chem.* **2005**, *15*, 3761.

(9) Rungta, A.; Natarajan, B.; Neely, T.; Dukes, D.; Schadler, L. S.; Benicewicz, B. C. *Macromolecules* **2012**, *45*, 9303.

(10) Li, Y.; Tao, P.; Viswanath, A.; Benicewicz, B. C.; Schadler, L. S.Langmuir **2013**, *29*, 1211.

(11) Norsten, T. B.; Jeoung, E.; Thibault, R. J.; Rotello, V. M. *Langmuir* **2003**, *19*, 7089.

(12) Helms, B.; Mynar, J. L.; Hawker, C. J.; Fréchet, J. M. J. *J. Am. Chem. Soc.* **2004**, *126*, 15020.

(13) Binder, W. H.; Sachsenhofer, R. *Macromol. Rapid Commun.* **2008**, *29*, 952.

(14) Guerrero, G.; Mutin, P. H.; Vioux, A. *Chem. Mater.* **2001**, *13*, 4367.

(15) Guerrero, G.; Alauzun, J. G.; Granier, M.; Laurencin, D.; Mutin, P. H. *Dalton Trans.* **2013**, *42*, 12569.

(16) Granqvist, C. G.; Hultåker, A. *Thin Solid Films* **2002**, *411*, 1.

(17) Tao, P.; Viswanath, A.; Schadler, L. S.; Benicewicz, B. C.; Siegel, R. W. *ACS Appl. Mater. Interfaces* **2011**, *3*, 3638.

(18) Liu, J.; Nakamura, Y.; Ogura, T.; Shibasaki, Y.; Ando, S.; Ueda, M. *Chem. Mater.* **2008**, *20*, 273.

(19) Su, H.-W.; Chen, W.-C. *J. Mater. Chem.* **2008**, *18*, 1139.

(20) Tao, P.; Li, Y.; Rungta, A.; Viswanath, A.; Gao, J.; Benicewicz, B. C.; Siegel, R. W.; Schadler, L. S. *J. Mater. Chem.* **2011**, *21*, 18623.

(21) Hanson, E. L.; Guo, J.; Koch, N.; Schwartz, J.; Bernasek, S. L. **2005**, 10058.

(22) Capozzi, C. J.; Li, Z.; Samuels, R. J.; Gerhardt, R. a. *J. Appl. Phys.* **2008**, *104*, 114902.

(23) Khaled, S. M.; Sui, R.; Charpentier, P. A.; Rizkalla, A. S. *Langmuir* **2007**, *23*, 3988.

(24) Matsuno, R.; Otsuka, H.; Takahara, A. *Soft Matter* **2006**, *2*, 415.

(25) Hojjati, B.; Charpentier, P. A. *J. Polym. Sci. Part aPolymer Chem.* **2008**, *46*, 3926.

(26) Hojjati, B.; Sui, R.; Charpentier, P. A. *Polymer (Guildf).* **2007**, *48*, 5850.

(27) Tchoul, M. N.; Fillery, S. P.; Koerner, H.; Drummy, L. F.; Oyerokun, F. T.; Mirau, P. A.; Durstock, M. F.; Vaia, R. A. *Chem. Mater.* **2010**, *22*, 1749.

(28) Aslan, A.; Bozkurt, A. *J. Mater. Res.* **2012**, *27*, 3090.

(29) Aamer, K. A.; Tew, G. N. *J. Polym. Sci. Part A Polym. Chem.* **2007**, *45*, 5618.

(30) Cengiz, N.; Kabadayioglu, H.; Sanyal, R. *J. Polym. Sci. Part A Polym. Chem.* **2010**, *48*, 4737.

(31) Eschweiler, N.; Keul, H.; Millaruelo, M.; Weberskirch, R.; Moeller, M. *Polym. Int.* **2014**, *63*, 114.

(32) Fukukawa, K.; Rossin, R.; Hagooly, A.; Pressly, E. D.; Hunt, J. N.; Messmore, B. W.; Wooley, K. L.; Welch, M. J.; Hawker, C. J. *Biomacromolecules* **2008**, *9*, 1329.

(33) Li, C.; Han, J.; Ryu, C. Y.; Benicewicz, B. C. *Macromolecules* **2006**, *39*, 3175.

(34) Li, Y.; Benicewicz, B. C. *Macromolecules* **2008**, *41*, 7986.

(35) Hussain, F.; Hojjati, M. *J. Compos. …* **2006**.

(36) Beecroft, L. L.; Ober, C. K. *Chem. Mater.* **1997**, *9*, 1302.

(37) Sanchez, C.; Julián, B.; Belleville, P.; Popall, M. *J. Mater. Chem.* **2005**, *15*, 3559.

(38) Schadler, L. S.; Kumar, S. K.; Benicewicz, B. C.; Lewis, S. L.; Harton, S. E. *MRS Bull.* **2011**, *32*, 335.

(39) Tao, P.; Viswanath, A.; Li, Y.; Rungta, A.; Benicewicz, B. C.; Siegel, R. W.; Schadler, L. S. *MRS Proc.* **2011**, *1359*, mrss11.

(40) Kim, H.; Miura, Y.; Macosko, C. W. *Chem. Mater.* **2010**, *22*, 3441.

(41) Wang, H.; Zeng, C.; Elkovitch, M.; Lee, L. J.; Koelling, K. W. *Polym. Eng. Sci.* **2001**, *41*, 2036.

(42) Sen, S.; Xie, Y.; Bansal, A.; Yang, H.; Cho, K.; Schadler, L. S.; Kumar, S. K. *Eur. Phys. J. Spec. Top.* **2007**, *141*, 161.

(43) Jordan, J.; Jacob, K. I.; Tannenbaum, R.; Sharaf, M. A.; Jasiuk, I. *Mater. Sci. Eng. A* **2005**, *393*, 1.

(44) Liu, J.; Gao, Y.; Cao, D.; Zhang, L.; Guo, Z. *Langmuir* **2011**, *27*, 7926.

(45) Tao, P. Epoxy and Silicone Optical Nanocomposites Filled with Grafted Nanoparticles, 2012.

(46) Akcora, P.; Liu, H.; Kumar, S. K.; Moll, J.; Li, Y.; Benicewicz, B. C.; Schadler, L. S.; Acehan, D.; Panagiotopoulos, A. Z.; Pryamitsyn, V.; Ganesan, V.; Ilavsky, J.; Thiyagarajan, P.; Colby, R. H.; Douglas, J. F. *Nat. Mater.* **2009**, *8*, 354.

(47) Kuang, Q.; Wang, X.; Jiang, Z.; Xie, Z.; Zheng, L. *Acc. Chem. Res.* **2014**, *47*, 308.

(48) Queffélec, C.; Petit, M.; Janvier, P.; Knight, D. A.; Bujoli, B. *Chem. Rev.* **2012**, *112*, 3777.

(49) Vosloo, J. J.; De Wet-Roos, D.; Tonge, M. P.; Sanderson, R. D. *Macromolecules* **2002**, *35*, 4894.

(50) Tao, P.; Viswanath, A.; Schadler, L. S.; Benicewicz, B. C.; Siegel, R. W. *Langmuir* **2011**, *3*, 3638.

(51) Rudnick, L. R. *Lubricant Additives: Chemistry and Applications, Second Edition*; CRC Press, 2009; p. 790.

(52) Kwak, Y.; Nicolaÿ, R.; Matyjaszewski, K. *Macromolecules* **2009**, *42*, 3738.

(53) Chong, ) Y. K.; Krstina, J.; Le, T. P. T.; Moad, G.; Postma, A.; Rizzardo, E.; Thang, S. H. *Macromolecules* **2003**, *36*, 2256.

(54) Shirasaki, Y.; Supran, G. J.; Bawendi, M. G.; Bulovic, V. *Nat Phot.* **2013**, *7*, 13.

(55) Kamat, P. V. *J. Phys. Chem. Lett.* **2013**, *4*, 908.

(56) Liu, W.; Greytak, A. B.; Lee, J.; Wong, C. R.; Park, J.; Marshall, L. F.; Jiang, W.; Curtin, P. N.; Ting, A. Y.; Nocera, D. G.; Fukumura, D.; Jain, R. K.; Bawendi, M. G. *J. Am. Chem. Soc.* **2010**, *132*, 472.

(57) Zhang, P.; Liu, S.; Gao, D.; Hu, D.; Gong, P.; Sheng, Z.; Deng, J.; Ma, Y.; Cai, L. *J. Am. Chem. Soc.* **2012**, *134*, 8388.

(58) Zimmer, J. P.; Kim, S.-W.; Ohnishi, S.; Tanaka, E.; Frangioni, J. V; Bawendi, M. G. *J. Am. Chem. Soc.* **2006**, *128*, 2526.

(59) Bruchez, M.; Moronne, M.; Gin, P.; Weiss, S.; Alivisatos, A. P. *Sci.* **1998**, *281* , 2013.

(60) Wang, M.; Oh, J. K.; Dykstra, T. E.; Lou, X.; Scholes, G. D.; Winnik, M. A.; Ms, C. *Macromolecules* **2006**, *39*, 3664.

(61) Yi, D. K.; Selvan, S. T.; Lee, S. S.; Papaefthymiou, G. C.; Kundaliya, D.; Ying, J. Y. *J. Am. Chem. Soc.* **2005**, *127*, 4990.

(62) Kloust, H.; Schmidtke, C.; Merkl, J.-P.; Feld, A.; Schotten, T.; Fittschen, U. E. A.; Gehring, M.; Ostermann, J.; Pöselt, E.; Weller, H. *J. Phys. Chem. C* **2013**, *117*, 23244.

(63) Schieber, C.; Bestetti, A.; Lim, J. P.; Ryan, A. D.; Nguyen, T.-L.; Eldridge, R.; White, A. R.; Gleeson, P. a; Donnelly, P. S.; Williams, S. J.; Mulvaney, P. *Angew. Chem. Int. Ed. Engl.* **2012**, *51*, 10523.

(64) Algar, W. R.; Krull, U. J. *Langmuir* **2006**, *22*, 11346.

(65) Zhan, N.; Palui, G.; Safi, M.; Ji, X.; Mattoussi, H. *J. Am. Chem. Soc.* **2013**, *135*, 13786.

(66) Aldeek, F.; Safi, M.; Zhan, N.; Palui, G.; Mattoussi, H. *ACS Nano* **2013**, *7*, 10197.

(67) Liu, W.; Greytak, A. B.; Lee, J.; Wong, C. R.; Park, J.; Marshall, L. F.; Jiang, W.; Curtin, P. N.; Ting, A. Y.; Nocera, D. G.; Fukumura, D.; Jain, R. K.; Bawendi, M. G. *J. Am. Chem. Soc.* **2010**, *132*, 472.

(68) Petryayeva, E.; Krull, U. J. *Langmuir* **2012**, *28*, 13943.

(69) Petryayeva, E.; Algar, W. R.; Krull, U. J. *Langmuir* **2013**, *29*, 977.

(70) Han, H.-S.; Martin, J. D.; Lee, J.; Harris, D. K.; Fukumura, D.; Jain, R. K.; Bawendi, M. *Angew. Chem. Int. Ed. Engl.* **2013**, *52*, 1414.

(71) Shen, L. *J. Funct. Biomater.* **2011**, *2*, 355.

(72) Shen, L.; Pich, A.; Fava, D.; Wang, M.; Kumar, S.; Wu, C.; Scholes, G. D.; Winnik, M. A. *J. Mater. Chem.* **2008**, *18*, 763.

(73) Allen, M. H.; Hemp, S. T.; Smith, A. E.; Long, T. E. *Macromolecules* **2012**, *45*, 3669.

(74) Weber, R. L.; Ye, Y.; Schmitt, A. L.; Banik, S. M.; Elabd, Y. a.; Mahanthappa, M. K. *Macromolecules* **2011**, *44*, 5727.

(75) Hoarfrost, M. L.; Segalman, R. A. *Macromolecules* **2011**, *44*, 5281.

(76) Vijayakrishna, K.; Jewrajka, S. K.; Ruiz, A.; Marcilla, R.; Pomposo, J. a.; Mecerreyes, D.; Taton, D.; Gnanou, Y. *Macromolecules* **2008**, *41*, 6299.

(77) Wiss, K. T.; Theato, P. *J. Polym. Sci. Part A Polym. Chem.* **2010**, *48*, 4758.

(78) Nilles, K.; Theato, P. *Polym. Chem.* **2011**, *2*, 376.

(79) Nilles, K.; Theato, P. *J. Polym. Sci. Part A Polym. Chem.* **2009**, *47*, 1696.

(80) Yanjarappa, M. J.; Gujraty, K. V; Joshi, A.; Saraph, A.; Kane, R. S. *Biomacromolecules* **2006**, *7*, 1665.

(81) Batz, H.-G.; Franzmann, G.; Ringsdorf, H. *Angew. Chemie Int. Ed. English* **1972**, *11*, 1103.

(82) Alb, A. M.; Enohnyaket, P.; Drenski, M. F.; Shunmugam, R.; Tew, G. N.; Reed, W. F. *Macromolecules* **2006**, *39*, 8283.

(83) Boyer, C.; Bulmus, V.; Davis, T. P.; Ladmiral, V.; Liu, J.; Perrier, S. *Chem. Rev.* **2009**, *109*, 5402.

(84) Chen, M.; Moad, G.; Rizzardo, E. *J. Polym. Sci. Part A Polym. Chem.* **2009**, 6704.

(85) Willcock, H.; O'Reilly, R. K. *Polym. Chem.* **2010**, *1*, 149.

(86) Schneider, Y.; Modestino, M. a.; McCulloch, B. L.; Hoarfrost, M. L.; Hess, R. W.; Segalman, R. a. *Macromolecules* **2013**, *46*, 1543.

(87) Hochbaum, A. I.; Yang, P. *Chem. Rev.* **2010**, *110*, 527.

(88) Law, M.; Goldberger, J.; Yang, P. *Annu. Rev. Mater. Res.* **2004**, *34*, 83.

(89) Duan, X.; Lieber, C. M. *Adv. Mater.* **2000**, *12*, 298.

(90) Gao, T.; Wang, T. *Cryst. Growth Des.* **2010**, *10*, 4995.

(91) Prudnikau, A.; Chuvilin, A.; Artemyev, M. *J. Am. Chem. Soc.* **2013**, *135*, 14476.

(92) Ning, Z.; Molnár, M.; Chen, Y.; Friberg, P.; Gan, L.; Ågren, H.; Fu, Y. *Phys. Chem. Chem. Phys.* **2011**, *13*, 5848.

(93) Widmer-Cooper, A.; Geissler, P. *Nano Lett.* **2014**, *14*, 57.

(94) Rajendran, V.; Lehnig, M.; Niemeyer, C. M. *J. Mater. Chem.* **2009**, *19*, 6348.

(95) Ma, N.; Sargent, E. H.; Kelley, S. O. *Nat. Nanotechnol.* **2009**, *4*, 121.

(96) Chen, S.; Zhu, J.; Shen, Y.; Hu, C.; Chen, L. *Langmuir* **2007**, *23*, 850.

(97) Li, X.; Nichols, V. M.; Zhou, D.; Lim, C.; Pau, G. S. H.; Bardeen, C. J.; Tang, M. L. *Nano Lett.* **2014**, *14*, 3382.

(98) Jang, W.; Koo, P.; Bryson, K.; Narayanan, S.; Sandy, A.; Russell, T. P.; Mochrie, S. G. *Macromolecules* **2014**, *47*, 6483.

(99) Greytak, A. B.; Allen, P. M.; Liu, W.; Zhao, J.; Young, E. R.; Popović, Z.; Walker, B. J.; Nocera, D. G.; Bawendi, M. G. *Chem. Sci.* **2012**, *3*, 2028.

(100) Shunmugam, R.; Tew, G. N. *J. Polym. Sci. Part A Polym. Chem.* **2005**, *43*, 5831.

(101) Luo, C.; Liu, Y.; Li, Z. *Soft Matter* **2012**, *8*, 2618.

(102) Auch, T. Hydrocarbon Industrial Complex Map In Detail - FracTracker Alliance http://www.fractracker.org/2014/01/us-hydrocarbon-map/ (accessed Oct 22, 2014).

(103) Yew, C. H. *Mechanics of Hydraulic Fracturing*; Elsevier, 1997; pp. 1–29.

(104) *Modern Shale Gas Development in the United States: A Primer | Department of Energy*; 2009.

(105) Raimbay, A.; Babadagli, T.; Kuru, E.; Develi, K. In *SPE/CSUR Unconventional Resources Conference – Canada*; Society of Petroleum Engineers, 2014.

(106) Holloway, M. D.; Rudd, O. *Kirk-Othmer Encyclopedia of Chemical Technology*; John Wiley & Sons, Inc.: Hoboken, NJ, USA, 2000.

(107) Aldhous, P. *New Sci.* **2012**.

(108) Karisny, S. *Wayne Law Rev.* **2011**, *57*.

(109) Beemster, B.; Beemster, R. *Report on the effects of shale gas extraction by means of hydraulic fracturing in the Republic of Ireland.*; 2011; pp. 1–59.

(110) Jackson, R. E.; Gorody, A. W.; Mayer, B.; Roy, J. W.; Ryan, M. C.; Van Stempvoort, D. R. *Ground Water 51*, 488.

(111) Seybold, C. A. *Commun. Soil Sci. Plant Anal.* **1994**, *25*, 2171.

(112) Gidley, J. L.; Penny, G. S.; McDaniel, R. R. *SPE Prod. Facil.* **2013**, *10*, 20.

(113) Reinicke, A.; Rybacki, E.; Stanchits, S.; Huenges, E.; Dresen, G. *Chemie der Erde - Geochemistry* **2010**, *70*, 107.

(114) Benicewicz, B. C.; Calundann, G. W. Shale oil and gas fracturing fluids containing additives of low environmental impact. US20140090850 A1, 2014.

(115) Zoback, M.; Kitasei, S.; Copithorne, B. *Addressing the environmental risks from shale gas development*; Worldwatch Institute, 2010; Vol. 21.

(116) Howarth, R. W.; Ingraffea, A.; Engelder, T. *Nature* **2011**, *477*, 271.

(117) Myers, T. *Ground Water* **2012**, *50*, 872.

(118) Radhakrishnan, B.; Ranjan, R.; Brittain, W. J. *Soft Matter* **2006**, *2*, 386.

(119) Heikkinen, J. J.; Heiskanen, J. P.; Hormi, O. E. O. *Polym. Adv. Technol.* **2006**, *17*, 426.

(120) Ranjan, R.; Brittain, W. J. *Macromolecules* **2007**, *40*, 6217.

(121) Pelet, J. M.; Putnam, D. *Macromol. Chem. Phys.* **2012**, *213*, 2536.

(122) Lai, J. T.; Filla, D.; Shea, R. *Macromolecules* **2002**, *35*, 6754.

(123) Tew, G. N.; Aamer, K. A.; Shunmugam, R. *Polymer (Guildf).* **2005**, *46*, 8440.